Atomic shell structure from Born probabilities: comparison to other shell descriptors and persistence in molecules

María Menéndez-Herrero, Julen Munárriz, Evelio Francisco, and Ángel Martín Pendás*

Depto. Química Física y Analítica. Universidad de Oviedo. 33006 Oviedo, Spain.

(*Electronic address: ampendas@uniovi.es)

(Dated: March 31, 2022)

Abstract

Real space chemical bonding descriptors, like the electron localization function or the Laplacian of the electron density, have been widely used in electronic structure theory thanks to their power to provide chemically intuitive spatial images of bonded and non-bonded interactions. This capacity stems from their ability to display the shell structure of atoms and its distortion upon molecular formation. Here we examine the spatial position of the N electrons of an atom at the maximum of the square of the wavefunction, the so-called Born maximum, as a shell structure descriptor for ground state atoms with $Z = 1 - 36$, comparing it to other available indices. The maximization is performed with the help of variational quantum Monte Carlo calculations. We show that many electron effects, mainly Pauli driven, are non-negligible, that Born shells are closer to the nucleus than any other of the examined descriptors, and that these shells are very well preserved in simple molecules.

I. INTRODUCTION

Although the orbital paradigm lies at the root of how modern chemistry is interpreted [1], much work has been devoted over the last forty years to build alternative frameworks that provide orbital invariant descriptions [2, 3]. During this time, it has become clear that chemical interpretations rely strongly on the jargon peculiar to the computational schemes used, the levels of theory employed to obtain the electronic structure, and many other approach-dependent features that cannot be easily translated across methodologies. As an example, charge-shift bonding, a purportedly new bonding mechanism that had not been recognized until recently [4], depends crucially on valence bond theory (VBT) concepts which are hard to accommodated outside the VBT realm, having thus been criticized [5]. Orbital invariant formalisms, on the other hand, build their insights through descriptors which are obtained from reduced density matrices (RDMs) of various orders, either in real or in momentum space [6, 7]. By construction, they are kept unchanged under any orbital transformation that leaves the wavefunction unaltered, and can be built and compared, in principle, with any methodology. Given the proximity of the chemical language to spatial thinking, most of these orbital invariant descriptors have been developed in real space and their use has become widespread [3].

In this scenario, the shell structure of atoms can be considered as one of the most fundamental chemical concepts, permeating all other bonding analyses. Atomic valences are chemically relevant, while cores tend to stay inert. In an orbital description, shells come out immediately from filling orbitals with the same principal quantum number through the Aufbau prescription. Provided that core orbitals maintain their individuality upon molecular formation (in the worst case a symmetry determined localization procedure might be necessary), the atomic cores are thought to persist after chemical bonds are formed. On the contrary, valences are heavily distorted in this process. It thus comes to no surprise that recovering the shell structure of atoms from the electron distribution itself, freeing ourselves from the orbital corset, has raised much interest in the past.

A large number of different shell descriptors have been described. A very reduced list includes the radial electron density distribution function, $D(r) = 4\pi r^2 \rho(r)$, which displays maxima that correlate with the expected electron shells for light atoms, but fails to locate the valence shells for heavy ones [8–10]. Given that each shell is associated to a different exponential decay of the density, a plot of $\log(\rho)$ shows a set of rectilinear steps, with different slopes, that can be sensed by $|\nabla\rho|/\rho$. In a similar way, the Laplacian of the density is able to show regions of local charge

accumulation and depletion, since it is easy to show that its sign determines whether the average value of the density in the immmediate neighborhood of a point is larger or smaller than the density at the point itself. If computed for an exponential patch $\rho(r) \approx Ne^{-}\zeta r$, $-\nabla^2\rho = Ne^{-\zeta r}(2\zeta/r - \zeta^2)$, so that each shell shows a pair of positive (accumulation) and negative (depletion) regions. Interestingly, the Laplacian is related to the local kinetic energy, E_{kin} defined by Hunter [11], which has also been used as a shell descriptor. Again, unfortunately, accumulation regions for the valence shells of heavy atoms cease to be resolved in both cases (starting past Ca in the case of $-\nabla^2\rho$ and in Ga in the case of $-E_{kin}$.

Another route to recover the atomic shell structure looks for electron localization regions, understood in terms of the curvature of the Fermi exclusion hole that surrounds any electron. Steep holes imply heavy same-spin electron exclusion, thus localized electrons, while the contrary occurs in the case of shallow holes [12]. This idea was used to build the electron localization function (ELF) by Becke and Edgecombe. Since the spherically averaged same-spin conditional pair density curvature is density dependent, both authors took the homogeneous electron gas (HEG) with the same density (at the one-electron level) as a reference value to build the ELF kernel χ that is finally Lorenztian transformed so that ELF lies between zero and one. Soon, Savin [13] noticed that the hole curvature is related to the excess kinetic energy of a fermionic system with respect to a bosonic one at the same density, the so-called Pauli kinetic energy, which allowed to use the ELF within density functional theory (DFT). As shown by Kohout and Savin [14], the ELF shows the shell structure even in heavy atoms, and the density integrated between successive ELF minima provides electron numbers in reasonable agreement with expectations, something which is not the case for the Laplacian. Given the role of the kinetic energy density in the development of electron localization measures, Schmider and Becke [15] proposed another measure, the localized orbital locator (LOL), this time dependent just on the ratio of the positive-definite kinetic energy density, τ, and that of the HEG. LOL is also clearly able to recover the shell structure, and decays asymptotically to zero, a condition that is not met for ELF if the last shell is composed of only *s* electrons. Finally, the dependence of ELF or LOL on the HEG reference was by-passed by Kohout [16], who showed how a localization localizability indicator (ELI) could be introduced by examining how many same-spin pair lie in a region containing a fixed electron charge. ELI collapses over the ELF in single-determinant approximations, is equally valid for non-correlated and correlated descriptions, and obviously recovers very well the atomic shell structure and its associated electron counts.

Not unexpectedly, all these shell descriptors have been also used in the molecular realm, where the electrons associated to the different atomic shells become distorted by the environmental potential. Even the inert atomic cores experience this effect, which can be sensed very clearly as core polarizations of different flavors by the Laplacian or the ELF, for instance [17]. Usually, the valence electrons condense into regions of charge concentration or electron localization, which provide a robust theoretical foundation for, e.g., the valence shell electron pair repulsion (VSEPR) model of Gillespie and coworkers [18]. The ELF, LOL, and ELI have been widely used to offer inspiring chemical images that can immediately be read by chemists: cores, lone pairs, bonded pairs become truly, vividly visible. ELF analyses, for instance, have spread globally as a computationally inexpensive way to access orbital invariant chemically appealing interpretations [19], for most of these descriptors are rather independent of the level of theory and the basis set used to compute them, at least semi-quantitatively speaking.

Although most of the original controversies regarding the ability of these descriptors to feel the shell structure are now settled, a few important points remain to be answered. On one hand, all of these scalar fields are built from the one- or two-particle density matrices (either in real or in momentum space). The electron density and the pair density keep information about the distribution of an electron or electron pair, respectively, once all the other electron have been averaged. On doing so, the spatial (or momentum) correlations that exist among the full N-electron set are washed out. To what extent this impacts the shell structure has not been appropriately studied. Related to this, it is significant that the distances at which the different descriptors show shell maxima or inter-shell minima differ considerably from one index to the other. This is a relevant observation, since changes in the theoretical level or basis set do not alter much the position of these critical points for any given descriptor. Just as an example, the distances at which the M valence shell maximum occurs for the ELF, LOL and $-\nabla^2\rho$ in the ^{1}S ground state of the Ar atom are close to 1.46, 1.19, and 1.08 au, respectively (vide infra), while the outermost maxima of the 3s and 3p densities lie between 0.95-0.97 au. By no means this range of variation can be neglected, nor it can be attributed to a difference between localization-based and density-based descriptors: LOL and ELF differ substantially, both being related to kinetic energy densities.

It is therefore relevant to examine how the multielectron nature of atomic shells impacts our established intuition. We do it in real space, examining how the global electron distribution adapts to the shell concept. Since providing an N-electron continuous measure similar to ELI or $-\nabla^2\rho$ is impractical, to say the least, we approach the problem from a more restricted perspective, by

locating the maxima of the full Born probability. This point of view has been advocated by several authors, starting with Artmann and Zimmerman [20, 21], who were followed by Savin and Scemama [22], and more recently by Lüchow and Schmidt, among others [23–27]. In this sense we locate the maximum of $|\Psi|^2$ for the ground state of atoms Li through Kr, and compare it to the above-mentioned measures. It is known that the position of the N electrons at the $|\Psi|^2$ maxima beautifully uncovers, as close to the chemist's language as possible, the Lewis structure in molecules [28], and we feel that this research program must be expanded in the near future. Since our aim is to show what qualitatively new insights can be learnt from this perspective, we do not push the theoretical level to the limit. In so doing, we also avoid possible criticisms regarding the meaning of ELF or LOL at high levels of theory. The maxima of $|\Psi|^2$ have been traditionally obtained from quantum Monte Carlo calculations, for walkers are already $3N$-dimensional objects, and we have also done so here. Thus, we have computed single-determinant wavefunctions for ^1S states, or the simplest symmetry-adapted configuration state functions (CSFs) for open-shell states, and found the location of the N spin-spatial coordinates of the electrons that maximize $|\Psi|^2$ through variational Monte Carlo (VMC) runs. These maxima are compared with those provided by ELF, LOL, and $-\nabla^2\rho$. Finally, we also examine how the shell structure revealed by Born probabilities is preserved in a set of simple molecules, also comparing with other localization measures.

II. METHODOLOGICAL AND COMPUTATIONAL DETAILS

Given the variability of the position of the atomic shell maxima or the shell electron counts offered by different descriptors, we do not pursue quantitative results in this work. On the contrary, we use a well-defined mean-field framework in which all the indices can be obtained from the same wavefunction. As briefly commented in the introduction, it is a well-known fact that high levels of theory, extended basis sets, and even inclusion of relativistic effects, have a minor impact on any of the ELF, LOL, or $-\nabla^2\rho$ images.

We have obtained closed-shell Hartree-Fock wavefunctions in the case of ^{1}S states, and symmetry-adapted intra-shell complete active space (CAS) ones in the case of open-shells, for the ground states of atoms Li-Kr, as well as for a set of closed-shell molecules with GAMESS [29], using the cc-pVDZ basis set. This is a minimal setup that suffices our purposes. LOL, ELF, and the Laplacian of the density have been readily obtained through the PROMOLDEN code [30].

Once these wavefunctions were obtained, pure variational quantum Monte Carlo calculations that must reproduce their Hartree-Fock energies were performed with AMOLQC [31]. Details can be found in the Supporting Information (SI, section 1). During the course of each VMC run, a detour to a minimization of $-\log(|\Psi|^2)$ was performed at equally spaced steps of the sampling procedure, using a combination of steepest descent and L-BFGS minimization algorithms [31]. This provides a set of maxima which are appropriately ordered. Although multiple non-equivalent chemically important maxima of $\Psi|^2$ are usually found in molecules, this is not usually the case in atoms, and we report here only the global ones unless explicitly stated.

In the absence of Coulomb correlation, opposite spin electrons are statistically independent for a single-determinant wavefunction. This means that the Born probability for such a model is the product of α and β components, a fact that gives rise to a non-physical maxima degeneracy related to the free rigid rotation of the α set of electrons with respect to the β one and vice versa. The introduction of Coulomb correlation lifts this degeneracy, although it is known that extensive configuration mixing is needed to achieve the final electron distribution. For instance, since Fermi correlation is far more intense than opposite-spin correlation, the maximum of $|\Psi|^2$ for a restricted single determinant built from four equivalent α sp^3 spinorbitals and its four β counterparts puts the α or β set two equivalent regular tetrahedra, both rotating freely around the nucleus. These two interpenetrated tetrahedra acquire a cubical disposition that minimizes the overall electron repulsion when correlation is accounted for. Interestingly, it is relatively easy to obtain qualitatively correct electron distributions with VMC by optimizing the parameters of a Jastrow factor starting from a HF determinant, so that $\Psi = e^U\Phi$, Φ being a single determinant or one of our minimal CSFs. In the last expression, the Jastrow factor is $J = e^U$ and U is expanded in terms of explicit interelectron, or electron-nucleus coordinates. In order to check the effect of $\alpha - \beta$ separation on the shell structure provided by the maximization of $|\Psi|^2$, we have also obtained the maxima of HF+J functions. Details of the specific Jastrows used in this work are found in the SI.

III. THE EFFECT OF LEAVING THE ONE- OR TWO-PARTICLE FRAMEWORK

As stated, one of our main goals in this work is to understand the effect that considering the true N-electron distribution, and not the images provided by compacted one- or two-electron projections, has on the atomic shell structure. The H and He atoms, which fill the K shell, are not

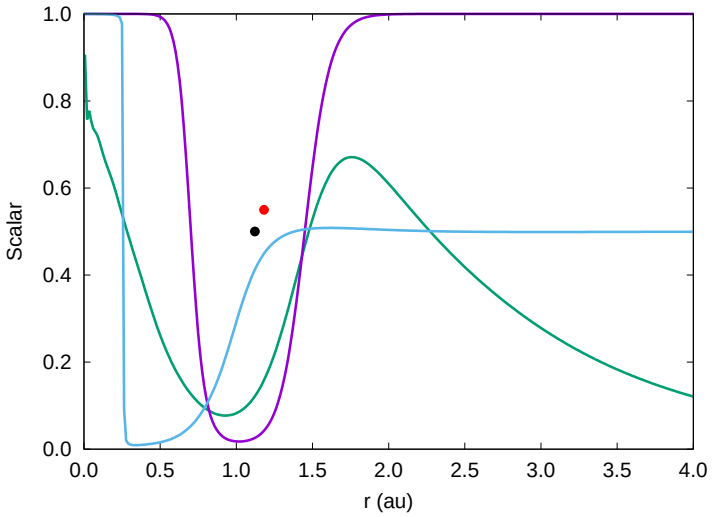

FIG. 1: ELF (purple), LOL (green), and L (cyan, plotted as $\arctan(L)/\pi + 1/2$) for the HF/cc-pVDZ ground state of Be. The black and red dots mark the distance at which the electrons of shell L lie at the maximum of $|\Psi|^2$ for the HF and the HF+J calculations, respectively.

considered, since no shell transition exists. We simply notice that in both cases, the maximum Born probability is obtained when the electron(s) are located at the nucleus, and that the existence of two opposite spin electrons (the K or $1s^2$ core) at the nucleus is maintained unaltered in all the other atoms examined. Similarly, $L = -\nabla^2\rho$ diverges to infinity at the nucleus. Notice the different meaning of L (the $n = 2$ shell) and L (minus the Laplacian of the density).

Lithium and Beryllium are the first two relevant systems to examine. Both have outermost s electrons, so that the ELF does not decay to zero at large distances, displaying just an intershell minimum, and tending asymptotically to one after it. LOL displays a K-L intershell minimum and an L maximum, decaying to zero, and L shows the well-known low-Z behavior with one maximum/minimum pair per shell. Data can be found in Table S1. Let us concentrate on Be, with HF determinant $\Psi = |1s\bar{1}s2s\bar{2}s|$. The ELF minimum is located at $r = 1.02$ au, while the LOL minimum/maximum lie at $r = 0.93$ and $r = 1.76$ au, respectively. The maximum/minimum pairs of the K and L shells for $-\nabla^2\rho$ are located at $r = 0.0, 0.23, 1.62$, and 3.0 au, respectively. The critical points of LOL are found to occur at smaller distances than their ELF equivalents (see Fig. S1). The behavior of all these scalars can be found in Fig. 1.

In order to understand how Fermi and Coulomb correlation determines the location of the maxima of Ψ^2, let us take the HF determinant and build the α (for instance) two-electron probability

distribution. This turns out to be

$$p^{\alpha} \approx (\phi_{1s}(\boldsymbol{r}_1)\phi_{2s}(\boldsymbol{r}_2) - \phi_{2s}(\boldsymbol{r}_1)\phi_{1s}(\boldsymbol{r}_2))^2, \tag{1}$$

where a normalization factor has been dropped. An obviously equivalent expression exists for the β block. The complete four electron probability density is simply its product. An obvious Fermi exclusion avoids the two same spin electrons from occupying the same position in space. Now, the location of the maximum of this two electron distribution is easily understood. Given the dominance of the ϕ_{1s} function, the maximum localizes either of the two electrons at the nucleus. The other is found at the r distance that maximizes

$$(\phi_{1s}(0)\phi_{2s}(r) - \phi_{2s}(0)\phi_{1s}(r))^2. \tag{2}$$

This very simple result shows that in the absence of the 1s electrons, the L shell probability maximum in Be would obviously appear at the position of the secondary maximum of $|\phi_{2s}|^2$. However, the presence of the same spin 1s electron interferes non-negligibly with this naïve image. From Eq. 2, it is clear that the second term of the sum decreases that distance, since the 1s function is more compact than the 2s one. Fig. 2 shows this effect pictorially. Since the β distribution is equivalent to the α one, the HF Born probability is thus maximum when two electrons (the K shell) are located at the nucleus and the other two (the L shell) at $r = 1.17$ au. These Born shells do have exactly the number of electrons dictated by the Aufbau filling rule. Notice that the L maximum of the 2s orbital is found at $r = 1.36$ au in this approximation, so that the 1s-2s interference effect is very relevant. Excluding ELF, which does not have an appropriate valence maximum, the sequence of positions of the LOL, L, and Born valence maxima are 1.76, 1.62, and 1.17 au, respectively, showing a considerable variability. Moreover, since at this level of theory the Laplacian is orbital-additive, one can also learn about the origin of all these discrepancies by dissecting the behavior of L into orbital contributions. $-\nabla^2\phi_{1s}^2$ diverges at the nucleus (although in the present gaussian primitive function approximation it gets only very large in its neighborhood) and displays a negative minimum at about 0.34 au, decaying to zero afterwards. In the case of $-\nabla^2\phi_{2s}^2$, a much shallower minimum appears at 0.33 au, followed by a positive maximum at 1.16 au. We stress that this outermost maximum of L for the 2s density appears at a substantially smaller distance than the maximum of the total electron density itself, at 1.36 au (see. Fig. 2). This is the result of the 3D nature of the Laplacian, which for a spherical density reads $\nabla^2\rho(r) = \rho''(r) - 2\rho'(r)/r$. When both the 1s and 2s contributions are added, the tail of the 1s L term moves the 2s L maximum to

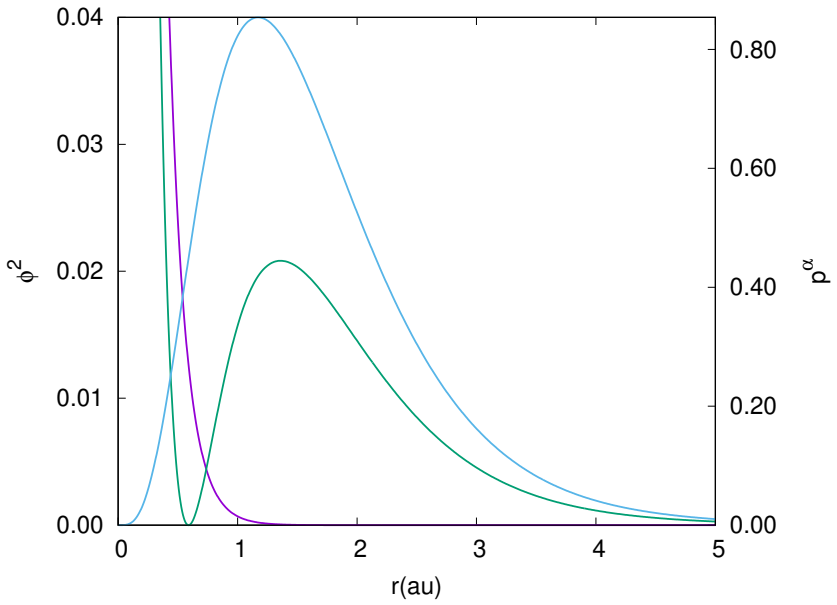

FIG. 2: $|\phi|^2$ (scaled to one at the nucleus) for the 1s (purple) and 2s (green) HF/cc-pVDZ orbitals of Be. The cyan curve (right *y* axis) depicts the behavior of Eq. 2.

its final position at 1.62 au. Interestingly, the 2s L maximum appears rather close to the maximum of the Born probability. A similar dissection can be performed if the ELF is computed from $1s^2$ or $2s^2$ determinants alone. In both cases ELF is constantly equal to one, and only when the 1s-2s interference is accounted for, the intershell minimum appears.

Introduction of Coulomb correlation via optimization of a simple Jastrow factor on top of the cc-pVDZ HF calculation leads to a decrease in the energy from -14.572 to -14.628 au, see Table S2. Now all the equivalent Born maxima display two opposite spin valence electrons with correlated positions, at a distance from the nucleus $r = 1.20$ au, on the surface of a nucleus-centered sphere, and at the two extremes of any of its diameters (see Fig. 3). This result is physically sensible, for Coulomb correlation should decrease the opposite spin interelectron repulsion. In a pattern that is repeated in many of our following examples, the distance at which Born shells appear are close to the intershell minima of the ELF. Since both L and the ELF have been widely used, care must be taken regarding to the meaning of these indices.

The B atom serves to introduce another interesting effect. The simplest single-determinant function of its $M_L = 0, M_S = 1/2$, ^{2}P ground state is $\Psi = |1s\bar{1}s2s\bar{2}s2p_0|$. Now the minority spin block is equivalent to that in Be, but the majority one has three electrons. Using the same arguments as in the previous paragraphs, at the HF level, the first of the two β electrons will occupy

the nucleus in the Born maximum probability distribution, and the second will appear at a distance from it, affected from the 1s-2s interference. To understand the distribution of the three α electrons, a generalization of Eq. 2 is immediately proposed, this times with six terms and, let us say, electron one at the nucleus. It is easy to show that p^{α} is maximized when the three electrons are equidistant along a line, with the central electron at the nucleus. This minimizes the Fermi repulsion of the two outside-of-nucleus electrons. Since the outermost maximum of the 2p density is slightly more internal than that of the 2s one, now the interference that occurs among the 1s, 2s, and 2p functions simultaneously leads to slightly smaller distances when we mix 1s,2s, and 2p than when only the 1s and 2s functions are involved. Thus, in the Born maximum, the majority spin electrons are slightly closer to the nucleus than the minority spin one. This argument is of rather general validity. In the cc-pVDZ function, these two distances are 0.82 and 0.84 au. Now, the ELF decays to zero at large distances, displaying a valence maximum. Similar to Be, the valence maxima occur at 1.40, 1.36, and 1.27 au for the ELF, LOL, and L, respectively, so that the shrinking on going from ELF to Born probabilities is again rather obvious. For the sake of completeness, the valence maxima of the 2s and 2p densities lie at 1.02 and 0.65 au, respectively.

Optimization of a Jastrow factor induces a separation of opposite spin electrons. As known since the times of Linnett [32], Fermi exclusion is much more intense than Coulomb's, so that we expect a reasonably triangular disposition of electrons with a larger α-nucleus-α than α-nucleus-β angle, coupled to a slight overall expansion. This is exactly what is found, and the HF+J Born maxima display the three valence electrons at the vertices of a close to equilateral triangle centered at the nucleus, with nucleus to vertex distances equal to 0.88 (α) and 0.89 (β) au, and α-nucleus-α and α-nucleus-β angles of 137 and 111 degrees, respectively. Although the proximity of these insights to Linnett's theory has already been put forward [23, 24], we stress that the geometry of the valence same-spin electron blocks is rather rigid, and that the effect of Coulomb correlation is considerably more subtle, so that rotations of the mutually interpenetrated blocks is relatively easy.

These arguments are rather robust. For instance, in ^{3}P carbon, we expect a valence equilateral triangle of majority spin electrons Coulomb interacting with a single minority spin one. This leads to a distorted tetrahedron, with again two different distances. Similarly, in ^{4}S nitrogen an almost regular tetrahedron of majority spin electrons is capped by a minority spin companion, which is situated over one face to form an overall slightly distorted triangular bipyramid. Actually, a simple force field differentiating same-spin from opposite-spin repulsions is able to reproduce

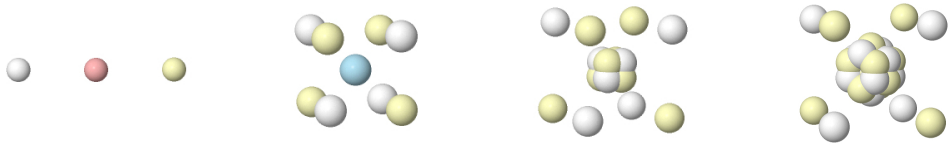

FIG. 3: Pictorial representation of the position of electrons (spins labeled by color) at the Born maximum for the ground states of Be, Ne, Ar, Kr as obtained from VQMC HF+J/cc-pVDZ calculations. The two K electrons at the nucleus are not shown. Subfigures are not drawn on the same scale.

remarkably well all these arrangements, showing that the minimization of electron repulsion can indeed be used as a simple didactic proxy (see the work by Luder, Ref. 33).

IV. SHELL STRUCTURE FROM BORN PROBABILITIES

Once the basic framework has been presented, we shift to the general picture that emanates from it. As it comes out, the maxima of the Born probability density show an extremely clear structure of electrons in quasi-spherical shells for a given principal quantum number n. Same spin electron blocks in a given shell minimize their Fermi repulsion as much as possible separately, and then these quasi-rigid opposite spin blocks can be seen to rotate with respect to each other to minimize their Coulomb repulsion. Given the present capabilities of the AMOLQC code, we have not attempted to include f electrons in our semi-quantitative discussion, and only atoms up to Kr are considered. HF+J data are presented in Table I, while Born Hartree-Fock data as well as ELF, LOL, and L ones can be found in Table S1.

Fig. 3 displays the structure of the Born probability maxima for Be, Ne, Ar, and Kr. This allows us to see the evolution of the electron arrangement as s, s+p, and s+p+d subshells are sequentially filled. Also, since we want to focus on the ability of Born maxima to show the atomic shell structure, we do not examine in detail all the geometrical arrangements found. This will be done in future works.

In agreement with the above-mentioned rules guided by the minimization of electron repulsions and, as it is well known, filling the s+p shell with two sets of four same-spin electrons leads to Linnett's double quartet: two interpenetrated tetrahedra that minimize their mutual repulsion when forming a regular cube centered at the nucleus that rotates freely in space. Distances for the L shells

in Ne and Ar are 0.370 and 0.162 au, respectively, and 0.887 au for the M shell of Ar, for instance (see Table S1). All the eight valence electrons of Ne are obviously found at the same distance from the nucleus. This is a particularly striking example of how the one-electron orbital picture can lead to biased intuitions. Although one-electron excitations (i.e. spectroscopic knowledge) are best understood with an orbital formalism in which 2s and 2p electrons play different roles, the spatial distribution of electrons, thus probably much of chemical reactivity, is probably better rationalized using other theoretical frameworks. Adding the 3s and 3p subshells in Ar allows us to clearly recognize how concentric shells are built. In Fig. 3, the K core of Ar has two electrons at the nucleus, the 2s+2p shell forms a cubic outer core, and finally the 3s+3p electrons form another cube at a clearly different distance. The principal quantum number determines the radius of the shell. Notice again that much finer information can be obtained from these maxima, e.g. it is clear from Figure 3 that the outer core is oriented (polarized) with respect to the valence, and that a complete alternation of α and β electron can also be distinguished. We do not pursue in this work extracting and analyzing this information any further.

Most interestingly, Kr shows how the s+p+d 18 electron filling occurs. Now the M shell includes the ten 3d electrons, and a quite globular distribution which is basically alien to the average chemist is found. There are nine same spin electrons that occupy the vertices of a tricapped trigonal prism, which is formed by three layers of staggered equilateral triangles. This is exactly the geometry expected for nine electron pairs in the VSEPR model, found for instance in the ReH_9^{2-} anion. The opposite electron block occupies an equivalent prism in such a way that three layers of regular hexagons in which all vertices alternate α and β electrons form the eighteen electron shell. Although all these electrons are not found at exactly the same distances from the nucleus, they are basically situated on the surface of a sphere. Out of the 3s+3p+3d shell, and at a larger distance, the 4s+4p octet forms another cubic onion shell. Much as in the case of Ne or Ar, it is relevant to stress that the eighteen M electrons form a compact shell that does not discriminate s from p or d, contrarily to what is done coventionally in transition metal chemistry. A depiction of the nine electron spin block polyhedron as well as of the interpenetration of the two opposite spin polyhedra to form the 18 electron distribution is found in Fig. 4.

We think that this spatial image should be particularly appealing to the chemist, providing a conceptual framework in which cores and valences are visually identified at a glance. The shell structure provided by the maximization of Born probabilities has obviously no counting problems. The number of electrons of each shell is an integer, that exactly coincides with that of the Aufbau

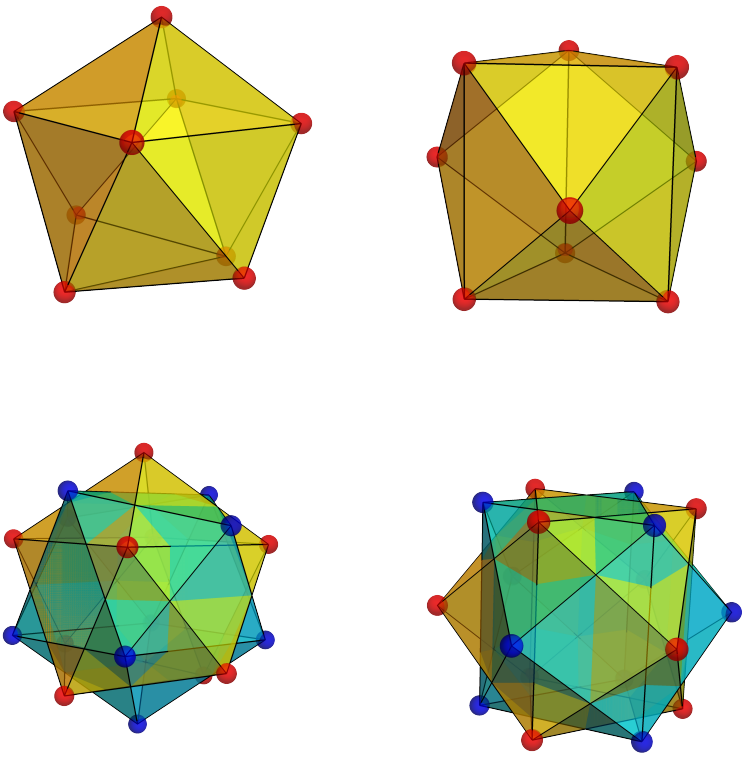

FIG. 4: Top: two views of the tricapped triangular prism (or monocapped square antiprism) distribution of the 9 electrons of a spin block in the 18 electrons M shell. The right panel shows the three layers of staggered equiliateral triangles. Bottom: Idem for the interpenetration of two of the above polyhedra to form the full M shell. The left panels allows to visualize how the two polyhedra (reddish and blueish) interpenetrate each other. The right one displays the layered disposition of the eighteen electrons in three paralell staggered layers of regular hexagons.

rule.

V. BORN SHELLS VERSUS ELF/LOL/LAPLACIAN SHELLS

We show very briefly in this section how the distances at which shell maxima occur for our selected ELF/LOL/L descriptors compare to those found from maximizing Born probabilities. Data are found in Tables I and S1, and a set of pictures equivalent to Fig. 1 for all the systems can be found in Fig. S1.

First, a general comment on ELF/LOL/L. In a given row, all of these indices show the expected

TABLE I: Atomic shell radii from Born probabilities for atoms H to Kr from Jastrow optimized Hartree-Fock (or intra-shell CASSCF in the case of open shells) cc-pVDZ calculations. For representative elements, underlined values correspond to the majority spin block for each shell, while not underlined ones reveal minority spin blocks. If the M shell contains d electrons, several distances appear which are summarized as a range. Pure HF maxima can also be be found in Table S1. Notice that the K shell electrons lie at the nuclear position.

System	L	M	System	L	M	N
H (^{2}S)	-		K (^{2}S)	0.146	0.792	2.207
He (^{1}S)	-		Ca (^{1}S)	0.144	0.762	2.584
Li (^{2}S)	1.755		Sc (^{2}D)	0.127	0.71-0.76	2.009 /2.014
Be (^{1}S)	1.182		Ti (^{3}F)	0.127	0.60-0.64	2.050 /2.056
B (^{2}P)	0.884/ 0.886		V (^{4}F)	0.118	0.52-0.60	1.710 /1.729
C (^{3}P)	0.663/ 0.699		Cr (^{7}S)	0.115	0.50-0.57	1.994
N (^{4}S)	0.545/ 0.587		Mn (^{6}S)	0.110	0.50-0.57	2.128 /2.144
O (^{3}P)	0.469/ 0.490		Fe (^{5}D)	0.104	0.43-0.51	1.621 /1.629
F (^{2}P)	0.392/ 0.401		Co (^{4}F)	0.100	0.41-0.48	1.683 /1.694
Ne (^{1}S)	0.370		Ni (^{3}F)	0.096	0.39-0.47	1.552 /1.554
Na (^{2}S)	0.311	2.087	Cu (^{2}S)	0.093	0.41-0.48	1.726
Mg (^{1}S)	0.276	1.712	Zn (^{1}S)	0.094	0.39-0.45	1.204
Al (^{2}P)	0.246	1.413/1.572	Ga (^{2}P	0.085	0.32-0.37	1.224 /1.272
Si (^{3}P)	0.222	1.218/1.371	Ge (^{3}P)	0.080	0.30-0.34	1.196 /1.230
P (^{4}S)	0.208	1.095/1.225	As (^{4}S)	0.077	0.28-0.33	1.090 /1.141
S (^{3}P)	0.188	1.040/1.071	Se (^{3}P)	0.075	0.27-0.32	1.083 /1.095
Cl (^{2}P)	0.175	0.959/0.966	Br (^{2}P)	0.072	0.26-0.31	1.050 /1.058
Ar (^{1}S)	0.162	0.887	Kr (^{1}S)	0.070	0.25-0.30	1.054

periodic behavior, displaying a shrinking of the effective atomic volumes as we increase the atomic number until we fill the noble gas configuration. Both LOL and L decay to zero at large distance while, as commented, the asymptotics of ELF depends on the s/not-s character of the last occupied subshell. In general, the distance at which shell maxima (and intershell minima) occur follow the sequence ELF>LOL>L. As it is well known, the Laplacian does not show the correct number

of shells past calcium for the transition metals, but the ELF maintains the appropriate number of intershell minima, and LOL displays also a number of maxima equal to the largest principal quantum number. The reasons for those behaviors have been widely studied. Fig. S1 also shows that transition metals with a $4s^1$ configuration, like Cr and Cu, show particularly shallow last shell LOL maxima, and specific ELF profiles.

As Born shells are regarded, Table S1 and Fig. S1 uncover that, in general, the introduction of Coulomb correlation by optimizing a simple Jastrow factor on top of a HF calculation increases slightly the interelectron distances, as expected from physical grounds. This translates into a concomitant swelling of the atomic shells. As a general rule, Born shells appear at the smallest distance from the nucleus out of all of the descriptors examined here. In our opinion, this is an important result that forces us to reconsider the quantitative role of indices based on one- or two-particle densities. Shifting from a one-particle, additive descriptor as the Laplacian, to an N-electron one like the Born probability leads to multi-electron interference phenomena which are not obvious from the one-particle case.

As a matter of fact, from Fig. S1 it stands out that the Born shell radii lie always close to the ELF or LOL intershell minima, and that if they correlate with any shell maxima, it is with those of the L function. This is not surprising, since the Laplacian measures pure spatial charge concentration/depletion, while ELF or LOL are mainly built from Pauli exclusion information, but the correspondence with ELF minima is striking. Shells built from different number of majority and minority spin electrons, as well as the M shells of transition metals that are filling the 3d subshell have electrons at slightly different distances from the nucleus. This variability is easy to follow in Fig. S1, being particularly large in groups 13-15.

VI. PERSISTENCE OF THE SHELL STRUCTURE IN MOLECULES

Molecular formation has a deep impact on valence electrons. After all, this is what Chemistry is about. As commented, most shell structure descriptors have been successfully used as chemical bonding indicators. With the aforementioned limitations in the case of heavy atoms, it was soon found that the Laplacian is able to display local valence maxima along bonds (the so-called bonded valence shell charge concentrations, bonded VSCCs) as well as along non-bonded directions (non-bonded VSCCs). These VSCCs correspond rather faithfully with the distribution of electron pairs predicted by the VSEPR model [34]. Similarly, the success of the ELF was very clearly based on

its ability to locate bonds as local ELF concentrations. Moreover, the peculiar topologies of these concentrations easily distinguish single bonds, that show a local maximum along the bond axis, from double, with two dumbbel-like maxima orthogonal to the bond axis, and triple bonds, which display toroidal concentrations around the bond direction in simple organic molecules. Lone pairs, also visible as local maxima, appear at their expected chemical positions. Using tools borrowed from the Quantum Theory of Atoms in Molecules (QTAIM) [2], each local maximum of any scalar can be linked to the attraction basin of its associated gradient field. Doing so, an electron population can be obtained by integrating the electron density over these 3D regions. In the case of the ELF, the population of cores and lone pair basins was shown to be close to two, and those of bonded basin around two in the case of single bonds and larger than two, although sometimes not exactly an integer multiple of this figure, in the case of multiple bonds. The population of Laplacian basins, on the contrary, does not correlate well with the expected number of electrons. In the same vein, the LOL was also shown [35] to display local maxima for covalent links between the bound centers and to distinguish also easily lone pairs, and in the case of the ELI [16], the match between the expected and computed basin populations is even better.

The ELF, LOL, and ELI fields, for instance, tend to be homeomorphic among themselves, but typically not with the Laplacian field which, as already evidenced in atoms, does not resolve all the shells and displays a minimum/maximum pair, instead of just one maximum critical point, per shell. Thus it is instructive to examine how the behavior of the N-electron Born probability compares with them, paying particular attention to the redistribution of the valence electrons. To that end, we take a few very simple molecules, methane, ethane, ammonia, water and hydrogen fluoride, and compute, at the same HF/cc-pVDZ level used for bare atoms before, their Laplacian and ELF fields to compare them to the global maxima of $|\Psi|^2$. LOL provides no qualitatively new insights over ELF, and we will just examine it in selected cases. To avoid the statistical independence of opposite-spin electrons at the HF level, only HF+J (see the SI for details) data will be reported. Again, this semi-quantitative level of theory suffices our purposes.

The Born probability maxima of simple organics and second-row hydrides have already been reported [22–24]. Although it is not the focus of this paper, it is important to recall here that several non-equivalent maxima (after permutational and spin related symmetries have been accounted for) are usually found in molecules which are immediately interpreted as different Lewis, or valence bond, electron arrangements. For instance, in LiH, the largest probability maximum places two electrons at the Li and H nuclei, the ionic Li^+H^- structure, while another lower probability local

maximum places only one electron at the H nucleus while the other three surround the Li one, thus corresponding to a neutral Li·H· structure. Ionic structures dominate the Born maxima of LiH, BeH_2, and BH_3. Since we want to consider the possible persistence of the shell structure of the neutral atoms reported, we skip these examples, and start with CH_4, dominated by a neutral Born maximum. This situation is maintained up to hydrogen fluoride. We also consider ethane, where a bond in which none of the atoms is H exists.

A. Methane and Ethane

We examine methane first. Since we want to determine the origin of the differences exhibited by shell structure descriptors based on the density, Fermi, and the full wavefunction, we have also obtained a set of localized orbitals that reconstruct the Hartree-Fock determinant. We have chosen a real space based localization procedure already described [36], that builds a set of localized orbitals from a pre-existing QTAIM partition of the total electron density of a system. This localization is useful in our real space context, but the results that follow are equally valid if a natural bond orbital (NBO) [37] perspective or any other single-determinant localization technique, like those of Ruedenberg or Pipel-Mezey [38, 39], are used instead. In this way, the five canonical orbitals of CH_4 are substituted by a 1s-like carbon core and four equivalent sp^3-like bond orbitals. Since (i) LOL is built to be large in regions where a single orbital dominates the wavefunction, and (ii) Savin has shown [40] that for well-localized orbitals the basins of ELF correspond to domains for which the probability of finding a pair of electrons is maximal, we expect that in each of the C-H bonding regions all the shell-structure descriptors should be related to their associated localized bond orbital.

Fig. 5 summarizes the results of such analysis. Starting from the C nucleus, it is very clear how the electron density in any of the equivalent C-H internuclear regions is dominated by the core function, ϕ_c, until about 0.5 au, to become completely determined by the bond orbital ϕ_b afterwards. Interestingly, the C-H bond critical point is almost solely dictated by ϕ_b, corroborating that past the core region, the C-H bonding domain is well described by a single orbital. Consideration of the detailed behavior of ELF, LOL, and L provides interesting insights. As the external C-H regions are dominated by s functions, ELF tends to one at large distances, so that its profile shows a single intershell minimum, located at 0.56 au from the C nucleus. LOL, in its turn, displays a richer structure, with a minimum at 0.51 au and a maximum at 1.68 au. (0.36 au away from the

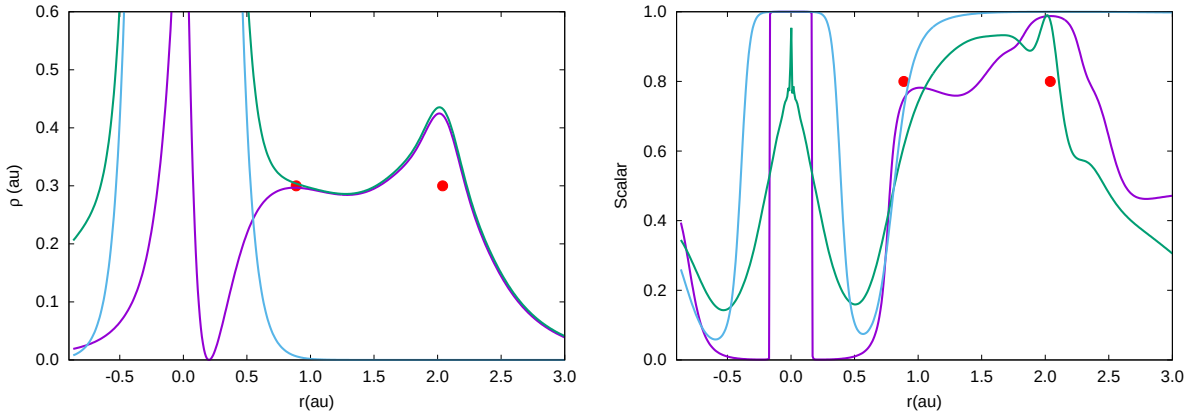

FIG. 5: Left panel: Electron densities along the C-H direction in methane, computed at the HF/cc-pVDZ level, dissected into core (c) and bond (b) contributions. Total ρ in green, ϕ_c^2 in cyan, and ϕ_b^2 in purple. The C atom is located at $r = 0.0$ and the H nucleus at $r = 2.04$ au. The position of the two electrons of the HF+J Born maximum along the C-H axis is marked by two red dots. Right panel: profiles of LOL (green), ELF (cyan), and $\arctan(-\nabla^2\rho)/\pi + 1/2$ (purple) along the same axis. All densities and distances in au.

H nucleus). The profile of $-\nabla^2\rho$ has a minimum at 0.225 au, developing a maximum at 1.015 au from the C atom. As in isolated atoms, the distances at which the critical points of these descriptors appear satisfy the same ordering, with ELF>LOL>L, being rather close to the values found in Table I. On top of this scenario, the HF+J Born probability maximum displays a neutral Lewis structure with the expected K shell of C with two opposite electrons at the nuclear position, one electron at each of the H nuclei, and a tetrahedral arrangement of four valence electrons along the C-H directions at 0.888 au from the C nucleus. Their positions are marked with a red dot in the Figure. Notice that this distance is again the smallest of all the others, and closer to the maximum of L than to that of ELF, just as in the bare atom.

From this point of view, not only the tetrahedral-like arrangement of the L electrons of the isolated carbon atom is maintained in the CH_4 molecule. Their distances to the C nucleus change from 0.72-0.74 au to 0.89 au, with a moderate 20% expansion expected from the attracting potential exerted by the neighboring hydrogens. As it was found in atoms, the position of the valence shell electrons at the Born maximum is close to that of the valence maximum of L, and also close to the LOL and ELF intershell minimum. The spin structure of the Born maximum, although known, requires also a comment. Three of the four C valence electrons display the same m_s value (e.g. they are α electrons), just as in the parent ^{3}P ground state of the C atom. Each of them is spin paired to the m_s value of its bond companion electron at the H nucleus. This has been found rather

general, but out of the scope of this contribution and will be published elsewhere. Notice that the *Lewis pair* corresponding to any given C-H bond is very well resolved at the Born maximum. One of its electrons is a *carbon-like* electron, while the other is a *hydrogen-like* electron. This structure is lost in ELF, while it persists in LOL and in L in this example (*vide infra*).

A relevant point regards the effect of the molecular potential, which leads to the well-known (partial) pair condensation, namely, the freezing or isolation of pairs around internuclear axes upon molecular formation [41]. In this case, the bonding region, past the C core, would be effectively dominated by the ϕ_b orbital, so the position of the electrons at the Born maximum, once the interference effects already commented are correctly taken into account, are determined by the maxima of this function. This is exactly what is found from Fig. 5. The position of the two electrons of each bond pair coincide very well with the maxima of the bond orbital.

To investigate a more general bonding situation where the terminal atom is not a Hydrogen moiety, we have chosen the ethane molecule. Fig. 6 shows ELF, LOL, and L along the C-C axis, as well as the structure of the Born maximum. The general pattern observed is easy to understand if an approximate additivity of atomic components is assumed for the three fields. Notice that the minima of the three scalars, at 0.225, 0.511, and 0.574 au from the C atoms, respectively, have not suffered any relevant change from their situation in methane. Similarly, the maximum of L appears at 0.945 au away from each C atom, very close to its CH_4 equivalent. However, in methane the maximum of LOL appeared at 1.68 au away from the C atom, while the barely distinguishable maximum of ELF was placed over the H atom, at 2.04 au. In an additive approximation, the superposition of the LOLs and ELFs of the two C atoms 2.88 au apart would yield a unique ELF/LOL maximum at the midpoint of the C-C internuclear axis, as it is actually found. This very simple analysis is rather general. ELF and LOL do not generally resolve the electrons in the pair, while L typically does, although, for instance, in F_2 only one bonded VSCC is found. Going to the Born probability maximum, two opposite spin electrons are found along the C-C direction, lying at 0.815 au from the closest carbon, while other three lie along the C-H direction at 0.914 au. These distances evidence a smaller expansion with respect to the atomic value along the C-C bond than along the C-H one. The latter is only slighly larger than the one found in methane. We stress how well the shell structure is maintained on going from the atom to the molecule.

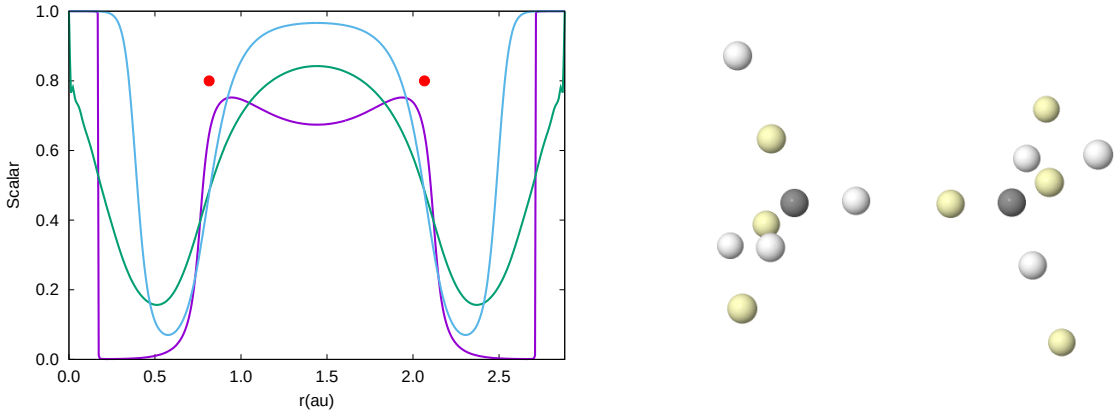

FIG. 6: Left panel: profiles of LOL (green), ELF (cyan), and $\arctan(-\nabla^2\rho)/\pi + 1/2$ (purple) along the C-C axis in HF/cc-pVDZ ethane, with C nuclei located at both ends of the abscissa. The position of the two electrons of the HF+J Born maximum along the C-C axis is marked by two red dots. Right panel: pictorial representation of the location of the electrons at the HF+J Born maximum in ethane. The grey spheres represent the C cores (with two opposite spin electrons), while the white and yellow spheres refer to different spin electrons.

B. The general picture

We now comment on the evolution of ELF, L, and the Born probability maximum in AH_n as we move from CH_4 to hydrogen fluoride. The first two descriptors have been obtained at our common HF/cc-pVDZ level. Since we want to separate appropriately spin blocks in the Born maximum, we choose the HF+J level. All the four systems display neutral (as opposed to ionic) Born maxima. As in CH_4, that we have presented in detail, ELF does not show well resolved A-H bond valence maxima, and those of LOL are either too close to the H atom maximum or non-existent. For that reason we do only consider the ELF maxima for lone pairs in some detail. Fig. 7 shows the population of the ELF valence basins and their $\eta \approx 0.9$ isosurfaces, the non-nuclear maxima of L for the four systems, as well as the position of the valence electrons at the Born maximum. Notice that in the HF molecule, and due to its cylindrical symmetry, the lone pairs appear as degenerate critical points on a ring surrounding the rear part of the F atom. As it is very clearly seen, the bonded and non-bonded (lone pair) maxima of L are found at about the same distance from the A nucleus, with the exception of the HF molecule, where the annular degeneracy forces a $(3,-1)$ critical point where the valence maximum should appear (the magenta balls in the plot). The Born maxima evince how the valence shell structure of the A atom is preserved, with

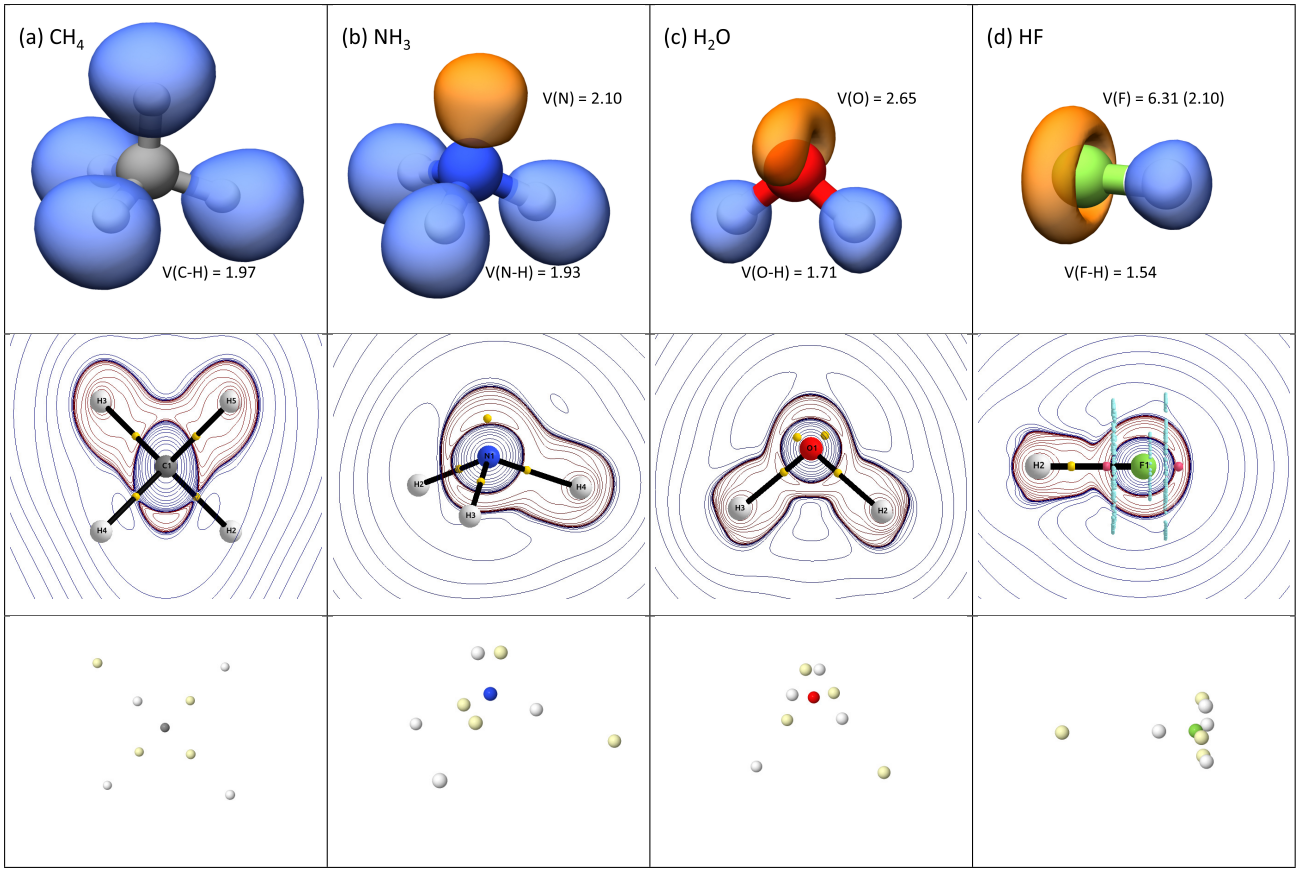

FIG. 7: Laplacian and Born probability maxima at the HF/cc-pVDZ and HF+J levels, respectively, for CH_4, NH_3, H_2O, and HF molecules. Top panels: ELF isosurfaces ($\eta \approx 0.9$) showing bond basins (in blue) as well as lone pair one (in orange). Basin populations are also shown in electrons. Middle panels: non-nuclear maxima of L, in yellow, as well as isocontours of the Laplacian on planes containing selected bonds. See the text for further information regarding the HF molecule. Bottom panels: pictorial representation of the location of the electrons at the HF+J Born maxima. The grey, blue, red, and green spheres represent the central atomic cores (holding two opposite spin electrons), while the white and yellow spheres refer to different spin electrons.

small expansions/contractions and slight rotations, when the molecules are formed. It is rather interesting to see how each of the L maxima corresponding to a lone pair is resolved into two spin-coupled separated electrons. Moreover, this separation is in a sense visible in the L field, since the isosurfaces close to the lone pair L maxima are considerably broader than in the case of the bonded ones. The Laplacian is, in a way, sensing the average lone pair electron distribution.

Table II displays the distances at which the non-nuclear (bonded and non-bonded) maxima of ELF, L and the Born probability occur. Comparison with Table I is very instructive. First we

TABLE II: Distances to the central atom at which the ELF, *L* and Born non-nuclear maxima appear in the CH_4, NH_3, H_2O, and HF molecules at the HF/cc-pVDZ or HF+J levels. the n and b labels refer to the bonded and non-boded (lone pair) cases. The asterisks in HF indicate that the critical points are degenerate (see the text for further details). Since majority/minority spin blocks at the Born maximum lie at slightly different distances from the central atom, their oscillation in the last digit is shown in parenthesis. All data in au.

Descriptor	CH_4	NH_3	H_2O	HF
ELF (n)	-	1.737	1.129	0.953
L (b)	0.962	0.795	0.683	0.597*
L (n)	-	0.717	0.618	0.545*
Born (b)	0.888	0.681(2)	0.555	0.476
Born (n)	-	0.581(5)	0.503(8)	0.439(9)

notice that the position of the non-bonded ELF maxima is the descriptor that correlates worst with its atomic equivalent. In ammonia, for instance, the ELF lone pair peaks at 1.74 au away from the N nucleus, 0.52 au farther than the valence ELF maximum in the N atom, while the LOL maximum occurs at 0.902 au, very close to the free atomic value. Fig. 8 shows how broad the ELF lone pair is, justifying this large ELF variability. The large distance at which the ELF maxima are found can also be sensed from the isosurfaces of Fig. 7. The disagreement between atomic and molecular ELF distances decreases as we evolve along the series. In hydrogen fluoride, the ELF lone pairs are at 0.95 au from the F atom, only 0.08 au more than in the isolated F atom. Notice that the non-bonded ELF maxima occur at distances larger than in the atom. This contrasts with ELF bonded ones, for instance those in the C-C bond in ethane, which lie along the internuclear axis. *L*, on the contrary, is considerably more stable. Besides methane, which has already been discussed, we find that the distances, both bonded and non-bonded, at which the molecular maxima occur are rather close to those in the atoms. Non-bonded VSCCs appear at a consistently smaller distance than bonded ones. This is the expected behavior from the VSEPR model. Finally, the Born maxima follow the wake of *L*, displaying even slightly more stable geometries with respect to their isolated atomic equivalent. Again, bonded maxima occur at systematically larger distances than non-bonded ones, as expected from molecular potential arguments (*vide supra*).

The results here reported are rather general, and a detailed account in a comprehensive set of

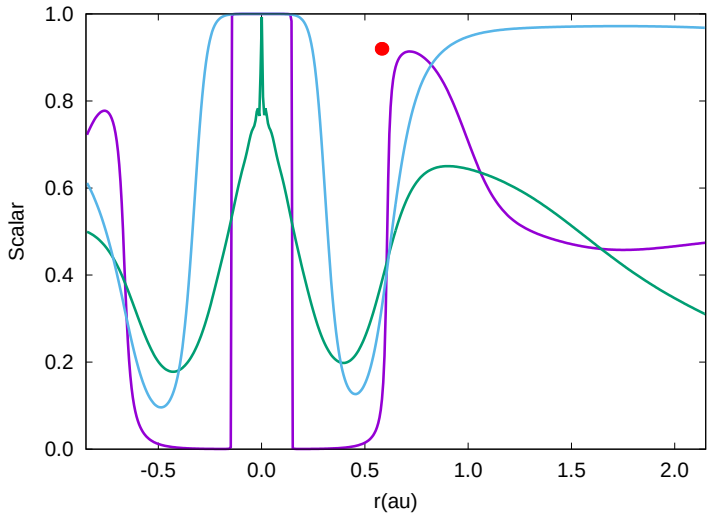

FIG. 8: Profiles of LOL (green), ELF (cyan), and $\arctan(-\nabla^2\rho)/\pi + 1/2$ (purple) along the C_{3v} axis in HF/cc-pVDZ ammonia, with the N nucleus located at $r = 0$ and the lone pair along the positive r axis. The distance of the center of mass of the two electrons of the HF+J Born maximum along the C_{3v} axis is marked by a red dot.

molecules spanning not only neutral but also ionic Born maxima will be published elsewhere. In the present context, we stress that the known (partial) transferability of both kinetic energy based shell structure descriptors like the ELF or the LOL when we go from the atomic to the molecular realm, as well as that of density based ones, like the Laplacian, is also found for Born probabilities. All atomic shell distances, be them intra-shell separations or shell-maxima in atoms show a general ordering ELF > LOL > L > Born which is maintained intact in the molecules here examined. Localization measures based on the curvature of the Fermi hole or on kinetic energy excesses or ratios with respect to the homogeneous electron gas place maxima at larger distances than those which use one- or multielectron spatial probability distributions. This has clear chemical implications that deserve to be explored further. Given the conceptual vicinity between the L and Born maxima, it is not unexpected that they also provide the closest results among those examined here. In many cases, L does not only resolve the position of non-bonded valence concentrations but also the valence shells of both the A and B atoms along the A-B bond direction. The latter become usually fused if either the ELF or the LOL are used. Therefore, for light atoms where L resolves all the atomic shells, this indicator becomes a computationally cheap coarse-grained alternative to Born maxima. The latter are found to be quite transferable and point towards a preservation of not only the distances at which atomic shells are found in molecules, but

to small redistributions of their 3D arrangement. This also deserves further investigation.

VII. CONCLUSIONS

Despite the success of the molecular orbital paradigm to rationalize chemical bonds, a considerable amount of work has been devoted over the years to consider orbital invariant alternatives, particularly in real space. One of the basic properties that any sensible chemical bonding descriptor must fulfill is the correct description of the shell structure of atoms and of its distortions upon molecular formation. Practically all of the many available shell structure indices rest on information about the average distribution of a representative electron or electron pair, as provided by the one- and two-particle reduced density matrices, and thus the influence of the full N-electron distribution on our picture of the atomic shell structure is still not well known. As we have shown, the $3N$-dimensional maxima of the Born probability, i.e. the square of the wavefunction, provide a means to access this kind of information, both in atoms and in molecules. Although this maximization was proposed long ago and it is being actively investigated at the moment, no direct account of its performance in providing the atomic shell structure, or of how it compares with other shell structure descriptors or provides complementary information is available.

We have obtained the Born maxima for atoms H to Kr from simple variational quantum Monte Carlo calculations and compared them to the results obtained from the Laplacian of the electron density, the electron localization function, and the localized orbital locator. Out of the four descriptors, the first two are based on direct probability distributions, while the others are related to the Fermionic behavior of electrons. We have not attempted finding the Born maximum for a 32 (s+p+d+f) electron shell yet, stopping our study at Kripton. Since our aim is comparative, a qualitative picture suffices our purposes, and single or quasi-single determinant expansions, where all the descriptors are well defined and can be obtained from the same wavefunction, have been used. In order to separate appropriately opposite spin pairs at the Born maximum, we have also optimized simple Jastrow factors that force that separation quite effectively.

We have first shown that changing from a one- to an N-particle picture leads to relevant interference effects. In a semi-analytical example, we show that Pauli exclusion leads to a measurable shrinkage of the distance at which the full probability has its maximum in comparison with that found from an orbital picture. As it is well known, Pauli-like shell descriptors like the ELF or LOL provide shell distances larger than those of density-based ones, like the Laplacian. Now we show

that Born maxima are closer to those of the minus Laplacian than to any other, providing a very clear indication that density and Pauli-based descriptors explore different spatial regions in atoms and molecules. So, although the Laplacian is unable to display the appropriate number of shells for heavy atoms, its shell distances compare well with Born maxima when this problem does not occur.

The Born maximum displays exquisitely structured shells in all the atoms examined. We show that the full 18 electron M shell corresponding to principal quantum number $n = 3$ is made of two interpenetrating polyhedra containing nine same spin electrons which vividly correspond to the tricapped trigonal prism (or monocapped square antiprism) geometry of inorganic chemistry. The number of electrons of each shell is obviously an exact integer.

As molecules form, the atomic valence shells distort considerably. Pauli-based descriptors typically reveal non-bonded concentrations such as lone pairs effortlessly, while tending to fuse the shell maxima of the two atoms involved in a bonded concentration. This tendency to fusion is much smaller in the Laplacian, that usually distinguishes the two valence shells of the two bonded atoms, and is minimized with the use of Born maxima. In cases in which a neutral maximum (without ionization) exists, the preservation of the atomic shells is rather impressive.

Summarizing, a detailed study of the position of the N electrons at the maximum of the square of the wavefunction in $Z = 1 - 36$ atoms provides an alternative shell structure descriptor which we think displays many advantages over other available indices. It takes into account, in principle, the full N electron correlations, which can lead to sizable effects. Shell distances are close to those provided by the Laplacian of the density, and tend to be substantially smaller than those of the ELF or LOL. The Born shell structure is delicately preserved in molecules.

Supplementary Material

The SM contains Methodological details regarding the electronic structure calculations, the Slater-Jastrow wavefunction, and the maximization of its square. Also plots of the ELF, LOL, L and the Born maxima for all the systems studied, including their energies, tables of the optimized Jastrow factors and coordinates of the electrons at the global Born maximum.

Acknowledgments

The authors thank the Spanish MICINN for financial support, grant PGC2018-095953-B-I00 and the FICyT, grant IDI-2021-000054. María Menéndez-Herreros specifically acknowledges the Spanish FICyT for the predoctoral grant PA-21-PF-BP20-034.

Author Declarations

Conflict of Interest

The authors have no conflicts to disclose.

Data Availability Statement

The data that support the findings of this study are available in the supporting information.

[1] B. M. Gimarc, *Molecular structure and bonding. The qualitative molecular orbital approach* (Academic Press, New York, 1979).

[2] R. F. W. Bader, *Atoms in Molecules* (Oxford University Press, Oxford, 1990).

[3] C. Gatti and P. Macchi, eds., *Modern Charge-density Analysis* (Springer, Dordrecht., 2012).

[4] S. Shaik, D. Danovich, W. Wu, and P. C. Hiberty, Nat. Chem. **1**, 443 (2009).

[5] J. L. Casals-Sainz, F. Jiménez-Grávalos, E. Francisco, and A. Martín Pendás, Chem. Commun. **55**, 5071 (2019).

[6] R. McWeeny, *Methods of Molecular Quantum Mechanics* (Academic Press, London, 1992), 2nd ed.

[7] J. Cioslowski, ed., *Many-electron densities and reduced density matrices* (Kluwer Academic Publishers, Dordrecht, 2000).

[8] J. T. Waber and D. T. Cromer, J. Chem. Phys. **42**, 4116 (1965).

[9] R. J. Boyd, Can. J. Phys. **56**, 780 (1978).

[10] A. M. Simas, R. P. Sagar, A. C. T. Ku, and V. H. S. Jr., Can. J. Chem. **66**, 1923 (1988).

[11] G. Hunter, Int. J. Quant. Chem. **29**, 197 (1986).

[12] A. D. Becke and K. E. Edgecombe, J. Chem. Phys. **92**, 5397 (1990).

[13] A. Savin, A. D. Becke, J. Flad, R. Nesper, H. Preuss, and H. G. von Schnering, Angew. Chem. Int. Ed. **30**, 409 (1991).

[14] M. Kohout and A. Savin, Int. J. Quantum Chem. **60**, 875 (1996).

[15] H. Schmider and A. Becke, J. Mol. Struct.: THEOCHEM **527**, 51 (2000).

[16] M. Kohout, Int. J. Quantum Chem. **97**, 651 (2003).

[17] J. Munárriz, M. Calatayud, and J. Contreras-García, Chem. Eur. J. **25**, 10938 (2019).

[18] R. Gillespie, *The VSEPR model of molecular geometry* (Dover Publications, Mineola, N.Y, 2012), ISBN 978-0486486154.

[19] B. Silvi and A. Savin, Nature **371**, 683 (1994).

[20] K. Artmann, Zeitschrift für Naturforschung A **1**, 426 (1946).

[21] H. K. Zimmerman and P. V. Rysselberghe, J. Chem. Phys. **17**, 598 (1949).

[22] A. Scemama, M. Caffarel, and A. Savin, J. Comput. Chem. **28**, 442 (2006).

[23] A. Lüchow, J. Comput. Chem. **35**, 854 (2014).

[24] Y. Liu, P. Kilby, T. J. Frankcombe, and T. W. Schmidt, Nat. Commun. **11**, 1210 (2020).

[25] L. Reuter and A. Lüchow, Phys. Chem. Chem. Phys. **22**, 25892 (2020).

[26] M. A. Heuer, L. Reuter, and A. Lüchow, Molecules **26**, 911 (2021).

[27] L. Reuter and A. Lüchow, Nat. Commun. **12**, 4820 (2021).

[28] G. N. Lewis, J. Am. Chem. Soc. **38**, 762 (1916).

[29] M. W. Schmidt, K. K. Baldridge, J. A. Boatz, S. T. Elbert, M. S. Gordon, J. H. Jensen, S. Koseki, N. Matsunaga, K. A. Nguyen, S. J. Su, et al., J. Comput. Chem. **14**, 1347 (1993).

[30] A. Martín Pendás and E. Francisco, promolden. A QTAIM/IQA code (Available from the authors upon request).

[31] A. Lüchow, S. Manten, C. Diedrich, A. Bande, T. C. Scott, A. Schwarz, R. Berner, R. Petz, A. Sturm, M. Hermsen, et al., amolqc (v7.1.0). Zenodo https://doi.org/10.5281/zenodo.4562745 (2021).

[32] J. W. Linnett, J. Am. Chem. Soc. **83**, 2643 (1961).

[33] W. F. Luder, J. Chem. Educ. **44**, 206 (1967).

[34] R. F. W. Bader, P. J. MacDougall, and C. D. H. Lau, J. Am. Chem. Soc. **106**, 1594 (1984).

[35] H. Jacobsen, Can. J. Chem. **86**, 695 (2008).

[36] A. Martín Pendás and E. Francisco, Phys. Chem. Chem. Phys. **20**, 21368 (2018).

[37] F. Weinhold and C. Landis, *Valency and Bonding. A Natural Bond Orbital Donor-Acceptor Perspective* (Cambridge Univ. Press, 2005).

[38] C. Edmiston and K. Ruedenberg, Rev. Mod. Phys. **35**, 457 (1963).

[39] J. Pipek and P. G. Mezey, J. Chem. Phys. **90**, 4916 (1989).

[40] A. Savin, J. Chem. Sci. **117**, 473 (2005).

[41] R. F. W. Bader and G. L. Heard, J. Chem. Phys. **111**, 8789 (1999).

Supporting Information

Atomic shell structure from Born probabilities: comparison to other shell descriptors and persistence in molecules

María Menéndez Herrero, Julen Munárriz, Evelio Francisco, and Ángel Martín Pendás*

Departamento de Química Física y Analítica. Facultad de Química. Universidad de Oviedo. 33006 Oviedo. Spain.

E-mail: ampendas@uniovi.es

Contents

1 Methodological details

1.1 Electronic structure calculations, ELF and LOL.

Provided that the aim of this work is to demonstrate how Born maxima can be used as a shell structure indicator, comparing it to other accepted indices, we have chosen as simple level of theory as possible, and all calculations have been performed at the single-determinant or subshell active space level, with the cc-pVDZ basis set. In the case of potassium, we have used the cc-pVDZ-X2C basis. Basis sets have been retrieved from the EMSL server[1]. Wavefunctions for the ground states of atoms and molecules have been obtained through the GAMESS suite[2]. All the Laplacian of the electron density, the ELF, and the LOL descriptors were obtained with the PROMOLDEN code[3] using the very same wavefunctions.

The electron localization function (ELF)[4], η, was obtained as

$$\eta = \frac{1}{1+\chi^2}, \tag{1}$$

where

$$\chi(\boldsymbol{r}) = \frac{D(\boldsymbol{r})}{D_0(\boldsymbol{r})} \tag{2}$$

is the ELF kernel as defined by Becke and Edgecombe,

$$D(\boldsymbol{r}) = \sum_i n_i |\nabla\phi_i(\boldsymbol{r})|^2 - \frac{|\nabla\rho(\boldsymbol{r})|^2}{4\rho(\boldsymbol{r})}, \tag{3}$$

where n_i is the occupation number of orbital ϕ_i and ρ is the electron density. $D_0(\boldsymbol{r}) = c_F\rho(\boldsymbol{r})^{5/3}$, with $c_F = \frac{3}{10}(3\pi^2)^{2/3}$, is the one-particle equivalent for the homogeneous electron gas.

Similarly, the localized orbital locator (LOL) scalar, $\nu(\boldsymbol{r})$, was obtained as

$$\nu(\boldsymbol{r}) = \frac{D_0(\boldsymbol{r})/t(\boldsymbol{r})}{1+(D_0(\boldsymbol{r})/t(\boldsymbol{r}))}, \tag{4}$$

where $t(\boldsymbol{r}) = \sum_i n_i|\nabla\phi_i(\boldsymbol{r})|^2$. t is the positive definite kinetic energy density[5].

1.2 The Slater-Jastrow wavefunction

An efficient and compact form of including electron correlation effects in Quantum Monte Carlo (QM) calculations is by multiplying a Slater determinant or a linear

combination of Slater determinants Φ by a Jastrow factor e^U according to Eq. 5

$$\Psi = \Phi e^U. \tag{5}$$

$\Phi = \Phi(\mathbf{r}_1, \ldots, \mathbf{r}_N)$ and U are respectively antisymmetric and symmetric functions of the cartesian coordinates of the N electrons of the system, $\mathbf{r}_1, \ldots, \mathbf{r}_N$. U is usually expressed as a linear combination of many-body terms. In this work, we will use the expression defined in Ref.[6]:

$$U = \sum_{A,i<j} U_{Aij}, \tag{6}$$

where the symbol A stands for nuclei, and i and j represent electrons. Each term U_{Aij} of Eq. 6 has the expression

$$U_{Aij} = \sum_{k}^{N(A)} \Delta(m_{kA}, n_{kA}) c_{kA} \left(\bar{r}_{iA}^{m_{kA}} \bar{r}_{jA}^{n_{kA}} + \bar{r}_{jA}^{m_{kA}} \bar{r}_{iA}^{n_{kA}} \right) \bar{r}_{ij}^{o_{kA}}. \tag{7}$$

The k sum runs over the $N(A)$ terms used to express the correlation function of atom A, where the c_{kA} are variational parameters that are optimized. The $\bar{r}$ functions represent scaled nuclear-electron and electron-electron distances, described by Eqs. 8 and 9, respectively

$$\bar{r}_{iA} = \frac{a_A r_{iA}}{1 + a_A r_{iA}}, \tag{8}$$

$$\bar{r}_{ij} = \frac{b_A r_{ij}}{1 + b_A r_{ij}}, \tag{9}$$

where r_{iA} is the distance between electron i and nucleus A, and r_{ij} the distance between electrons i and j. The parameters m_{kA}, n_{kA} and o_{kA} are integers, and the function Δ is one for $m \neq n$ and $\frac{1}{2}$ for $m = n$. Finally, a_A and b_A are optimizable parameters which in this work are taken as $a_A = b_A = 1$.

Different choices for the abovementioned N, m, n and o parameters define the Jastrow factor used. Optimized $c's$ are found in Section 5.

1.3 Optimization of the wavefunction with *Amolqc*

In this work, a Slater-Jastrow wavefunction ansatz has been used according to Eq. 5 in variational Monte Carlo (VQMC) calculations. The prefactor Φ was obtained

at the HF/cc-pVDZ level of theory using the GAMESS program[2]. This is a single Slater determinant in the case of ^1S atomic states or closed systems, and a symmetry-adapted intra-shell complete active space (CAS) linear combination of Slater determinants in the case of open-shell atoms. Thus, the non-Jastrow VQMC exact energy should replicate that of the standard electronic structure code if no other correction (e.g. a cusp correction) is applied.

The optimization of the Jastrow factors was performed through the *Amolqc* QMC code[7]. In a first step, samples of 1500 walkers were used, after which an optimization with respect to the variance of the energy was carried out. A new sample of 1500 walkers is then generated using as trial wavefunction the one containing the new parameters, which is followed by another optimization, this time with respect to the energy. The reference energies used in each case were those obtained from the HF/cc-pVDZ calculation for each system.

1.4 Search for maxima of $|\Psi|^2$

Instead of proceeding with the search of the maxima of $|\Psi|^2$, it is more efficient (and equivalent) to perform the minimization of the function $-\ln(|\Psi|^2)$. Both this minimization and the sampling of $|\Psi|^2$ to generate the $\{\mathbf{r}_i\}$ $(i = 1, \ldots, N)$ electronic distributions are also performed with the *Amolqc* program[7]. The variational Monte Carlo (VMC) method is used to sample $|\Psi|^2$ in the regions where it is large via the Metropolis-Hastings algorithm[8;9]. Then, the algorithms to perform a local minimization of $-\ln(|\Psi|^2)$ are invoked. To reduce the computational cost of these local minimizations, a combination of two methods is used. First, the steepest descent (SD) algorithm is applied and, after five steps, the code is switched to the L-BFGS algorithm[10] to avoid the well known size-step problem of SD.

2 ELF, LOL, $-\nabla^2\rho$, Born HF and HF+J maxima and minima

Table S1: Distances, in au, at which the several scalars examined in the manuscript show minima and maxima, together with Born maxima, computed at the HF and HF+J levels with the cc-pVDZ basis set (except K, see Section 1 above for more details). For ELF, $-\nabla^2\rho$, and LOL, the K shell maximum is always located at the nucleus. In the case of Born maxima, and for representative elements, underlined values correspond to the majority spin block for each shell, while not underlined ones reveal minority spin blocks. If the M shell contains d electrons, several distances appear which are summarized as a range. Notice that the K shell electrons lie at the nuclear position.

		K		L		M		N	
		r_{max}	r_{min}	r_{max}	r_{min}	r_{max}	r_{min}	r_{max}	r_{min}
Li (^{2}S)	ELF		1.600						
	$-\nabla^2\rho$		0.485	2.499	4.625				
	LOL		1.445	2.685					
	HF+J			1.755					
	HF			1.723					
Be (^{1}S)	ELF		1.018						
	$-\nabla^2\rho$		0.228	1.615	3.018				
	LOL		0.927	1.757					
	HF+J			1.182					
	HF			1.122					
B (^{2}P)	ELF		0.782	1.646					
	$-\nabla^2\rho$		0.269	1.268	2.073				
	LOL		0.712	1.357					
	HF+J			<u>0.884</u>					
				0.886					
	HF			<u>0.818</u>					
				0.842					
C (^{3}P)	ELF		0.647	1.399					
	$-\nabla^2\rho$		0.222	1.184	1.465				

	LOL	0.596	1.174	
	HF+J		<u>0.663</u>	
			0.699	
	HF		<u>0.620</u>	
			0.675	
N (^{4}S)	ELF	0.479	1.226	
	$-\nabla^2\rho$	0.189	0.754	1.559
	LOL	0.427	0.918	
	HF+J		<u>0.545</u>	
			0.587	
	HF		<u>0.492</u>	
			0.562	
O (^{3}P)	ELF	0.413	1.039	
	$-\nabla^2\rho$	0.166	0.665	1.100
	LOL	0.371	0.806	
	HF+J		<u>0.469</u>	
			0.490	
	HF		<u>0.403</u>	
			0.442	
F (^{2}P)	ELF	0.367	0.913	
	$-\nabla^2\rho$	0.147	0.605	0.857
	LOL	0.329	0.726	
	HF+J		<u>0.392</u>	
			0.401	
	HF		<u>0.344</u>	
			0.361	
Ne (^{1}S)	ELF	0.301	0.838	
	$-\nabla^2\rho$	0.133	0.488	0.844
	LOL	0.264	0.605	
	HF+J		0.370	
	HF		0.305	

Na (^{2}S)	ELF	0.264	0.740	2.245		
	$-\nabla^2\rho$	0.126	0.436	0.856	3.368	5.124
	LOL	0.235	0.536	2.026	3.617	
	HF+J		0.311		2.087	
	HF		0.262		2.069	
Mg (^{1}S)	ELF	0.235	0.655	1.666		
	$-\nabla^2\rho$	0.115	0.395	0.766	2.557	3.774
	LOL	0.205	0.475	1.536	2.697	
	HF+J		0.276		1.712	
	HF		0.236		1.648	
Al (^{2}P)	ELF	0.215	0.585	1.426	2.446	
	$-\nabla^2\rho$	0.105	0.355	0.676	2.166	2.788
	LOL	0.186	0.435	1.306	2.166	
	HF+J		0.246		1.413	
					1.572	
	HF		0.216		1.388	
					1.602	
Si (^{3}P)	ELF	0.196	0.525	1.266	2.026	
	$-\nabla^2\rho$	0.095	0.325	0.615	2.058	2.013
	LOL	0.174	0.395	1.165	1.186	
	HF+J		0.222		1.218	
					1.371	
	HF		0.199		1.210	
					1.406	
P (^{4}S)	ELF	0.175	0.465	1.036	2.006	
	$-\nabla^2\rho$	0.095	0.295	0.565	1.536	2.478
	LOL	0.156	0.355	0.956	1.646	
	HF+J		0.208		1.095	
					1.225	
	HF		0.183		1.076	
					1.228	

S (^{3}P)	ELF		0.165	0.435	0.936	1.746			
	$-\nabla^2\rho$		0.085	0.275	0.526	1.376	2.140		
	LOL		0.145	0.325	0.865	1.466			
	HF+J			0.188		1.040			
						1.071			
	HF			0.169		1.029			
						1.060			
						1.068			
Cl (^{2}P)	ELF		0.155	0.395	0.855	1.526			
	$-\nabla^2\rho$		0.075	0.255	0.485	1.246	1.816		
	LOL		0.135	0.305	0.796	1.316			
	HF+J			0.175		0.959			
						0.966			
	HF			0.157		0.937			
						0.944			
Ar (^{1}S)	ELF		0.145	0.365	0.745	1.456			
	$-\nabla^2\rho$		0.075	0.235	0.455	1.075	1.803		
	LOL		0.125	0.285	0.685	1.186			
	HF+J			0.162		0.887			
	HF			0.147		0.852			
K (^{2}S)	ELF		0.142	0.331	0.668	1.303	3.315		
	$-\nabla^2\rho$		0.074	0.222	0.412	0.993	1.573		
	LOL		0.115	0.263	0.628	1.073	3.058	4.868	
	HF+J			0.146		0.792		2.207	
	HF			0.137		0.729		2.086	
Ca (^{1}S)	ELF		0.128	0.304	0.614	1.167	2.518		
	$-\nabla^2\rho$		0.074	0.196	0.385	0.898	1.424	3.841	4.854
	LOL		0.115	0.250	0.574	0.979	2.343	3.801	
	HF+J			0.144		0.762		2.584	
	HF			0.130		0.668		2.381	
Sc (^{2}D)	ELF		0.125	0.285	0.575	1.076	2.387	6.059	

	$-\nabla^2\rho$	0.065	0.205	0.365	0.836	1.356	
	LOL	0.101	0.236	0.533	0.912	2.221	3.585
	HF+J		0.127		0.71-0.76		<u>2.009</u>
							2.014
	HF		0.123		0.59-0.63		<u>2.203</u>
							2.209
Ti (^{3}F)	ELF	0.114	0.274	0.533	1.006	2.289	7.554
	$-\nabla^2\rho$	0.061	0.182	0.344	0.777	1.126	
	LOL	0.101	0.222	0.492	0.857	2.140	3.490
	HF+J		0.127		0.60-0.64		2.050
							<u>2.056</u>
	HF		0.160		0.54-0.58		2.080
							<u>2.072</u>
V (^{4}F)	ELF	0.115	0.840	0.506	0.950	2.194	6.824
	$-\nabla^2\rho$	0.061	0.182	0.330	0.737	1.181	
	LOL	0.101	0.209	0.465	0.816	2.059	3.355
	HF+J		0.118		0.52-0.60		1.710
							<u>1.729</u>
	HF		0.111		0.48-0.60		<u>1.951</u>
							1.971
Cr (^{7}S)	ELF	0.101	0.236	0.466	0.897	2.531	5.717
	$-\nabla^2\rho$	0.061	0.169	0.304	0.695	1.128	
	LOL	0.088	0.196	0.439	0.776	2.532	3.247
	HF+J		0.115		0.50-0.57		1.994
	HF		0.105		0.45-0.52		1.903
Mn (^{6}S)	ELF	0.101	0.223	0.438	0.857	2.072	6.298
	$-\nabla^2\rho$	0.061	0.155	0.290	0.655	1.046	
	LOL	0.087	0.195	0.411	0.736	1.951	3.125
	HF+J		0.110		0.50-0.57		<u>2.128</u>
							2.144
	HF		0.101		0.41-0.50		<u>1.778</u>

							1.796
Fe (^{5}D)	ELF	0.101	0.209	0.425	0.804	2.004	5.813
	$-\nabla^2\rho$	0.047	0.155	0.277	0.614	0.992	
	LOL	0.088	0.181	0.398	0.695	1.910	2.976
	HF+J		0.104		0.43-0.51		<u>1.621</u>
							1.629
	HF		0.096		0.39-0.50		<u>1.695</u>
							1.707
Co (^{4}F)	ELF	0.088	0.207	0.397	0.776	1.951	5.462
	$-\nabla^2\rho$	0.061	0.155	0.263	0.587	0.951	
	LOL	0.075	0.169	0.371	0.666	1.870	2.869
	HF+J		0.100		0.41-0.48		<u>1.683</u>
							1.694
	HF		0.092		0.37-0.45		1.634
							<u>1.642</u>
Ni (^{3}F)	ELF	0.087	0.195	0.384	0.735	1.897	5.178
	$-\nabla^2\rho$	0.047	0.142	0.263	0.560	0.898	
	LOL	0.074	0.169	0.357	0.628	1.843	2.761
	HF+J		0.096		0.39-0.47		<u>1.552</u>
							1.554
	HF		0.088		0.35-0.41		<u>1.559</u>
							1.560
Cu (^{2}S)	ELF	0.088	0.181	0.357	0.707	2.397	9.080
	$-\nabla^2\rho$	0.047	0.142	0.250	0.533	0.871	
	LOL	0.074	0.155	0.344	0.614	2.801	3.288
	HF+J		0.093		0.41-0.48		1.726
	HF		0.084		0.33-0.39		1.622
Zn (^{1}S)	ELF	0.074	0.182	0.344	0.682	1.789	7.459
	$-\nabla^2\rho$	0.047	0.128	0.236	0.506	0.830	
	LOL	0.074	0.155	0.318	0.588	1.708	2.856
	HF+J		0.094		0.39-0.45		1.204

	HF		0.081		0.31-0.37		1.459	
Ga (^2P)	ELF	0.074	0.169	0.331	0.655	1.586	3.004	
	$-\nabla^2\rho$	0.047	0.128	0.222	0.492	0.790		
	LOL	0.074	0.142	0.304	0.561	1.492	1.951	
	HF+J		0.085		0.37-0.32		1.224	
							1.272	
	HF		0.080		0.31-0.35		1.331	
							1.483	
Ge (^{3}P)	ELF	0.074	0.169	0.317	0.628	1.505	1.938	
	$-\nabla^2\rho$	0.047	0.128	0.223	0.479	0.749		
	LOL	0.061	0.141	0.290	0.533	1.397	1.775	
	HF+J		0.080		0.30-0.34		1.196	
							1.230	
	HF		0.077		0.29-0.34		1.236	
							1.310	
As (^{4}S)	ELF	0.074	0.155	0.302	0.587	1.276	2.752	
	$-\nabla^2\rho$	0.047	0.128	0.209	0.452	0.709		
	LOL	0.060	0.142	0.276	0.506	1.195	2.005	
	HF+J		0.077		0.28-0.33		1.090	
							1.141	
	HF		0.073		0.23-0.33		1.149	
							1.278	
Se (^{3}P)	ELF	0.074	0.155	0.290	0.560	1.195	2.262	
	$-\nabla^2\rho$	0.047	0.115	0.209	0.439	0.682		
	LOL	0.061	0.128	0.277	0.479	1.127	1.802	
	HF+J		0.075		0.27-0.32		1.083	
							1.095	
	HF		0.073		0.27-0.31		1.104	
							1.174	
Br (^{2}P)	ELF	0.074	0.142	0.277	0.547	1.114	2.099	
	$-\nabla^2\rho$	0.034	0.115	0.196	0.425	0.641	1.749	2.018

	LOL	0.061	0.128	0.263	0.466	1.046	1.667	
	HF+J		0.072		0.31-0.26		1.050	
							<u>1.055</u>	
							<u>1.058</u>	
	HF		0.071		0.28-0.30		1.081	
							1.085	
							<u>1.091</u>	
							<u>1.093</u>	
Kr (^{1}S)	ELF	0.063	0.142	0.266	0.520	1.013	1.992	
	$-\nabla^2\rho$	0.182	0.115	0.196	0.398	0.614	1.478	2.113
	LOL	0.061	0.128	0.250	0.439	0.952	1.560	
	HF+J		0.070		0.25-0.30		1.054	
	HF		0.066		0.24-0.30		1.026	

3 Radial evolution of ELF, LOL, $-\nabla^2\rho$, Born HF and HF+J maxima

Fig. S1. Plots of the radial evolution of ELF (blue), LOL (orange), and L (green, plotted as $arctan(L)/\pi + 1/2$) for the ground states of the Li-Kr atoms. The grey and red dots (or ranges) mark the distances at which the electrons lie at the maximum of the square of the wavefunction for the VQMC HF and HF+J calculations, respectively. r stands for the distance with respect to the nucleus.

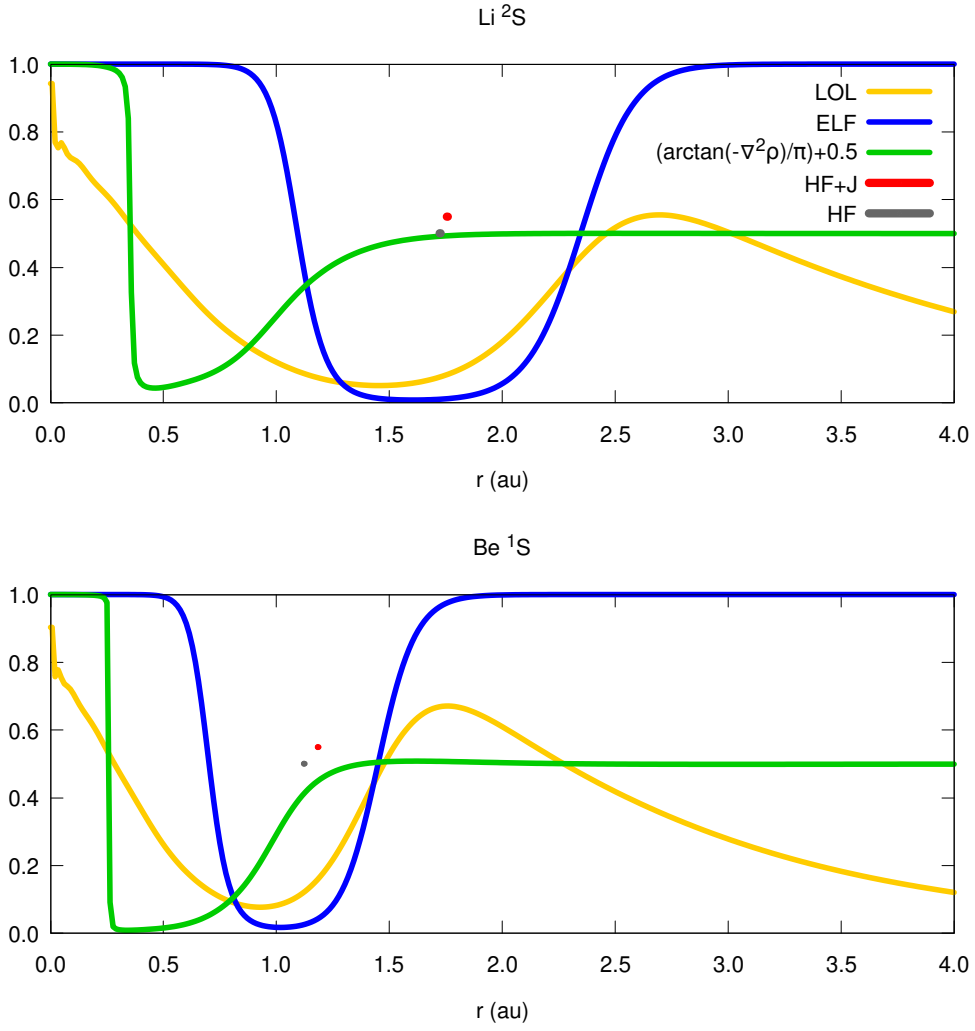

B ^{2}P

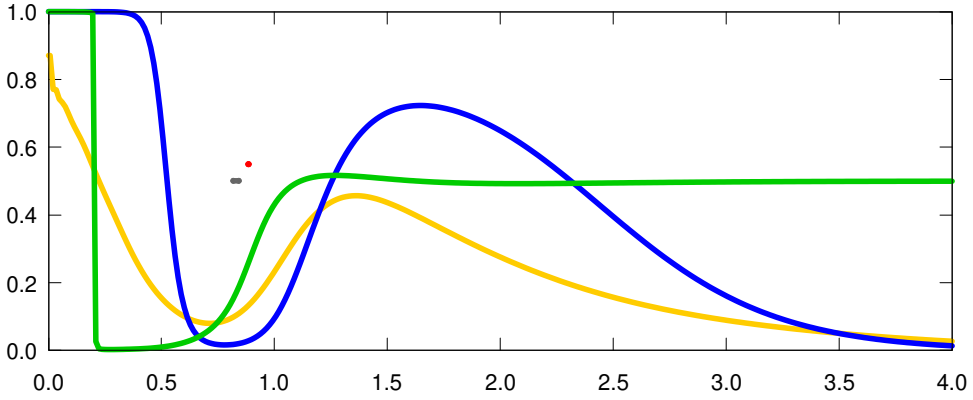
1.0
0.8
0.6
0.4
0.2
0.0
0.0
0.5
1.0
1.5
2.0
2.5
3.0
3.5
4.0
r (au)

C ^{3}P

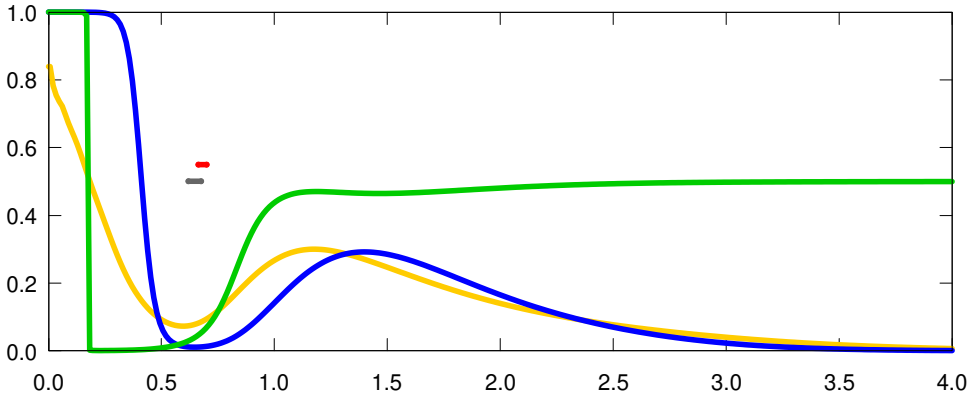
1.0
0.8
0.6
0.4
0.2
0.0
0.0
0.5
1.0
1.5
2.0
2.5
3.0
3.5
4.0
r (au)

N ^{4}S

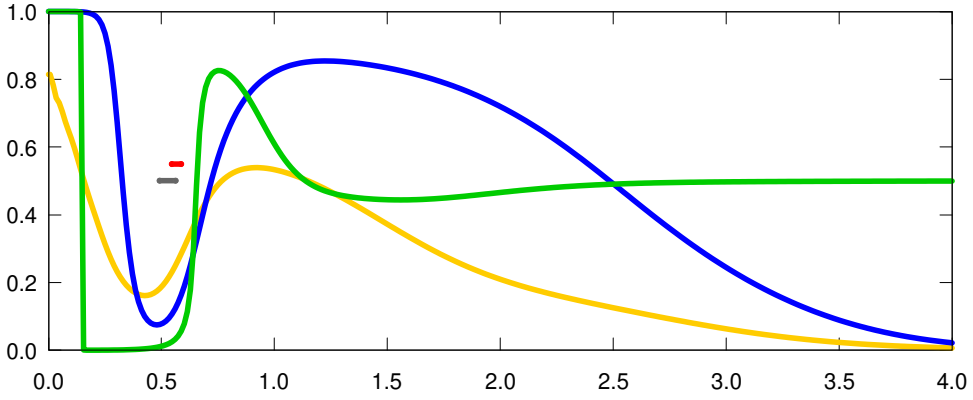
1.0
0.8
0.6
0.4
0.2
0.0
0.0
0.5
1.0
1.5
2.0
2.5
3.0
3.5
4.0
r (au)

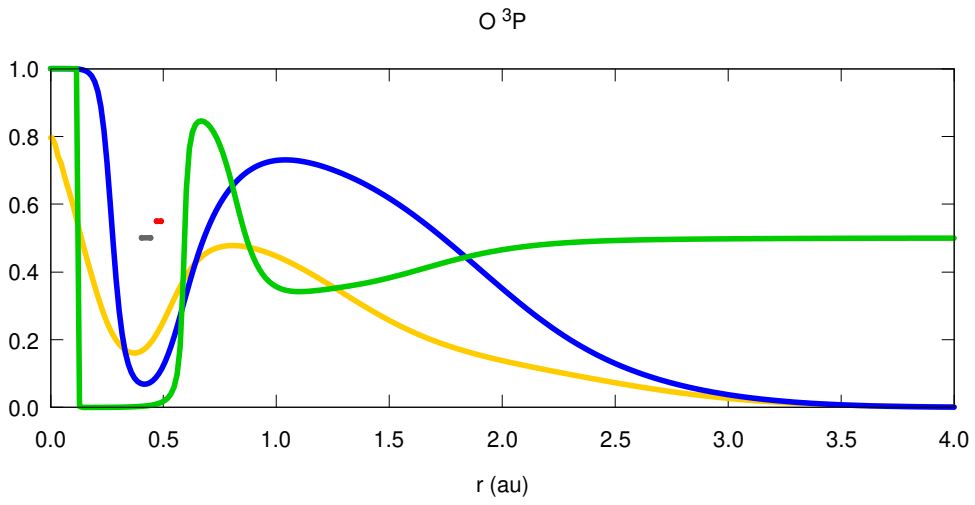
O 3P
1.0
0.8
0.6
0.4
0.2
0.0
0.0
0.5
1.0
1.5
2.0
2.5
3.0
3.5
4.0
r (au)

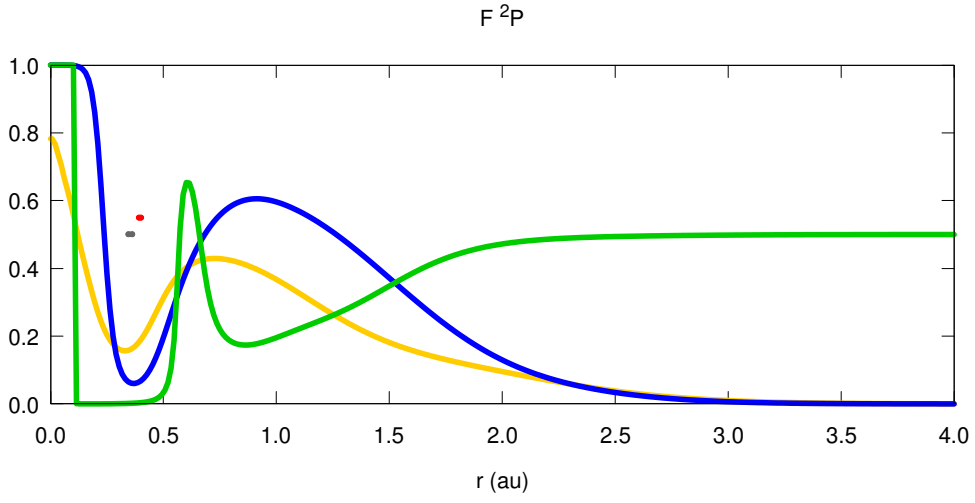
F 2P
1.0
0.8
0.6
0.4
0.2
0.0
0.0
0.5
1.0
1.5
2.0
2.5
3.0
3.5
4.0
r (au)

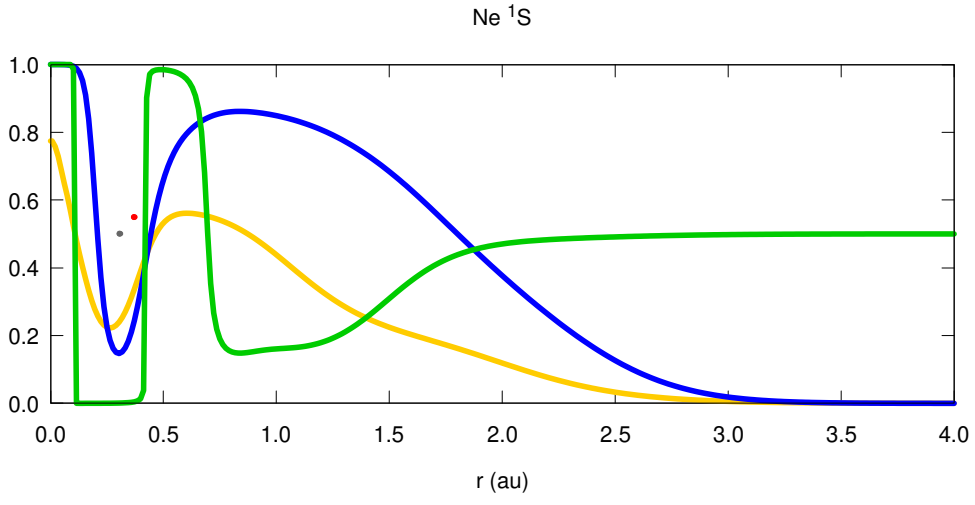
Ne 1S
1.0
0.8
0.6
0.4
0.2
0.0
0.0
0.5
1.0
1.5
2.0
2.5
3.0
3.5
4.0
r (au)

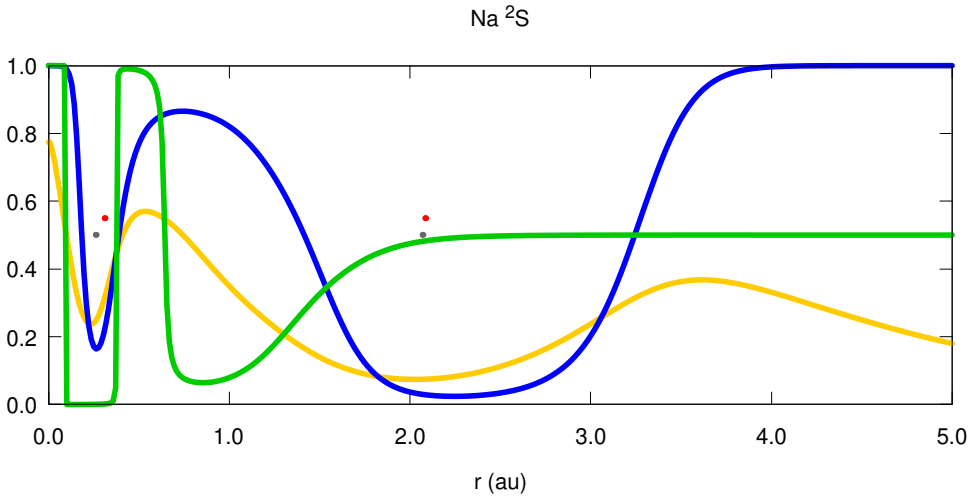
Na ^{2}S
1.0
0.8
0.6
0.4
0.2
0.0
0.0
1.0
2.0
3.0
4.0
5.0
r (au)

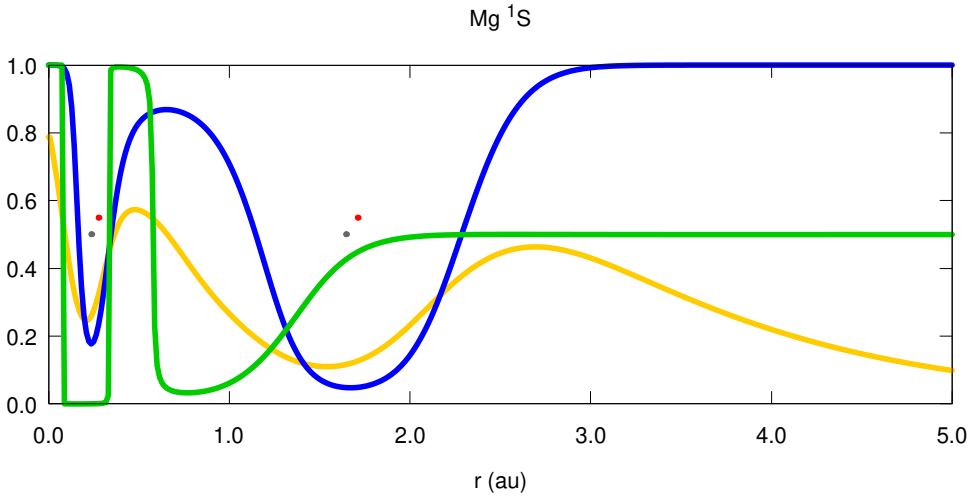
Mg ^{1}S
1.0
0.8
0.6
0.4
0.2
0.0
0.0
1.0
2.0
3.0
4.0
5.0
r (au)

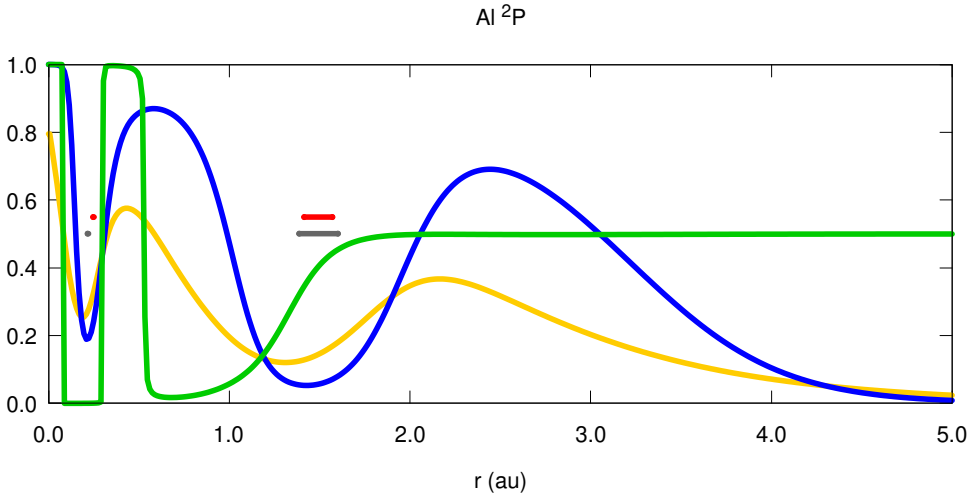
Al ^{2}P
1.0
0.8
0.6
0.4
0.2
0.0
0.0
1.0
2.0
3.0
4.0
5.0
r (au)

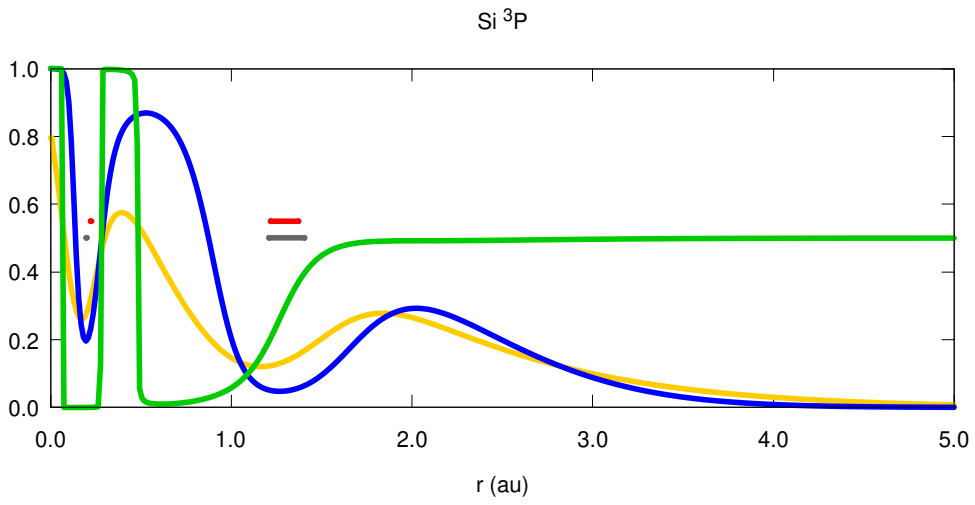
Si ^{3}P
1.0
0.8
0.6
0.4
0.2
0.0
0.0
1.0
2.0
3.0
4.0
5.0
r (au)

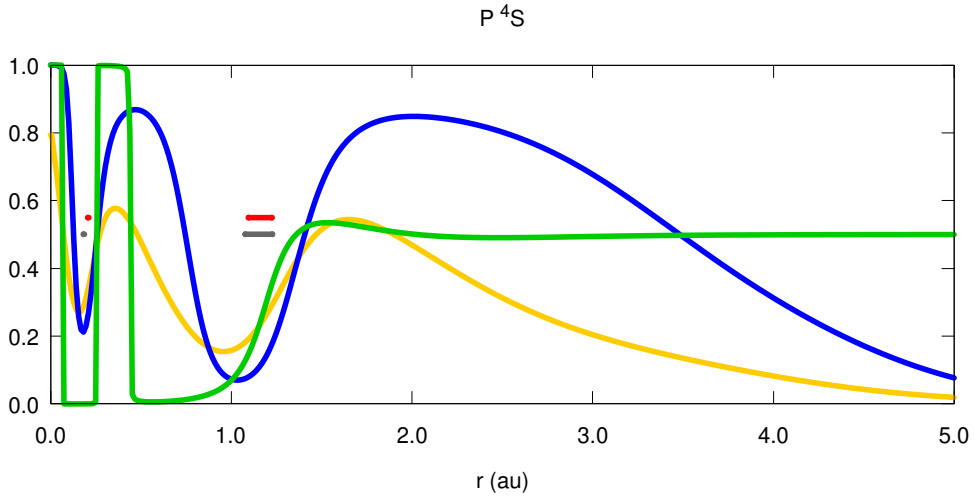
P ^{4}S
1.0
0.8
0.6
0.4
0.2
0.0
0.0
1.0
2.0
3.0
4.0
5.0
r (au)

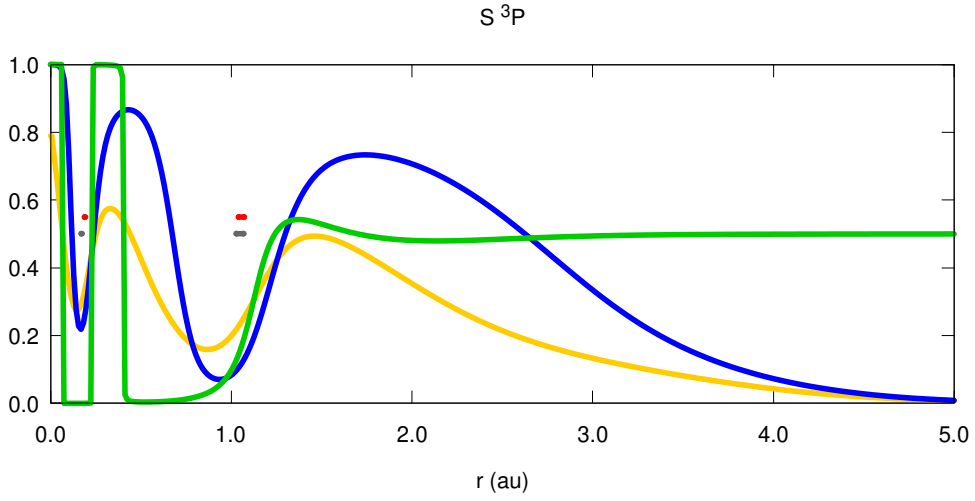
S ^{3}P
1.0
0.8
0.6
0.4
0.2
0.0
0.0
1.0
2.0
3.0
4.0
5.0
r (au)

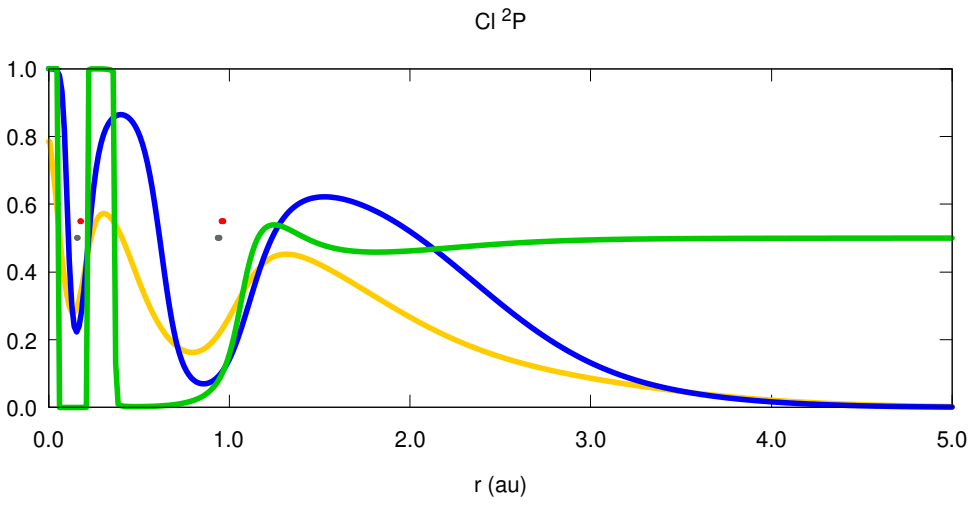
Cl ^{2}P
1.0
0.8
0.6
0.4
0.2
0.0
0.0
1.0
2.0
3.0
4.0
5.0
r (au)

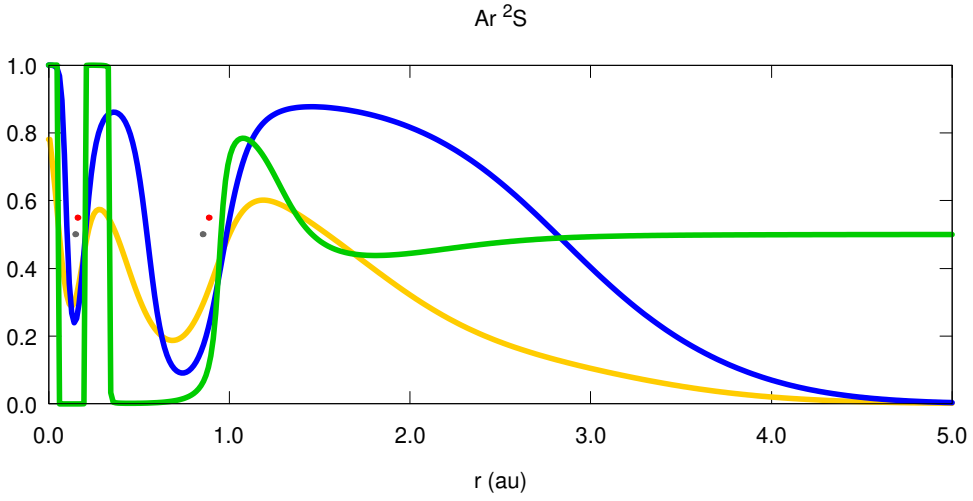
Ar ^{2}S
1.0
0.8
0.6
0.4
0.2
0.0
0.0
1.0
2.0
3.0
4.0
5.0
r (au)

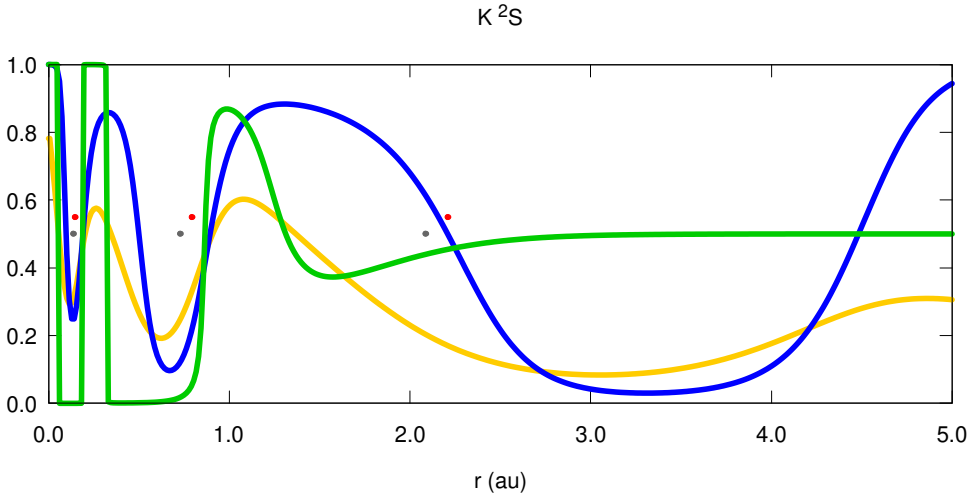
K ^{2}S
1.0
0.8
0.6
0.4
0.2
0.0
0.0
1.0
2.0
3.0
4.0
5.0
r (au)

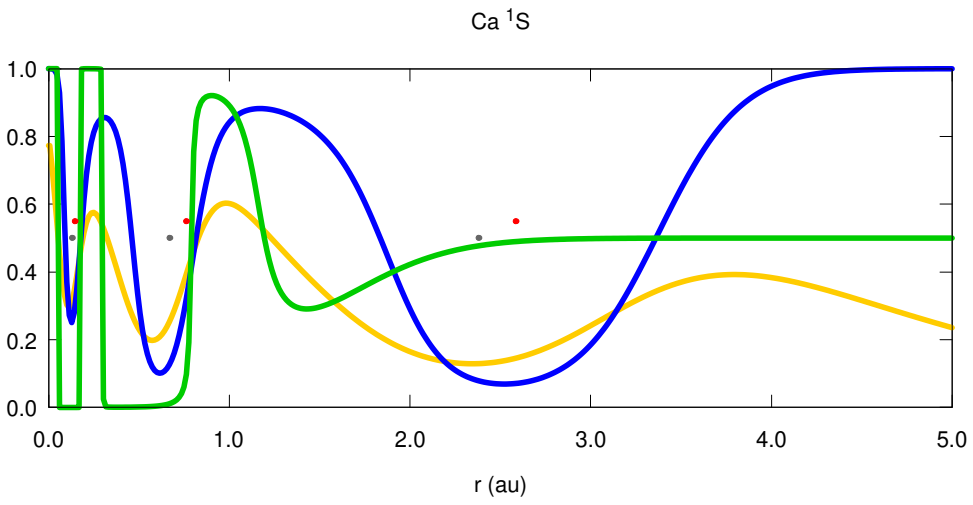
Ca ^{1}S
1.0
0.8
0.6
0.4
0.2
0.0
0.0
1.0
2.0
3.0
4.0
5.0
r (au)

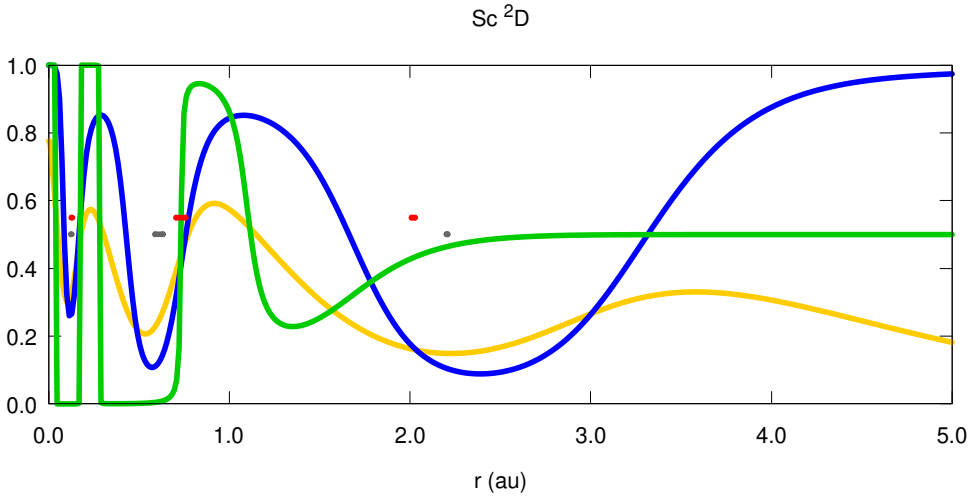
Sc ^{2}D
1.0
0.8
0.6
0.4
0.2
0.0
0.0
1.0
2.0
3.0
4.0
5.0
r (au)

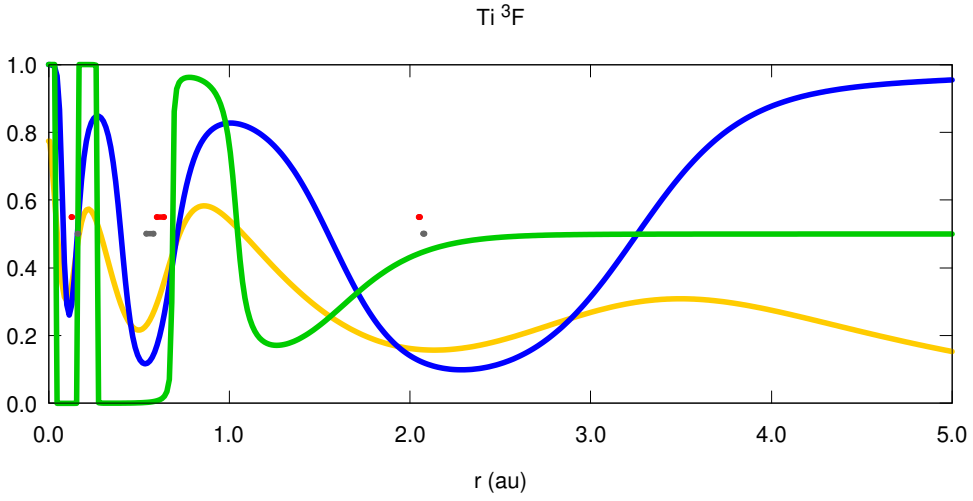
Ti ^{3}F
1.0
0.8
0.6
0.4
0.2
0.0
0.0
1.0
2.0
3.0
4.0
5.0
r (au)

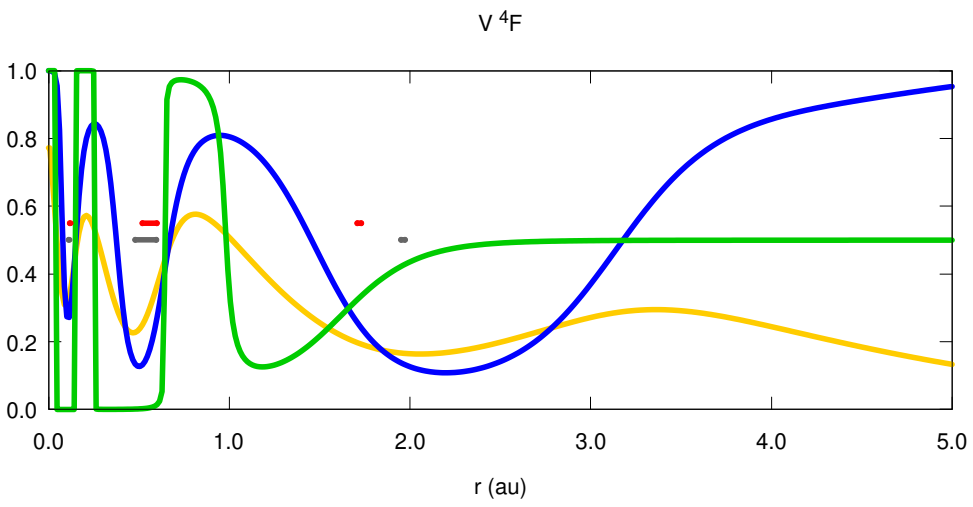
V ^{4}F
1.0
0.8
0.6
0.4
0.2
0.0
0.0
1.0
2.0
3.0
4.0
5.0
r (au)

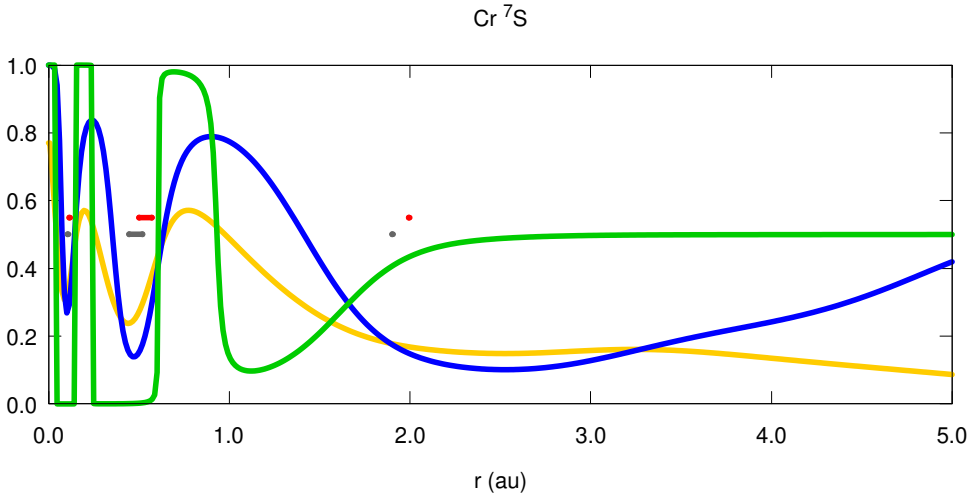
Cr ^{7}S
1.0
0.8
0.6
0.4
0.2
0.0
0.0
1.0
2.0
3.0
4.0
5.0
r (au)

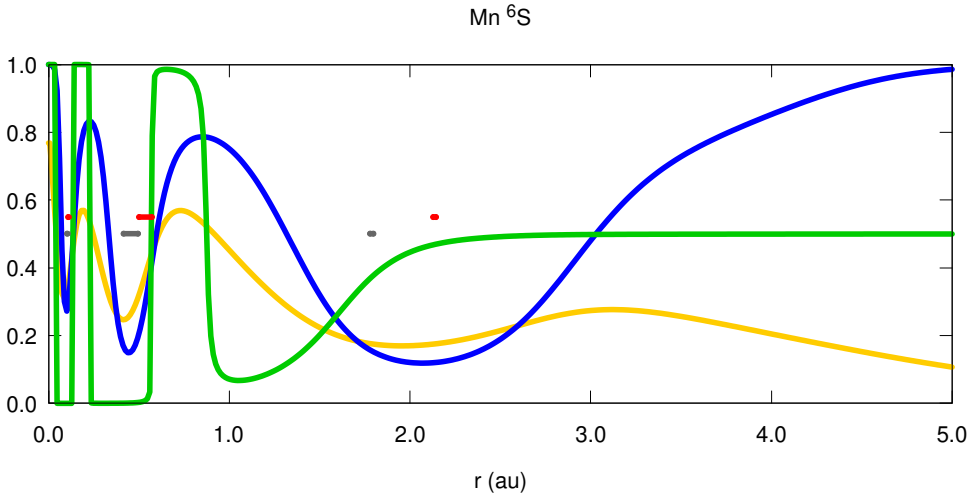
Mn ^{6}S
1.0
0.8
0.6
0.4
0.2
0.0
0.0
1.0
2.0
3.0
4.0
5.0
r (au)

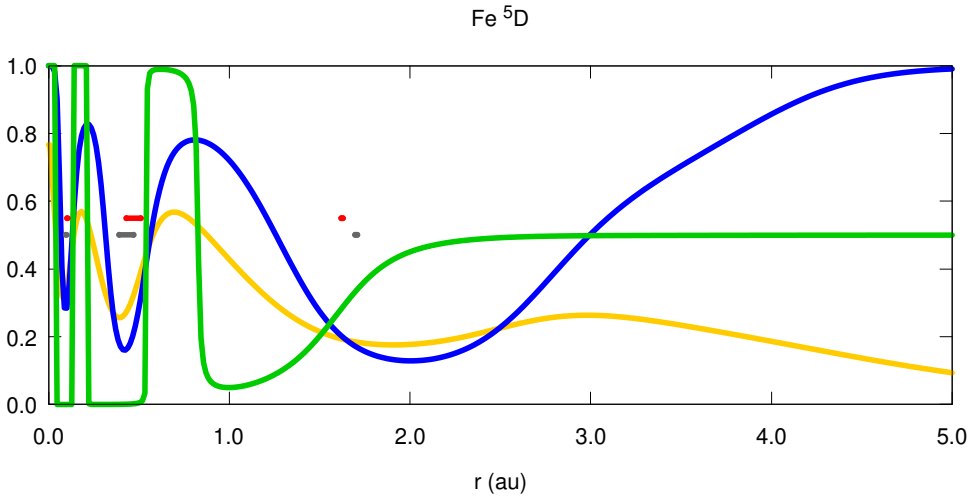
Fe ^{5}D
1.0
0.8
0.6
0.4
0.2
0.0
0.0
1.0
2.0
3.0
4.0
5.0
r (au)

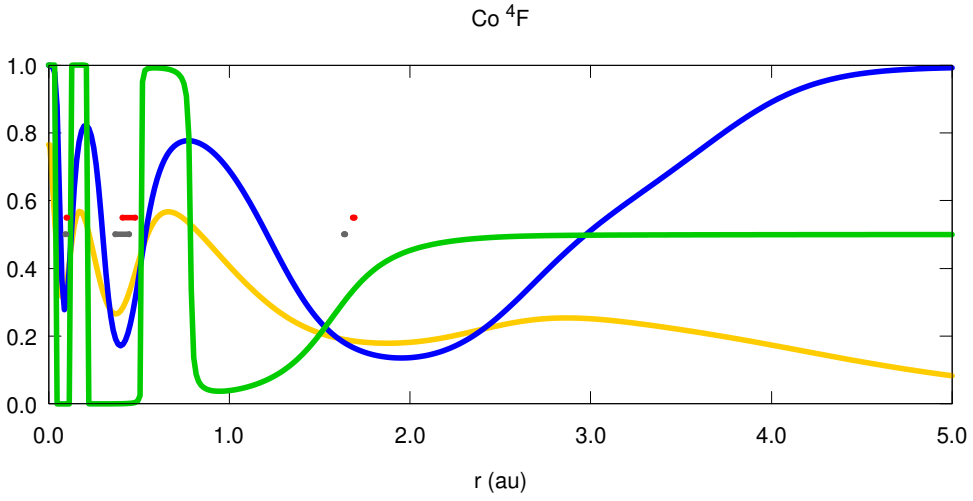
Co ^{4}F
1.0
0.8
0.6
0.4
0.2
0.0
0.0
1.0
2.0
3.0
4.0
5.0
r (au)

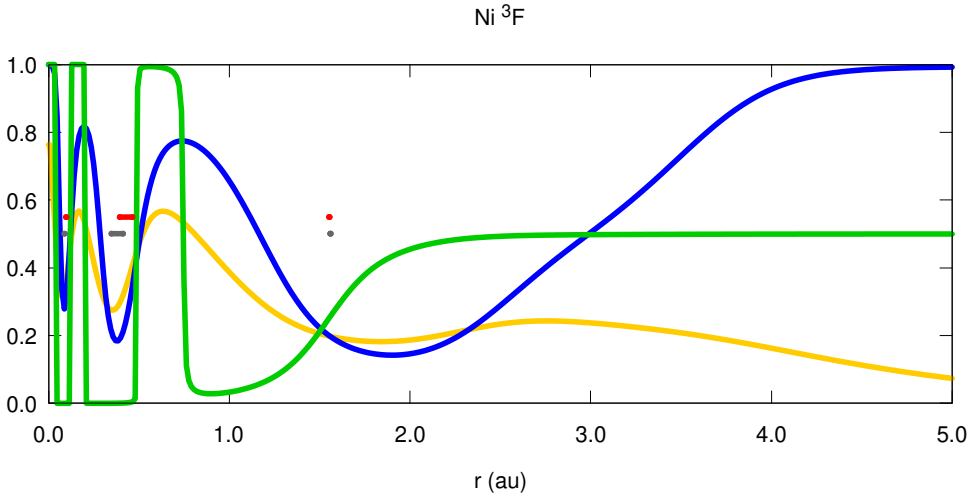
Ni ^{3}F
1.0
0.8
0.6
0.4
0.2
0.0
0.0
1.0
2.0
3.0
4.0
5.0
r (au)

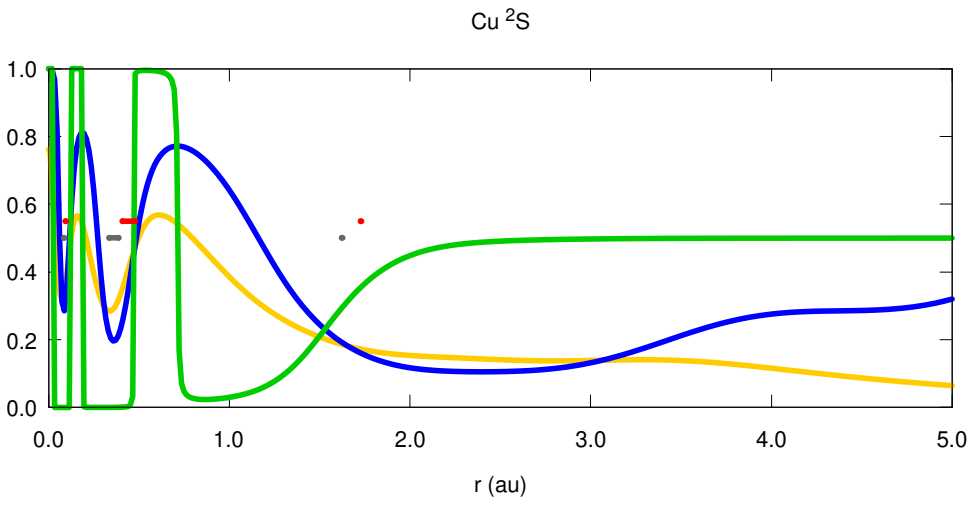
Cu 2S
1.0
0.8
0.6
0.4
0.2
0.0
0.0
1.0
2.0
3.0
4.0
5.0
r (au)

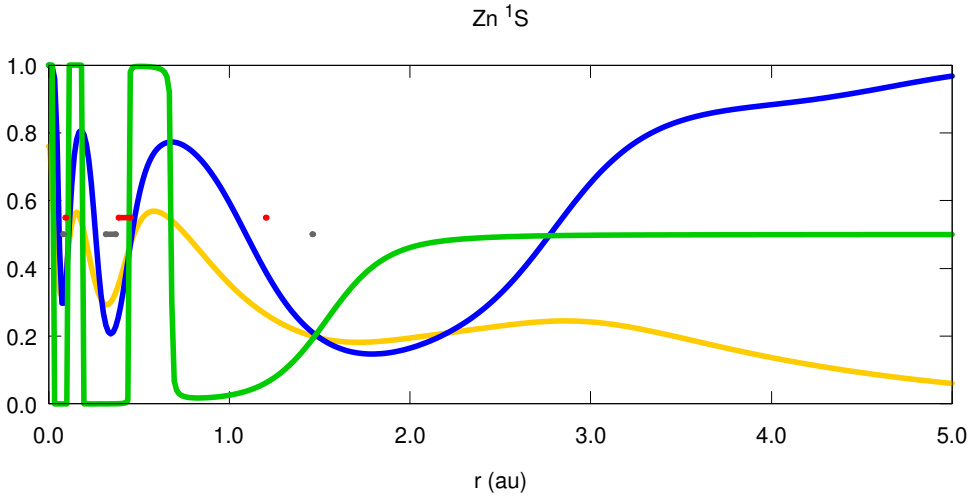
Zn 1S
1.0
0.8
0.6
0.4
0.2
0.0
0.0
1.0
2.0
3.0
4.0
5.0
r (au)

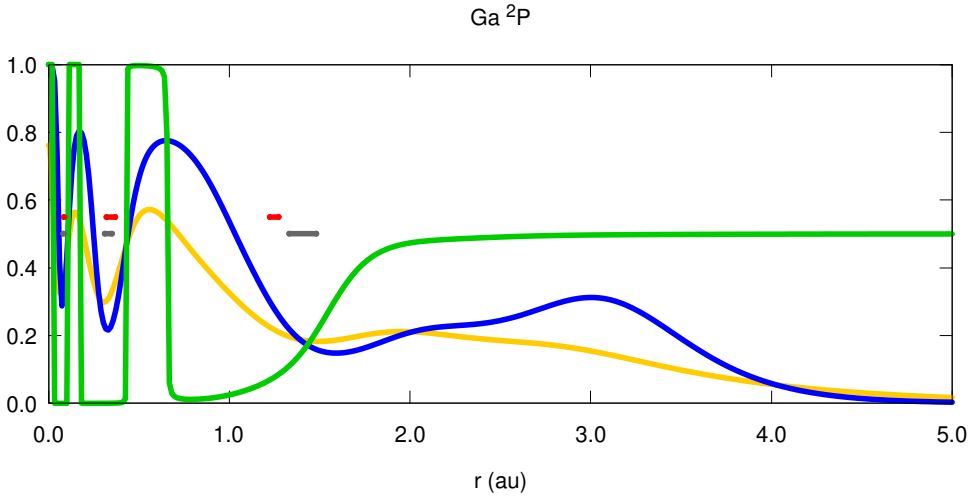
Ga 2P
1.0
0.8
0.6
0.4
0.2
0.0
0.0
1.0
2.0
3.0
4.0
5.0
r (au)

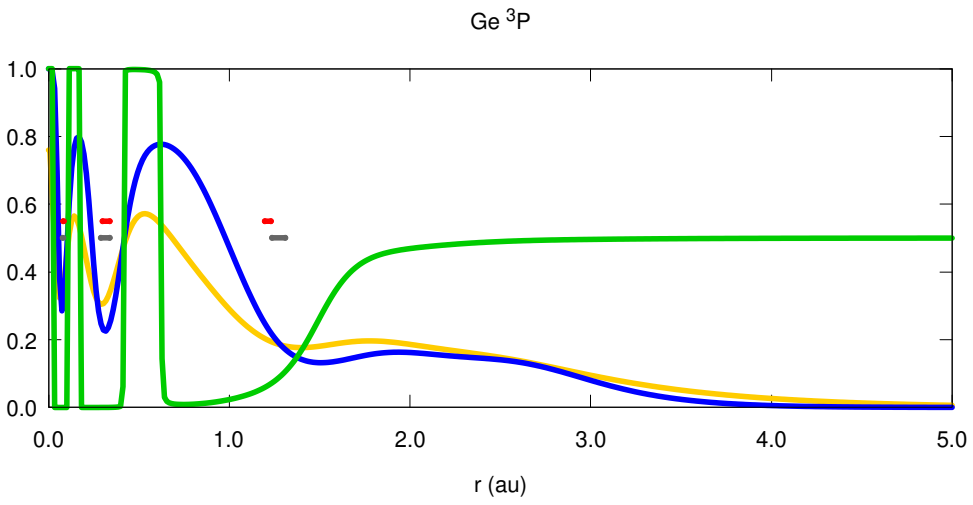
Ge 3P
1.0
0.8
0.6
0.4
0.2
0.0
0.0
1.0
2.0
3.0
4.0
5.0
r (au)

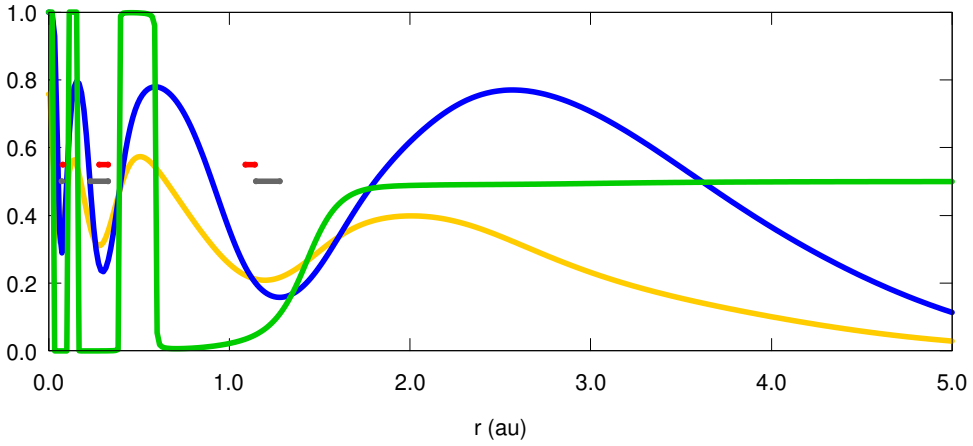
As 4S
1.0
0.8
0.6
0.4
0.2
0.0
0.0
1.0
2.0
3.0
4.0
5.0
r (au)

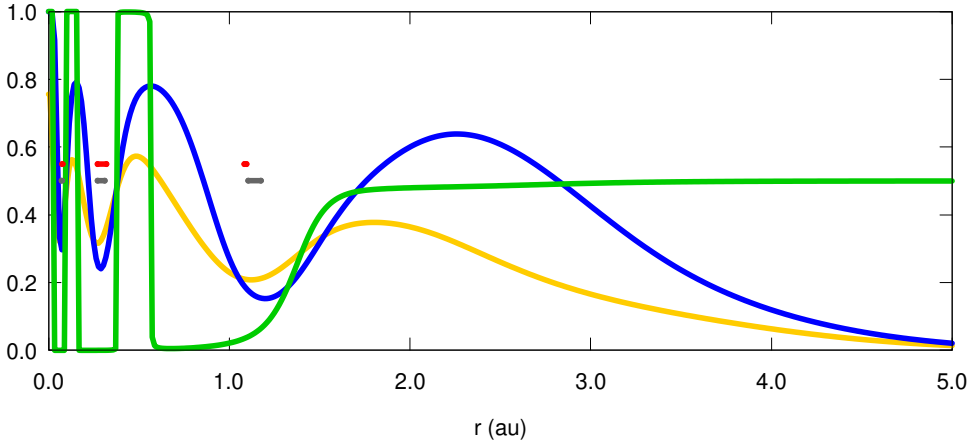
Se 3P
1.0
0.8
0.6
0.4
0.2
0.0
0.0
1.0
2.0
3.0
4.0
5.0
r (au)

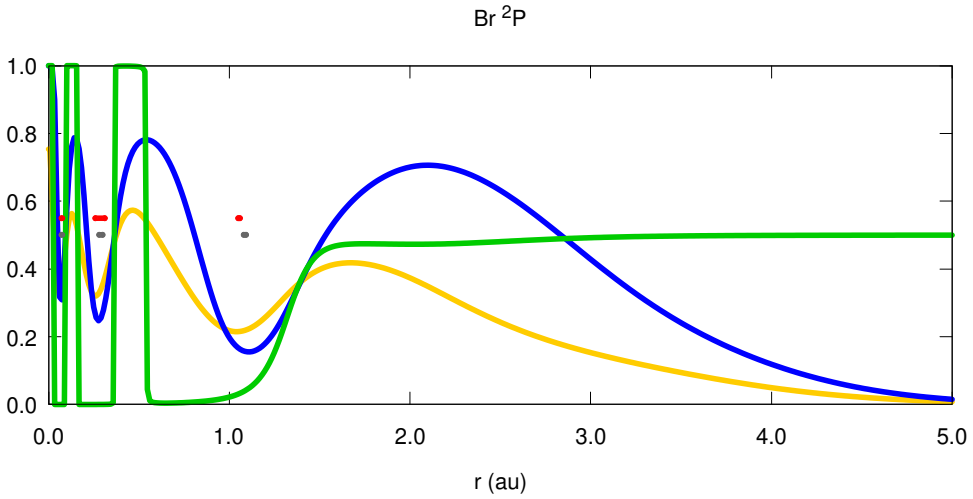
Br ^{2}P
1.0
0.8
0.6
0.4
0.2
0.0
0.0
1.0
2.0
3.0
4.0
5.0
r (au)

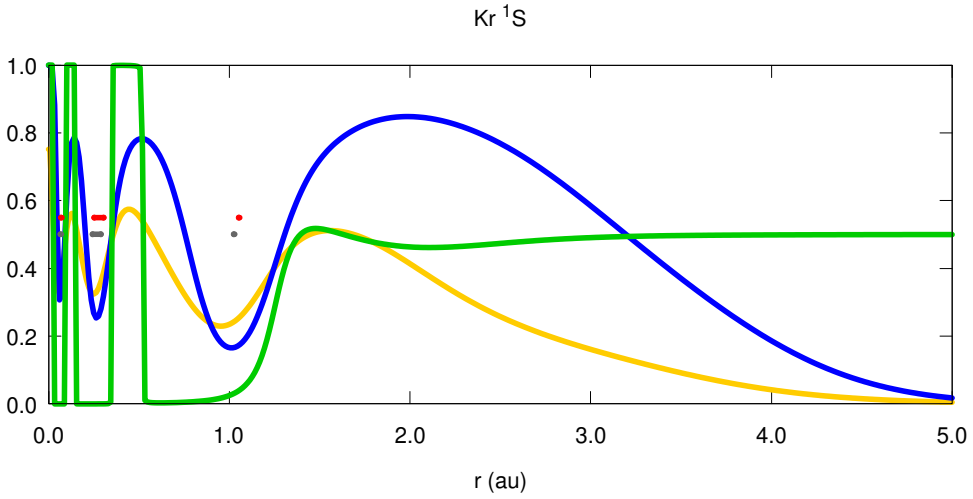
Kr ^{1}S
1.0
0.8
0.6
0.4
0.2
0.0
0.0
1.0
2.0
3.0
4.0
5.0
r (au)

4 Energies

Table S2: Energies (in au) for the HF/cc-pVDZ calculations (or intrashell CASSCF ones) performed with GAMESS[2] as compared to the HF+J/cc-pVDZ VMQMC results obtained with *Amolqc*[7] for atoms Li-Kr. First and second entries in each atom correspond to HF and HF+J calculations, respectively. Some VMQC calculations cannot be considered fully converged, but their Born maxima are consistent with the rest, being thus included.

Atom	Energy (Eh)				
Li (^{2}S)	-7.4324198797	Na (^{2}S)	-161.8530266435	K (^{2}S)	-599.1589148688
	-7.4747 ± 0.0012		-162.146 ± 0.013		-599.7 ± 0.7
Be (^{1}S)	-14.572337631	Mg (^{1}S)	-199.6082970286	Ca (^{1}S)	-676.7498235562
	-14.628 ± 0.003		-199.916 ± 0.016		-677.5 ± 0.2
B (^{2}P)	-24.4083204164	Al (^{2}P)	-241.7932028455	Sc (^{2}D)	-759.7350659316
	-24.602 ± 0.004		-242.161 ± 0.018		-758.95 ± 0.05
C (^{3}P)	-37.6824178815	Si (^{3}P)	-288.8464369231	Ti (^{3}F)	-848.4050840372
	-37.76 ± 0.04		-289.16 ± 0.02		-848.48 ± 0.11
N (^{4}S)	-54.388414237	P (^{4}S)	-340.7090141164	V (^{4}F)	-942.8831996507
	-54.490 ± 0.006		-341.11 ± 0.02		-943.16 ± 0.09
O (^{3}P)	-74.7875130746	S (^{3}P)	-397.4928397492	Cr (^{7}S)	-1043.35499896
	-74.945 ± 0.008		-397.86 ± 0.03		-1043.93 ± 0.05
F (^{2}P)	-99.3718619401	Cl (^{2}P)	-459.4671805869	Mn (^{6}S)	-1149.8646918089
	-99.487 ± 0.012		-459.87 ± 0.03		-1149.86 ± 0.11
Ne (^{1}S)	-128.4887755517	Ar (^{1}S)	-526.7998653097	Fe (^{5}D)	-1262.4418394408
	-128.718 ± 0.018		-527.26 ± 0.04		-1262.81 ± 0.14
				Co (^{4}F)	-1381.4123745687
					-1382.05 ± 0.09
				Ni (^{3}F)	-1506.8674501472
					-1507.46 ± 0.09
				Cu (^{2}S)	-1638.9615728573
					-1637.7 ± 0.4

Zn (^{1}S)	-1777.8466552079
	-1766.4 ± 0.7
Ga (^2P)	-1923.1118507221
	-1921.9 ± 0.3
Ge (^{3}P)	-2075.194260589
	2073.1 ± 0.3
As (^{4}S)	-2234.1661191505
	-2232.4 ± 0.4
Se (^{3}P)	-2399.7934879131
	-2396.4 ± 0.4
Br (^{2}P)	-2572.3649093745
	-2570.5 ± 0.7
Kr (^{1}S)	-2751.9748718143
	-2752.3 ± 0.4

5 Jastrow Factors

Table S4: Optimized c_{kA} coefficients and m, n, o exponents (see Eq. 7) for the Jastrow factors of the Li-Kr atoms and the CH_4, H»O, NH_3, HF and C_2H_6 molecules.

m	n	o	Li (^{2}S)	Be (^{1}S)	B (^{2}P)	C (^{3}P)	N (^{4}S)	O (^{3}P)	F (^{2}P)	Ne (^{1}S)
0	0	1	0.50000	0.50000	0.50000	0.50000	0.50000	0.50000	0.50000	0.50000
0	0	2	-0.11837	0.35626	0.22519	-0.30163	-0.22696	-0.28757	-0.57618	-0.46260
0	0	3	1.25185	-1.12013	-1.15077	0.17182	-0.19125	0.07705	0.35987	0.63859
0	0	4	-1.22020	1.10267	1.27545	-0.14770	0.47955	0.37095	-0.04002	-0.22152
2	0	0	0.12504	0.15277	0.04201	0.01286	-0.00860	-0.03426	-0.00516	-0.03356
3	0	0	-0.91186	-1.27497	-0.58707	-0.26299	-0.03338	0.17048	-0.06721	0.23202
4	0	0	1.61450	3.21442	1.66338	0.62255	-0.17295	-0.93600	-0.13308	-1.52305
2	2	2	-1.44821	-3.22536	-2.20962	-1.00095	-0.55128	0.04675	-0.36272	0.83571

m	n	o	Na (^{2}S)	Mg (^{1}S)	Al (^{2}P)	Si (^{3}P)	P (^{4}S)	S (^{3}P)	Cl (^{2}P)	Ar (^{1}S)
0	0	1	0.50000	0.50000	0.50000	0.50000	0.50000	0.50000	0.50000	0.50000
0	0	2	-0.93833	-0.90504	-0.88816	-1.05995	-0.85870	-0.88860	-0.84474	-0.97043
0	0	3	2.04824	1.76097	1.58601	1.72469	1.26859	1.25958	1.02858	1.41428
0	0	4	-1.42415	-1.09497	-0.92255	-1.01532	-0.55573	-0.55076	-0.27496	-0.62367
2	0	0	0.00215	0.00626	0.01198	0.00390	0.01932	0.01402	0.01396	0.00880
3	0	0	-0.13193	-0.21382	-0.29575	-0.21716	-0.38414	-0.35450	-0.37649	-0.32350
4	0	0	-0.35748	-0.03486	0.28924	0.22199	0.65408	0.63099	0.74921	0.59231
2	2	2	0.32010	0.00008	-0.32497	-0.22356	-0.72406	-0.70665	-0.87442	-0.71179

m	n	o	K (^{2}S)	Ca (^{1}S)	Sc (^{2}D)	Ti (^{3}F)	V (^{4}F)	Cr (^{7}S)	Mn (^{6}S)	Fe (^{5}D)	Co (^{4}F)
0	0	1	0.50000	0.50000	0.50000	0.50000	0.50000	0.50000	0.50000	0.50000	0.50000
0	0	2	-1.58137	-1.39895	-0.85544	-1.14895	-1.74036	-1.13877	-1.81959	-1.41073	-1.16749
0	0	3	2.84006	2.28671	0.83609	1.83001	3.14558	1.78005	3.33578	2.46907	1.87847
0	0	4	-1.88857	-1.33081	-0.10908	-0.91337	-2.03631	-0.91209	-2.16167	-1.46971	-1.03308
2	0	0	-0.00022	-0.00029	0.00128	-0.00062	0.00093	-0.00319	0.00083	-0.00142	-0.00329
3	0	0	-0.20102	-0.17492	-0.27159	-0.23250	-0.17977	-0.21386	-0.18066	-0.21690	-0.22716
4	0	0	0.43570	0.26082	0.43476	0.29737	0.41533	0.23071	0.43477	0.34463	0.27398
2	2	2	-0.32508	-0.21528	-0.41271	-0.33442	-0.34546	-0.22448	-0.39070	-0.34783	-0.24516

m	n	o	Ni (^{3}F)	Cu (^{2}S)	Zn (^{1}S)	Ga (^2P)	Ge (^{3}P)	As (^{4}S)	Se (^{3}P)	Br (^{2}P)	Kr (^{1}S)
0	0	1	0.50000	0.50000	0.50000	0.50000	0.50000	0.50000	0.50000	0.50000	0.50000
0	0	2	-1.19553	-2.78535	-0.70652	-1.98603	-2.04748	-2.01456	-2.10408	-2.03610	-1.37662
0	0	3	1.97268	4.69714	1.01678	3.73423	3.85209	3.76784	4.13658	3.79220	2.37461
0	0	4	-1.09473	-1.99991	-0.38202	-2.42369	-2.50338	-2.47412	-2.80896	-2.42189	-1.40297
2	0	0	-0.00142	-0.01819	-0.00442	0.00233	0.00367	0.00444	-0.00053	0.00175	-0.00390
3	0	0	-0.25720	3.21018	0.00164	-0.19949	-0.22068	-0.22759	-0.16948	-0.20492	-0.23582
4	0	0	0.38294	0.28846	0.16190	0.61666	0.70772	0.71748	0.49599	0.67431	0.36419
2	2	2	-0.38801	-0.34033	-0.16486	-0.68025	-0.73016	-0.75527	-0.53281	-0.76555	-0.35688

m	n	o	CH_4	NH_3	H_2O	HF	C_2H_6
0	0	1	0.50000	0.50000	0.50000	0.50000	0.50000
0	0	2	-0.24796	-0.41309	-0.55181	-0.49976	-0.37792
0	0	3	0.15833	0.80045	1.13254	0.14410	0.98116
0	0	4	-0.12613	-0.27605	-0.60457	0.12307	-0.51720
2	0	0	0.04728	-0.01333	-0.02210	-0.14792	-0.00409
3	0	0	-0.47510	0.04489	0.10367	0.79021	0.00375
4	0	0	1.24478	-0.51832	-0.85523	-1.64667	-0.15506
2	2	2	-1.24412	0.19862	0.54056	1.08764	-0.03252
2	0	2	-0.14719	-0.07797	-0.03739	0.00384	-0.06043
2	2	2	0.66943	0.21175	-0.07313	-0.16493	0.22083
4	0	2	-1.42723	-0.29454	0.15551	0.21680	-0.38143
2	0	4	1.10491	0.12576	-0.06811	-0.25772	0.23779

6 Electron coordinates at the HF Born maximum.

Nuclei are always located at the origin of the reference system. Majority spin electrons followed by minority spin ones. All data in au.

Li

0.000000 0.000000 0.000000
0.421021 0.465077 -1.604987
0.000000 0.000000 0.000000

Be

0.000000 0.000000 0.000000
-1.040667 0.317501 -0.275763
1.059810 -0.263955 -0.258784
0.000000 0.000000 0.000000

B

0.000007 -0.000006 -0.817714
0.000001 -0.000004 0.817680
0.000000 0.000000 0.000000
0.841612 0.000154 0.000075
0.000000 0.000000 0.000000

C

0.550702 0.000897 -0.285043
0.000000 0.000000 0.000000
-0.028222 -0.000045 0.619002
-0.522495 -0.000852 -0.333868
0.000000 0.000000 0.000000
-0.547411 -0.394533 -0.000032

N

0.452959 0.102266 -0.162067

-0.284045 -0.131542 -0.379356

0.021393 -0.368988 0.324478

0.000000 0.000000 0.000000

-0.190307 0.398264 0.216945

0.000000 0.000000 0.000000

-0.512166 -0.031832 0.228844

O

0.000000 0.000000 0.000000

0.122054 0.219704 -0.315277

0.124408 0.174560 0.341495

-0.407731 -0.024291 -0.000181

0.156534 -0.370646 -0.026044

0.442312 0.001004 -0.000001

0.000000 0.000000 0.000000

-0.442312 -0.001004 -0.000000

F

0.000000 0.000000 0.000000

-0.011966 0.331751 0.103234

-0.278540 -0.169014 0.120292

0.288161 -0.149481 0.123338

0.002313 -0.013118 -0.344136

0.166533 0.320455 -0.000000

-0.360440 -0.015811 0.000000

0.000000 0.000000 0.000000

0.193880 -0.304648 -0.000000

Ne

0.290334 0.089594 -0.022201
-0.049682 -0.115557 0.277475
-0.056950 -0.212889 -0.210355
-0.183702 0.238851 -0.044919
0.000000 0.000000 0.000000
-0.100984 0.021407 -0.286632
-0.100738 -0.259376 0.124056
0.000000 0.000000 0.000000
-0.102928 0.236677 0.161875
0.304650 0.001291 0.000701

Na

0.919778 0.264971 1.834583
0.218399 -0.145186 0.011813
-0.116465 -0.036245 -0.231858
0.061809 0.253578 0.028129
-0.163573 -0.072098 0.192255
0.000000 0.000000 0.000000
0.110869 -0.177160 0.158491
0.000000 0.000000 0.000000
0.121333 -0.002647 -0.232527
-0.253501 -0.058710 -0.032986
0.021298 0.238517 0.107021

Mg

0.121635 -0.103864 0.175085
0.015915 0.235654 0.021566
0.089911 -0.066568 -0.209112
1.564740 0.507609 -0.104216
-0.226986 -0.065070 0.012430
0.000000 0.000000 0.000000
0.602824 -1.346749 -0.734723
-0.090211 0.197396 0.093853

-0.066529 -0.017096 -0.227019

-0.079766 -0.188211 0.120209

0.000000 0.000000 0.000000

0.236687 0.007504 0.012736

Al

-0.000002 0.000005 -1.601623

-0.037819 0.201314 -0.069832

-0.000004 0.000007 1.601611

0.191749 -0.067387 -0.074291

-0.155746 -0.131876 -0.071993

0.000000 0.000000 0.000000

0.001805 -0.002039 0.215458

1.388305 -0.000232 -0.000133

0.069262 -0.063878 0.195162

0.076242 -0.134917 -0.151518

0.070972 0.200881 -0.039727

0.000000 0.000000 0.000000

-0.215992 -0.002085 -0.003916

Si

-1.222127 -0.004374 0.696204

1.215462 0.004339 0.707789

0.000000 0.000000 0.000000

0.000636 -0.198657 -0.000929

0.178018 0.066805 -0.053980

-0.042307 0.064997 0.181801

0.006707 0.000019 -1.406362

-0.136344 0.066142 -0.126898

-0.162505 -0.112912 0.009832

0.063019 0.009046 -0.188320

0.142510 -0.079014 0.113921

-0.042633 0.183166 0.064568

0.981793 0.707710 0.000249

0.000000 0.000000 0.000000

P

-0.900136 -0.834106 -0.051544

0.181433 0.334942 1.167701

0.000000 0.000000 0.000000

0.121442 0.113125 -0.075454

-0.315216 0.984090 -0.663951

-0.115472 -0.059351 -0.127994

1.033921 -0.484928 -0.452207

0.087066 -0.142111 0.073911

-0.093036 0.088336 0.129537

-0.561304 -0.908175 -0.132059

-0.162649 0.039448 -0.075696

-0.026158 -0.080047 0.163245

0.095764 0.154275 0.022450

0.000000 0.000000 0.000000

0.092778 -0.114104 -0.110062

S

-0.032748 1.067088 -0.004065

-0.066398 0.154661 -0.010311

0.512921 -0.342288 -0.862074

-0.988873 -0.381218 -0.003184

0.010095 -0.067224 -0.154272

0.504898 -0.335911 0.869258

0.000000 0.000000 0.000000

0.154244 0.009438 0.067385

-0.097954 -0.096848 0.097197

-0.000490 0.168286 0.000532

0.062172 -0.056732 0.147494

0.097053 -0.055763 -0.127715

-0.005173 1.028913 -0.000001

0.005163 -1.028947 -0.000001

-0.158731 -0.056850 -0.020318
0.000000 0.000000 0.000000

Cl

0.006245 0.139135 0.071846
0.000000 0.000000 0.000000
0.172873 -0.878089 0.300156
-0.013045 -0.113592 0.107169
0.003906 0.017408 -0.939410
0.666018 0.582194 0.328726
0.130895 -0.021648 -0.083397
-0.843846 0.279758 0.316504
-0.124094 -0.003893 -0.095611
0.000488 -0.000009 -0.158292
0.423117 -0.835677 -0.000010
0.136630 0.055899 0.052836
-0.020151 -0.146405 0.052362
0.000000 0.000000 0.000000
-0.935050 0.050323 -0.000010
0.509932 0.785674 -0.000010
-0.116959 0.090515 0.052047

Ar

-0.705269 0.454947 0.149410
0.446588 0.365853 -0.627228
-0.093518 -0.010466 0.112357
0.133467 0.033431 0.050479
0.000000 0.000000 0.000000
-0.216084 -0.792013 -0.229623
0.005343 -0.127991 -0.071198
-0.045292 0.105025 -0.091639
0.474765 -0.028787 0.707442
-0.074817 -0.001691 -0.126012
0.000000 0.000000 0.000000

0.631119 0.246250 0.517450

0.041187 -0.136432 0.034196

0.230960 -0.709575 -0.412146

-0.161136 0.617323 -0.565378

-0.085116 0.053511 0.106636

0.118746 0.084612 -0.014820

-0.700943 -0.153997 0.460074

K

-0.074786 -0.069978 0.090482

0.681845 -0.253500 0.005088

0.092813 0.075091 0.066060

0.003365 0.707855 0.163714

0.063296 -0.087123 -0.083796

1.461582 1.574323 -1.887796

-0.081405 0.081928 -0.072647

-0.289112 -0.094864 -0.660374

-0.402505 -0.366289 0.499821

0.000000 0.000000 0.000000

-0.057843 -0.074021 -0.099065

-0.006539 -0.593097 0.427923

0.029964 0.124362 -0.047702

-0.666447 0.301135 -0.009479

0.000000 0.000000 0.000000

0.190555 -0.191790 -0.679580

0.482420 0.483736 0.261141

0.114488 -0.061502 0.041823

-0.086609 0.011162 0.104945

Ca

-0.609942 0.262774 0.158904

-0.116839 0.054281 0.019370

0.000000 0.000000 0.000000

2.147029 -0.883466 -0.529224

-0.005431 -0.126414 0.029833

0.333569 0.430233 -0.387565

0.347244 -0.111005 0.560020

0.088088 0.058578 0.075553

0.034006 0.013635 -0.124725

-0.084467 -0.576379 -0.327986

-0.587708 -0.142796 0.284699

0.000000 0.000000 0.000000

0.399228 -1.242187 1.991961

-0.098103 -0.082696 0.020893

-0.022907 0.068018 -0.108730

-0.105807 0.348415 -0.577702

0.110808 -0.066695 -0.013112

0.366732 0.369743 0.418974

0.010166 0.081476 0.100785

0.324272 -0.567507 -0.138612

Sc

0.430727 0.432387 -0.125801

-0.097920 -0.038730 -0.062524

-1.547018 1.521860 -0.381999

0.000000 0.000000 0.000000

0.044207 0.102009 -0.051500

-0.431360 -0.429714 -0.125462

0.428884 -0.428899 -0.123664

-0.032035 0.023211 0.115980

0.000252 -0.000233 0.625703

-0.409508 0.409588 -0.117063

0.086174 -0.086913 -0.001696

1.616056 -0.148671 -1.498873

-0.228724 0.121693 -0.564118

0.080884 0.089459 0.021358

0.445844 0.410142 0.135536

0.056020 -0.108573 0.008651

0.000000 0.000000 0.000000

-0.090531 0.006062 0.082665

0.237044 -0.573682 0.007964

-0.463872 0.042742 0.429621

-0.046507 0.013061 -0.112551

Ti

-0.346886 -0.415336 0.000062

-0.001514 -0.000804 -0.570903

0.067630 -0.094682 0.000701

-0.066008 -0.000071 -0.095334

0.000000 0.000000 0.000000

0.369094 0.440082 -0.000069

-1.553629 -1.371384 0.006545

-0.368010 0.419022 -0.000409

-0.001595 0.000029 0.570473

0.066852 0.094896 0.000409

-0.067570 0.000218 0.094217

0.383648 -0.437592 0.000442

0.091432 -0.018866 0.069141

-0.266220 -0.517406 -0.109613

-0.052966 -0.101133 -0.022800

0.934637 1.816337 0.392178

-0.074487 0.071661 0.053033

0.035945 0.048192 -0.099407

-0.092533 0.363112 -0.443758

-0.217224 0.230064 0.486997

0.570806 -0.085819 0.064208

0.000000 0.000000 0.000000

V

-0.348785 -0.348785 0.136400

0.063463 -0.065390 0.063463

0.136401 -0.348785 -0.348785

-0.348785 0.136398 -0.348785

-0.347614 0.297686 0.297684

-0.065391 0.063463 0.063463

-1.126624 -1.126642 -1.126624

0.297685 -0.347614 0.297685

0.277718 0.277718 0.277718

-0.063046 -0.063046 -0.063047

0.000000 0.000000 0.000000

0.297684 0.297686 -0.347614

0.063463 0.063463 -0.065390

-0.011257 0.013357 -0.109092

-0.237278 -0.266628 0.413070

0.007367 -0.319503 -0.442473

-0.073242 0.063802 0.052642

0.000000 0.000000 0.000000

-1.844255 -0.467492 -0.514775

0.102522 0.028722 0.030334

-0.281555 0.454808 -0.108639

-0.017881 -0.105842 0.026159

0.520783 0.133688 0.140634

Cr

0.035135 -0.098447 -0.019834

-0.413156 0.260613 0.023594

-0.120043 -0.161896 -0.445591

0.000000 0.000000 0.000000

0.078465 0.067811 -0.012047

-0.038903 0.008275 0.098680

-0.160636 -0.051383 0.483685

-0.074663 0.024911 -0.069075

0.144610 -0.491385 -0.004927

1.724269 0.600966 0.536009

0.344558 -0.065373 0.274123

0.123390 0.412256 0.219510

0.414961 -0.008029 -0.247205

0.013027 0.368325 -0.323543

-0.354527 -0.268854 0.020625

0.109559 0.505812 -0.037882

0.030834 0.001791 0.100790

0.000000 0.000000 0.000000

-0.514308 -0.067244 -0.015795

0.219958 -0.254686 -0.395016

0.184792 -0.183883 0.448690

0.055571 0.070700 -0.055008

-0.102553 0.023703 -0.005799

0.016148 -0.096193 -0.039982

Mn

-0.145604 -0.375060 0.217551

0.067011 0.065977 0.038664

-0.078930 -0.006585 0.060808

-0.031040 0.027823 -0.092740

1.281887 -1.045483 -0.652985

0.334278 -0.021041 -0.243322

-0.069753 0.091193 0.442552

0.305924 0.353456 0.101934

0.342985 -0.198843 0.216856

0.041730 -0.090300 -0.004919

-0.201080 0.359322 0.045708

-0.448944 -0.056364 -0.065623

-0.087687 0.200288 -0.425567

-0.034446 -0.345715 -0.288961

0.000000 0.000000 0.000000

-0.286461 -0.238394 -0.326661

1.035354 0.878326 1.176154

-0.004681 0.100228 -0.007654

0.093366 -0.030924 -0.021293

-0.023894 -0.027612 0.093772

0.000000 0.000000 0.000000

-0.064870 -0.041745 -0.064906

-0.014909 0.479317 -0.089942

0.459644 -0.158814 -0.040353

-0.162609 -0.085781 0.452029

Fe

-0.119210 0.166825 -0.380269

-0.065923 -0.311723 -0.284545

0.269369 -0.339019 0.131052

-1.343016 -1.020480 -0.172181

-0.208737 -0.288795 0.157840

0.043602 0.070506 -0.047406

0.061236 -0.075095 0.009758

-0.030884 0.033249 0.086168

-0.094908 0.089414 0.433204

0.338662 0.018323 -0.267461

0.000000 0.000000 0.000000

-0.012307 0.431106 0.023653

-0.075043 -0.027108 -0.052034

-0.415434 0.099344 0.005359

0.314695 0.137235 0.184807

-0.000656 -0.446884 -0.091887

-0.620691 0.620596 -1.464361

-0.039654 0.039655 -0.077844

0.000088 -0.000088 0.468841

-0.000384 0.433180 -0.088174

-0.433180 0.000384 -0.088174

0.094874 0.016179 -0.000554

-0.038842 0.038843 0.079200

0.000000 0.000000 0.000000

-0.016182 -0.094873 -0.000553

0.446884 0.000656 -0.091887

Co

0.349819 0.219382 0.117221

0.248091 -0.279988 0.166675

-0.019837 0.040697 -0.081747

-0.036538 0.051746 0.400316

0.076042 0.036640 0.040092

-0.085671 0.349437 0.079050

-0.993140 0.994220 0.814627

-0.024331 0.235209 -0.358229

0.012778 -0.089665 -0.013041

0.282320 -0.074716 -0.224655

0.000000 0.000000 0.000000

-0.395764 0.066941 -0.056170

-0.071217 0.009231 0.056351

-0.112483 -0.264736 -0.291522

-0.220088 -0.304491 0.163060

0.059472 0.733255 1.458996

-0.069535 -0.035081 0.048927

0.000000 0.000000 0.000000

-0.320335 -0.277942 0.000999

-0.168138 0.282438 -0.286386

0.034846 -0.065540 -0.054808

0.065429 0.030247 0.056885

0.317185 0.275749 0.001309

-0.030655 0.070174 -0.051851

-0.156735 0.263130 0.267378

0.166446 -0.279335 -0.283919

0.159172 -0.267002 0.272017

Ni

-0.248516 -0.033084 0.297804

0.338202 0.081377 -0.029055

-0.096950 -0.332416 0.044174

0.015396 0.085576 -0.010817

-0.087041 -0.009941 0.006201

-0.280410 -0.096852 -0.252055

0.000000 0.000000 0.000000

-0.268046 0.281705 -0.017122

0.038630 -0.027668 0.076214

0.060753 0.223585 -0.308065

0.183981 -0.241872 -0.272625

1.047237 1.138511 -0.192788

0.030045 -0.044832 -0.071790

0.092540 0.287139 0.239943

0.217067 -0.175720 0.297791

0.900694 -0.900696 -0.900721

0.264221 -0.264221 0.103235

-0.050726 -0.052956 0.050726

-0.103235 -0.264221 -0.264221

0.050417 -0.050417 -0.050417

-0.225687 -0.261846 0.225687

-0.225687 0.225687 -0.261846

0.000000 0.000000 0.000000

0.052957 0.050726 0.050725

0.261846 0.225687 0.225687

-0.050726 0.050726 -0.052957

0.264221 0.103235 -0.264221

-0.206601 0.206601 0.206601

Cu

0.027746 0.051798 0.060667

0.283770 -0.049636 -0.231639

-0.094037 -0.178844 -0.266022

0.038494 -0.076892 0.008223

-0.086090 -0.005614 0.004342

0.302988 0.007062 0.215739

-0.071231 -0.107722 0.308217

0.021966 0.034378 -0.073758

-0.157248 0.270377 0.201405

-0.175392 0.213066 -0.245939

-0.026102 -0.133650 -1.616716

0.000000 0.000000 0.000000

0.184470 0.319804 -0.048159

0.101288 -0.374495 0.042437

-0.375817 -0.101528 0.027577

0.063942 -0.235186 0.233142

-0.070927 -0.048753 0.004969

-0.074025 -0.090470 -0.316373

-0.306986 0.172322 -0.117925

0.314692 0.076540 0.181529
-0.014536 0.065287 -0.051484
0.000000 0.000000 0.000000
-0.273685 -0.274061 -0.003460
0.208097 0.188348 -0.243028
0.068042 -0.044428 -0.028784
0.017537 0.031647 0.076258
0.011130 0.359482 0.091876
-0.200392 0.060514 0.306632
0.257225 -0.257542 -0.132406

Zn

0.026288 -0.237742 0.262140
0.000000 0.000000 0.000000
-0.354226 -0.011673 0.017808
-0.104726 0.331904 -0.051409
-0.052982 -0.032580 0.052368
-0.113418 0.012058 -0.354872
-0.111591 0.142099 0.305265
-0.037728 0.012471 -0.073236
0.066690 -0.049565 -0.006190
0.022609 0.071495 0.030941
0.208461 0.157236 -0.179168
-0.108173 -0.282615 -0.093025
0.274732 0.106462 0.192245
0.281363 -0.222487 -0.101379
0.811131 1.203193 -0.149939
-0.067490 -0.039442 -0.022368
-0.020787 0.179425 0.326064
0.271185 -0.214352 0.139482
-0.065381 -0.324016 -0.129105
-0.346802 0.055531 0.050735
-0.016975 0.048859 0.065323
-0.112673 -0.190715 0.226183
0.000000 0.000000 0.000000
0.229197 -0.040859 -0.263761

-0.166642 0.024369 -0.312199

0.262166 0.170001 0.051467

0.951346 0.963016 -0.543715

0.060250 -0.055293 0.015974

-0.051443 0.337634 -0.084420

0.022105 0.046197 -0.062906

Ga

0.204990 -0.119325 0.239581

0.000000 0.000000 0.000000

0.000002 0.045614 -0.066142

-0.204994 -0.119314 0.239582

-0.000009 -0.338087 -0.003602

0.000007 0.248070 0.251960

0.000006 0.253382 -0.246618

-0.063259 -0.046529 -0.000496

0.266877 0.153278 0.001632

-1.482888 0.003843 0.000044

1.482888 0.003844 0.000034

0.204988 -0.114194 -0.242070

0.063257 -0.046532 -0.000496

0.000001 0.044194 0.067099

-0.204996 -0.114182 -0.242069

-0.266869 0.153292 0.001634

0.111418 0.165171 0.293000

0.092148 0.285942 -0.064898

-0.066844 0.041557 -0.016326

0.036870 0.026860 0.066187

0.000000 0.000000 0.000000

-0.193154 -0.050973 0.233704

0.334165 0.013654 -0.028773

-0.018105 -0.075977 0.009225

0.112331 -0.258208 -0.187181

-0.277106 0.220223 -0.016103

0.116046 -0.247753 0.200097

0.049174 0.005024 -0.060913

-0.259440 -0.194549 -0.098633

0.743782 0.761062 -0.799350

-0.040104 0.066685 -0.326534

Ge

-0.256038 -0.044883 -0.191323

1.210593 0.461249 -0.191832

-0.159877 -0.124484 0.252806

0.267534 0.106386 -0.039482

-1.006753 0.822506 -0.191932

0.045645 -0.037291 0.050590

0.018628 -0.015220 -0.073849

-0.007080 0.259842 -0.191327

-0.210567 -1.278260 -0.191831

0.090104 0.181495 0.252802

-0.072069 -0.019743 0.012195

-0.050898 -0.283376 -0.039476

0.004975 0.074559 0.012194

0.128025 -0.104599 -0.294034

0.228555 -0.186724 0.164316

-0.237532 0.194062 0.086487

0.000000 0.000000 0.000000

0.052689 -0.057054 -0.002146

0.247281 0.045377 0.199228

0.176047 -0.289687 -0.010271

0.075299 0.313792 0.015368

0.009763 0.040683 0.063047

0.000912 0.003794 1.236122

0.252581 0.063749 -0.192467

-0.036426 -0.151802 0.246584

-0.031464 -0.131112 -0.259615

-0.196149 0.171429 -0.192464

-0.288336 -0.178251 -0.010268

0.011227 0.046787 -0.058662

-0.199758 0.152651 0.199230

0.000000 0.000000 0.000000

-0.072842 -0.026931 -0.002145

As

-0.216547 -0.127142 0.178879

0.052651 -0.039581 -0.036149

-0.270550 0.140161 -0.044769

1.142587 0.387125 0.398456

0.121297 -0.227793 0.168061

0.004943 -0.013130 0.071766

-0.048316 0.037304 -0.270782

-0.105989 -0.258747 -0.129087

0.000000 0.000000 0.000000

-0.907367 0.639521 0.627424

-0.128767 -1.247870 0.228479

-0.043265 0.171115 0.252378

0.076156 0.302069 -0.089717

-0.066163 -0.022814 -0.021195

0.005829 0.073917 -0.012159

0.242947 0.076971 0.110007

0.247088 -0.112282 -0.177299

-0.115762 0.215758 -1.246670

-0.285053 0.145175 0.061125

-0.051882 0.004434 0.273271

-0.058557 0.046187 0.009631

0.056879 0.024319 0.039365

0.076600 0.274991 0.122648

0.228738 -0.138452 0.158241

0.000000 0.000000 0.000000

-0.037546 0.202032 -0.227839

-0.240704 -0.184007 -1.108585

-0.015470 -0.070902 0.019711

0.020554 0.001530 -0.070081

0.274856 0.091824 -0.108221

-0.195241 -0.087196 -0.178326

0.114087 -0.210042 -0.192364

-0.127402 -0.283250 0.098007

Se

0.000667 -0.237208 0.201979

0.111848 0.272519 -0.020628

-0.032636 -0.012792 -0.061413

0.063814 0.025791 -0.016113

0.546421 0.219541 0.985854

-0.195096 0.149537 -0.163904

0.108557 0.045276 -0.271352

-0.037636 -0.241395 -0.166145

-0.109616 0.994614 -0.614909

0.000000 0.000000 0.000000

0.624109 -0.772395 -0.626477

-0.163126 0.169457 0.204308

0.146829 0.057921 0.212263

-0.242778 -0.097949 0.030216

0.269419 -0.118706 -0.022861

-1.006996 -0.415794 0.207843

-0.037454 0.050222 0.037143

0.007951 -0.062526 0.036499

0.179061 0.211745 0.102244

0.056707 0.000163 0.042274

0.180733 -0.210625 0.101598

0.000242 -0.060706 -0.040330

0.000000 0.000000 0.000000

-0.179055 -0.212056 0.101609

0.000864 -0.219345 -0.223019

-0.000245 0.060828 -0.040145

-0.056704 -0.000292 0.042278

-0.000879 0.220023 -0.222349

0.000010 -0.000453 0.297108

0.229949 0.001114 -0.132021

-0.229958 -0.000711 -0.132009

1.104227 0.004717 -0.005130

-0.180727 0.210314 0.102251

-1.104227 -0.004701 -0.005098

Br

0.133306 -0.221344 0.152309

0.604277 -0.665408 -0.617774

-0.165227 -0.116607 0.152264

0.150140 -0.135941 -0.151853

-0.258905 0.113202 -0.025964

-0.036970 0.043358 0.037943

-0.043165 -0.036381 -0.042449

0.270545 0.081656 0.025648

0.000000 0.000000 0.000000

0.021481 0.096926 0.265827

0.016950 0.283724 -0.000461

-0.679091 -0.586735 0.619792

0.038535 -0.041124 0.042575

0.041861 0.038525 -0.038076

-0.009840 0.097932 -0.266144

-0.158739 -0.204391 -0.151617

0.656145 0.596477 0.642510

-0.580577 0.668295 -0.644548

0.015819 -0.066615 -0.000001

-0.197338 0.036404 -0.203996

0.249261 -0.043119 -0.000001

1.064742 -0.187238 0.000000

0.136326 0.163199 0.210814

0.070950 -0.187702 -0.204000

-0.068367 0.003707 -0.000000

0.000000 0.000000 0.000000

-0.197338 0.036397 0.203997

0.024826 0.029721 -0.059100

0.136326 0.163206 -0.210808

-0.373815 1.014394 0.000000

0.070950 -0.187709 0.203993

-0.179553 -0.214952 -0.000004

-0.086805 0.237602 0.000004

0.024825 0.029719 0.059102

-0.695676 -0.832842 -0.000000

Kr

-0.808472 -0.237608 -0.578317

0.506180 -0.850743 0.254076

0.002564 0.165320 -0.217332

-0.031452 0.056351 -0.015411

0.045693 0.008419 0.269095

0.133914 -0.189333 0.071080

-0.041918 -0.039881 0.036826

0.061293 -0.172440 -0.223822

0.051951 0.017452 0.037399

-0.216474 0.130693 0.103098

0.000000 0.000000 0.000000

-0.196312 -0.035317 -0.138011

0.070379 0.253386 0.075492

-0.317742 0.475472 0.852061

-0.167114 -0.208548 0.110313

0.623184 0.624214 -0.524443

0.264731 0.043046 -0.051335

0.022597 -0.029682 -0.057551

-0.215595 0.116071 -0.153737

-0.027291 -0.115756 -0.211396

-0.792001 -0.273293 0.592526

-0.002190 -0.065987 0.006562

0.018256 -0.142671 0.232741

0.011105 0.242247 0.005049

0.215090 0.084747 0.145344

0.037222 1.019014 -0.068996

-0.202572 -0.182572 0.014239

-0.115637 -0.406210 -0.930676

0.871232 -0.345893 0.417557

-0.059525 0.022073 -0.025949

0.007508 0.024432 0.061228

0.188145 0.098447 -0.196210

0.054513 0.017095 -0.037946

0.184607 -0.199472 -0.026491

-0.172089 0.101648 0.186075

0.000000 0.000000 0.000000

7 Electron coordinates at the HF+J Born maximum.

Nuclei at the origin of the reference System. Majority spin electrons followed by minority spin ones. All data in au.

Li

-0.983110 -0.206543 1.439148

0.000000 0.000000 0.000000

0.000000 0.000000 0.000000

Be

1.124140 0.348840 -0.110005

0.000000 0.000000 0.000000

0.000000 0.000000 0.000000

-1.124140 -0.348840 0.110005

B

-0.096541 0.000016 -0.878938

0.000000 0.000000 0.000000

-0.096536 0.000013 0.878940

0.000000 0.000000 0.000000

0.886482 -0.000113 0.000008

C

0.000000 0.000000 0.000000

0.332072 -0.028695 0.573239

-0.662503 -0.026459 0.001936

0.328697 -0.028679 -0.575191

0.052226 0.697255 0.000033

0.000000 0.000000 0.000000

N

-0.065333 -0.496101 0.215572

0.000000 0.000000 0.000000

0.525291 0.125492 -0.071955

-0.226381 -0.014715 -0.496833

-0.266413 0.383190 0.281151

0.243323 0.015816 0.534014

0.000000 0.000000 0.000000

O

0.259897 -0.389940 0.019344

-0.258816 -0.020541 -0.390904

0.000000 0.000000 0.000000

-0.258917 0.018125 0.390928

0.257840 0.391886 -0.019321

0.489962 0.001352 -0.000012

-0.489961 -0.001112 -0.000012

0.000000 0.000000 0.000000

F

0.259897 -0.389940 0.019344

-0.258816 -0.020541 -0.390904

0.000000 0.000000 0.000000

-0.258917 0.018125 0.390928

0.257840 0.391886 -0.019321

0.489962 0.001352 -0.000012

-0.489961 -0.001112 -0.000012

0.000000 0.000000 0.000000

Ne

0.000000 0.000000 0.000000

-0.048714 -0.236653 0.280604

0.166258 -0.174449 -0.281144

0.211319 0.282630 0.112165

-0.328863 0.128472 -0.111625

0.328863 -0.128472 0.111625

-0.211319 -0.282630 -0.112165

-0.166258 0.174449 0.281144

0.048714 0.236653 -0.280604

0.000000 0.000000 0.000000

Na

-0.132270 0.234251 0.162271

-0.459142 -2.025387 0.203708

0.212537 0.119866 -0.197891

0.140750 -0.195331 0.196784

0.000000 0.000000 0.000000

-0.218999 -0.149882 -0.162061

-0.211371 -0.115691 0.197250

0.000000 0.000000 0.000000

-0.140106 0.199737 -0.197569

0.133027 -0.229940 -0.162483

0.220333 0.154203 0.161967

Mg

-0.022171 -0.274335 -0.007153

0.096206 0.090067 -0.242424

-0.248118 0.110293 0.049093

0.820101 -1.081776 1.043863

0.000000 0.000000 0.000000

0.173828 0.074312 0.200160

0.022171 0.274335 0.007156

-0.096206 -0.090069 0.242423

0.000000 0.000000 0.000000

-0.820100 1.081775 -1.043866

-0.173828 -0.074310 -0.200161

0.248118 -0.110292 -0.049094

Al

0.000000 0.000000 0.000000

-0.048714 -0.236653 0.280604

0.166258 -0.174449 -0.281144

0.211319 0.282630 0.112165

-0.328863 0.128472 -0.111625

0.328863 -0.128472 0.111625

-0.211319 -0.282630 -0.112165

-0.166258 0.174449 0.281144

0.048714 0.236653 -0.280604

0.000000 0.000000 0.000000

Si

0.000000 0.000000 0.000000

-0.048714 -0.236653 0.280604

0.166258 -0.174449 -0.281144

0.211319 0.282630 0.112165

-0.328863 0.128472 -0.111625

0.328863 -0.128472 0.111625

-0.211319 -0.282630 -0.112165

-0.166258 0.174449 0.281144

0.048714 0.236653 -0.280604

0.000000 0.000000 0.000000

P

-1.083484 -0.120081 -0.553536

-0.048731 -0.168665 -0.107339

0.000000 0.000000 0.000000

-0.170244 0.090267 0.065316

-0.093719 0.565938 1.079675

0.114464 -0.055567 0.161724

0.402787 -1.137169 0.233560

0.107086 0.126540 -0.118142

0.833393 0.523792 -0.725075

0.051632 0.166282 0.108080

-0.358475 1.013574 -0.208496

0.000000 0.000000 0.000000

0.172368 -0.096587 -0.063949

-0.112738 0.052374 -0.162923

-0.108397 -0.129982 0.120380

S

-0.894473 0.588643 -0.014457

-0.104141 -0.109614 -0.111961

0.000000 0.000000 0.000000

0.887812 0.598162 0.014492

0.019693 -0.592714 -0.891620

-0.009239 -0.592831 0.891714

0.106552 -0.106978 0.112249

-0.113318 0.107182 0.105210

0.110882 0.109399 -0.105498

0.117120 -0.107838 -0.102466

-0.005484 1.040120 -0.000002

0.101380 0.110264 0.115734

-0.114675 -0.110099 0.102777

-0.103848 0.107663 -0.116070

0.004643 -1.040130 -0.000001

0.000000 0.000000 0.000000

Cl

0.000000 0.000000 0.000000

0.141830 0.036921 -0.094680

0.790120 -0.443501 -0.336038

-0.001385 0.098506 0.144523

-0.000004 0.001042 0.964376

-0.142729 0.033041 -0.094763

-0.777855 -0.464681 -0.336046

0.002284 -0.168435 0.044794

-0.012192 0.905269 -0.338724

0.001364 -0.097062 -0.147271

-0.836108 0.469331 0.017454

0.823131 0.491748 0.017456

0.012899 -0.959125 0.017423

0.000000 0.000000 0.000000

0.143315 -0.034389 0.094578

-0.142375 -0.038284 0.094498

-0.002294 0.169010 -0.042293

Ar

-0.094482 -0.129958 -0.021853

0.114644 0.003357 -0.114558

0.799909 -0.031006 0.381179

-0.090044 0.134508 -0.009661

-0.627093 -0.018434 0.626680

-0.074217 0.747748 -0.470616

0.069812 -0.007909 0.146141

0.000000 0.000000 0.000000

-0.098446 -0.698303 -0.537396

0.000000 0.000000 0.000000
0.074218 -0.747748 0.470615
-0.069812 0.007909 -0.146141
0.090044 -0.134508 0.009661
-0.799910 0.031006 -0.381178
0.094482 0.129959 0.021853
0.627093 0.018435 -0.626681
-0.114644 -0.003358 0.114558
0.098446 0.698303 0.537397

K

0.000000 0.000000 0.000000
0.108074 -0.093093 -0.028777
-0.089187 0.008221 -0.114930
1.176379 1.598649 0.965871
-0.074381 -0.046378 0.116151
0.055613 0.131494 0.027628
0.721132 0.199771 -0.188796
-0.010183 -0.767659 0.234558
-0.479146 0.101933 -0.636104
-0.245583 0.447204 0.579035
-0.107970 0.093384 0.028953
0.089230 -0.008046 0.114927
-0.055610 -0.131592 -0.027593
0.000000 0.000000 0.000000
-0.739472 -0.200467 0.197929
0.015149 0.761723 -0.226394
0.476145 -0.093369 0.629572
0.074614 0.046636 -0.116079
0.257215 -0.455571 -0.593699

Ca

-0.516090 0.559990 0.031854
0.034483 -0.376083 0.661897

0.106732 0.018502 0.094691
0.000000 0.000000 0.000000
-0.198004 -0.479585 -0.539136
-0.100046 0.101542 0.019927
0.671107 0.298810 -0.142137
-0.058931 -0.129870 0.019014
0.052256 0.009775 -0.133555
1.439113 -0.548259 -2.075442
0.100046 -0.101542 -0.019928
-0.034482 0.376080 -0.661898
-0.671106 -0.298812 0.142137
0.058931 0.129870 -0.019014
0.000000 0.000000 0.000000
-0.052255 -0.009775 0.133555
-0.106733 -0.018501 -0.094690
0.516091 -0.559987 -0.031851
0.198001 0.479588 0.539134
-1.439108 0.548241 2.075450

Sc

0.099920 -0.588075 0.132598
0.557475 0.292130 -0.215805
-0.022065 -0.107490 -0.077344
0.020777 -0.039423 0.126633
0.108882 0.066533 -0.045027
-0.107132 0.081064 -0.004608
-1.369720 1.067556 0.167047
0.654555 -1.050232 1.167658
-0.218750 0.308301 0.504432
-0.449020 -0.021513 -0.479835
0.000000 0.000000 0.000000
0.107809 -0.080886 0.005250
-0.108702 -0.066465 0.044976
-0.020638 0.039022 -0.127494
0.230902 -0.361257 -0.487587
0.021655 0.108645 0.077192

-0.131752 0.600667 -0.219402

0.452130 0.044039 0.476459

1.133189 0.083197 -2.123192

0.000000 0.000000 0.000000

-0.552364 -0.280870 0.236987

Ti

0.043980 0.000523 0.119301

-0.069856 -0.104555 -0.018627

0.395863 -0.451444 0.005232

0.000000 0.000000 0.000000

-0.072305 0.102875 -0.018634

-0.000155 -0.000013 -0.609719

0.000626 0.000018 0.628827

0.385085 0.460674 0.005209

0.097303 0.001146 -0.081084

1.984781 0.023416 -0.510621

-0.416831 0.477142 0.005243

-0.405440 -0.486859 0.005267

0.000000 0.000000 0.000000

-0.044740 -0.000532 -0.118829

0.069692 0.104581 0.018881

-0.097050 -0.001144 0.081706

-0.505219 -0.005962 0.361307

0.517991 0.006130 0.377907

0.072142 -0.102905 0.018887

-2.002345 -0.023670 -0.464904

-0.003792 0.513812 -0.361844

0.008351 -0.513774 -0.361821

V

0.297721 0.297954 0.297954

0.325482 0.327190 -0.381391

-0.370368 0.148671 -0.371740

0.325482 -0.381391 0.327191
-0.069555 0.067810 0.067812
0.000000 0.000000 0.000000
0.067780 0.067745 -0.069696
-0.370367 -0.371739 0.148671
-0.967184 -0.997238 -0.997207
0.067780 -0.069699 0.067743
-0.067128 -0.067033 -0.067035
-0.379805 0.326996 0.326996
0.149477 -0.370600 -0.370600
0.068164 -0.067948 -0.067950
-0.116734 -0.113510 0.556883
0.000000 0.000000 0.000000
-0.067797 -0.067818 0.067946
-0.067796 0.067949 -0.067816
-0.319966 -0.337796 -0.337800
0.581545 -0.107074 -0.107069
-1.718933 0.134457 0.134448
-0.116728 0.556884 -0.113511
0.067848 0.067935 0.067938

Cr

-0.441672 0.030297 -0.298351
0.043821 -0.327095 -0.438378
0.087963 -0.004328 -0.074068
-0.198656 0.528387 0.092464
0.474785 -0.264330 0.003104
0.000000 0.000000 0.000000
0.155620 -0.047376 0.548907
0.153763 0.283548 -0.442073
-0.046278 0.106561 -0.001817
0.372346 0.320333 0.112809
0.038222 -0.026669 0.106540
-0.109187 -0.503798 0.145839
-1.831983 -0.716066 0.327224
-0.404318 -0.013547 0.285799

-0.078273 -0.076503 -0.032929

0.048200 -0.104760 0.002958

-0.034802 0.023333 -0.107385

0.000000 0.000000 0.000000

-0.090073 0.003064 0.071346

-0.193179 -0.508917 -0.151123

0.077679 0.078685 0.032966

0.562052 0.028782 -0.086424

-0.240708 0.392993 -0.329091

-0.118830 0.120876 0.539910

Mn

-0.222790 -0.347569 -0.204516

-0.107037 0.027497 -0.003486

-0.112100 0.123565 0.431555

0.016177 -0.090188 0.062130

0.354196 1.140824 1.322024

-0.527381 0.054951 0.049259

0.369447 0.250917 -0.248100

0.057158 0.082820 0.041234

0.337726 -0.325369 -0.197842

-0.010070 -0.431780 0.313167

0.036226 -0.018610 -0.101394

-0.073483 0.492822 0.030049

-0.153388 0.136613 -0.466037

0.406213 0.022685 0.287530

0.000000 0.000000 0.000000

-0.034696 0.022611 0.101362

0.114557 -0.348315 -0.380481

0.449064 0.271118 0.136807

-0.214934 -0.244334 0.424357

-0.011666 0.088775 -0.063442

-0.353939 0.349395 -0.193624

0.105922 -0.029073 0.003147

-0.899600 -1.134105 -1.068650

0.000000 0.000000 0.000000

-0.059141 -0.082352 -0.041179

Fe

-0.345416 0.006919 -0.313074
0.086724 0.050302 0.031335
-0.086722 0.050306 0.031334
0.000000 0.000000 0.000000
0.334063 -0.300542 0.164428
-0.347868 0.309079 0.184856
0.347868 0.309076 0.184858
-0.334067 -0.300540 0.164425
0.000028 0.704013 -1.460672
-0.000000 -0.401159 -0.260406
0.000002 0.371199 -0.218356
-0.000002 -0.007927 0.427436
0.000000 -0.007201 -0.102782
-0.000003 -0.096258 0.038473
0.345419 0.006917 -0.313071
-0.480122 -0.001171 0.095366
-0.084883 -0.050418 -0.032436
-0.000000 -0.471717 0.099813
0.000000 0.000000 0.000000
0.000000 0.004500 0.103863
0.000000 0.485332 0.103991
0.000003 0.096352 -0.038701
0.084880 -0.050423 -0.032436
0.000000 -0.006121 -0.511918
-0.000038 -0.206897 1.615336
0.480121 -0.001172 0.095366

Co

-0.317950 -0.058206 -0.353554
0.084402 0.045421 -0.027618
0.180431 -0.141334 -0.337837

-0.067424 0.004228 -0.076059

0.000000 0.000000 0.000000

-0.314868 0.324244 0.068863

-0.036429 0.048869 0.079316

0.020460 -0.095947 0.026024

1.241887 0.145815 -1.127120

-0.350974 -0.158638 0.149623

0.438748 -0.077722 0.077830

0.094671 0.328544 -0.289463

0.035345 -0.085542 0.445354

0.033393 -0.475995 0.023575

0.187323 0.355584 0.221038

-0.351339 -0.311750 -0.039134

-0.084838 -0.042301 0.032525

0.213108 -0.319912 -0.293116

-0.212661 0.304210 -0.294626

0.152081 -0.300015 0.315817

-0.019201 0.093180 -0.031991

0.351097 0.300745 -0.032026

0.066740 0.003117 0.074825

0.000000 0.000000 0.000000

-1.142235 -0.054516 1.249474

0.037191 -0.054390 -0.076019

-0.146553 0.291139 0.316232

Ni

0.290133 0.341690 -0.101262

0.000000 0.000000 0.000000

0.989078 -0.783695 0.902986

-0.049124 0.043524 0.072079

0.064915 0.060258 -0.040714

-0.061520 -0.031200 -0.066757

0.045565 -0.076005 0.034805

-0.068465 -0.405656 -0.151091

-0.196216 0.307745 -0.145966

0.016465 -0.001179 -0.438289

-0.430624 -0.084763 -0.012161

-0.174944 0.251859 0.343455

-0.068750 -0.271212 0.323124

0.374458 -0.184785 -0.096679

0.264863 0.051990 0.289489

0.000000 0.000000 0.000000

0.118325 0.292062 -0.295906

0.057752 0.046672 0.061765

-0.297398 0.294330 0.114387

0.052900 -0.050567 -0.063860

0.247956 0.297947 0.252407

-0.051533 0.064438 -0.047020

-0.060181 -0.058883 0.048292

-0.291144 -0.112488 -0.292534

-0.930346 0.836251 -0.922118

-0.299836 -0.252841 0.249751

0.233229 -0.236417 0.231730

0.247280 -0.256330 -0.299287

Cu

-0.539525 -0.011266 0.456853

0.000000 0.000000 0.000000

-3.209961 -0.760238 -1.588981

-0.180892 0.343459 -0.575034

-0.101761 2.405846 2.947849

0.512367 -1.352627 3.274608

-0.007511 0.028231 0.087696

-0.084070 -0.008786 -0.036751

1.403606 3.496416 -0.616320

0.043723 -0.081487 -0.002466

0.573563 0.310838 0.316302

-2.538693 2.820272 -0.208212

0.048340 0.062321 -0.048146

2.825644 0.292435 -2.185073

0.187917 -0.681888 -0.160147

-0.082840 0.361266 -0.629153

-0.047972 -0.062237 0.048483

0.000000 0.000000 0.000000

0.008557 -0.028635 -0.087359

0.418432 -1.264133 3.211624

2.706606 0.358169 -2.164424

-0.315300 -1.813194 -2.925469

-1.822262 -2.873052 0.595654

-0.044168 0.081103 0.001695

-3.092130 -0.738408 -1.543065

0.294945 -0.662167 -0.068259

0.499632 0.407704 0.378673

-0.603518 0.048416 0.369425

0.084070 0.010045 0.037479

Zn

-0.146865 0.115733 -0.387254

-0.432518 0.028322 0.006087

-0.152516 -0.300710 0.192284

-0.028288 -0.346318 -0.259180

0.000000 0.000000 0.000000

-0.034138 0.032809 0.082407

0.704019 0.942292 -0.257981

0.325113 -0.278063 0.150579

-0.069159 -0.039800 -0.049176

-0.097676 0.113778 0.428025

0.033142 0.071017 -0.049794

0.294169 0.203348 0.161082

0.314553 0.035315 -0.270284

0.069481 -0.063226 0.014408

-0.086558 0.407064 -0.007064

-0.325112 0.278063 -0.150580

-0.294169 -0.203348 -0.161081

-0.314553 -0.035314 0.270283

-0.704031 -0.942284 0.257976

0.000000 0.000000 0.000000

0.034138 -0.032810 -0.082407

-0.069482 0.063226 -0.014408

0.069158 0.039800 0.049177

0.146864 -0.115734 0.387254

0.097676 -0.113779 -0.428025

0.152517 0.300710 -0.192284

0.086557 -0.407065 0.007063

-0.033142 -0.071017 0.049794

0.432518 -0.028323 -0.006087

0.028289 0.346318 0.259180

Ga

-0.132132 0.175004 -0.298496

-0.024344 0.027035 -0.076618

0.241535 0.047087 0.247660

0.241536 -0.044772 -0.248089

-0.132133 0.270333 0.215977

1.276083 -0.004350 0.000806

-1.271548 -0.002808 0.000519

0.000000 0.000000 0.000000

0.162506 0.273984 -0.050767

-0.031353 -0.075741 0.014034

-0.125951 -0.260307 -0.208172

-0.314635 -0.000541 0.000100

0.082337 -0.007022 0.001301

-0.024344 0.052691 0.061845

0.178521 -0.297451 0.055116

-0.125951 -0.168440 0.287616

0.139907 -0.267799 -0.216719

-0.082734 0.007941 -0.001472

-0.147145 -0.277040 0.051333

0.024506 -0.027235 0.076564

0.000000 0.000000 0.000000

0.323811 0.013896 -0.002574

0.113221 0.161846 -0.286686

-0.253319 0.035029 0.251399

-0.181408 0.290357 -0.053801

0.032472 0.074602 -0.013823

0.139907 -0.172373 0.298280

-0.253319 -0.057369 -0.247260

0.024506 -0.052858 -0.061723

0.113220 0.253817 0.209667

0.262819 1.175479 -0.217800

Ge

0.048823 0.315358 -0.071125

-0.004441 -0.002951 0.079481

0.008913 -0.075234 -0.029787

-0.072381 1.217250 0.175814

0.000000 0.000000 0.000000

0.309646 -0.077160 -0.071127

-0.289871 0.102622 -0.165226

1.094152 -0.538303 0.175815

-0.172270 0.168443 0.229759

0.088553 -0.224075 0.229756

-0.065906 0.037364 -0.029787

0.207534 0.137902 0.221141

-1.011046 -0.671821 0.184457

-0.233683 -0.155280 0.091173

0.054464 0.036192 -0.298007

-0.017690 -0.306989 -0.165229

0.064205 0.042663 -0.018086

0.294779 -0.100259 0.162480

0.006002 0.003988 -0.078863

0.021770 0.310600 0.162482

-0.009046 0.075324 0.029936

0.000000 0.000000 0.000000

-0.064951 -0.043159 0.016495

-0.096027 0.221345 -0.222957

-0.318455 0.074630 0.081174

0.166857 -0.174276 -0.222959

0.065938 -0.037521 0.029936

0.106733 0.070922 -1.188922

0.236983 0.157472 -0.103274
-0.054569 -0.322499 0.081171
-0.207052 -0.137582 -0.216409
-0.044505 -0.029575 0.293161

As

0.160525 0.037041 -0.227772
-0.174896 -0.002415 -0.260017
0.067415 0.303477 -0.039499
-0.026222 0.054556 -0.046865
0.071428 0.020664 0.026735
-0.245267 -0.184318 0.069478
0.321227 0.028406 0.084885
-1.026182 -0.233273 -0.446320
0.241951 -0.767983 0.799445
-0.258791 0.174668 0.042075
-0.048991 -0.003677 0.058933
-0.016878 1.040865 0.472209
0.000213 -0.069238 -0.038076
0.796153 -0.041863 -0.816761
0.067366 -0.292066 -0.146145
-0.002872 0.121680 0.290073
0.070621 -0.193218 0.190423
0.000000 0.000000 0.000000
-0.091667 0.681910 -0.845181
-0.000419 0.068702 0.038951
0.000000 0.000000 0.000000
0.261396 -0.173462 -0.046611
0.027088 -0.054950 0.046459
0.244129 0.187620 -0.070375
0.048455 0.004402 -0.059349
-0.158287 -0.043410 0.234147
-0.071584 -0.021136 -0.025813
-0.064772 -0.308332 0.037044
0.180882 0.001780 0.260604
-0.322601 -0.030727 -0.079469

0.000440 -0.120011 -0.292147
-0.075474 0.194118 -0.186338
-0.069105 0.289284 0.151228

Se

0.225350 0.055979 0.133984
-0.225332 -0.055200 0.134339
-0.057289 -0.015421 -0.044366
-0.016297 0.061902 0.041884
0.000000 0.000000 0.000000
-0.000020 -0.000879 -0.302718
0.127674 0.254688 -0.105258
-0.053870 0.219157 0.227162
0.016303 -0.061658 0.042240
0.057283 0.015163 -0.044463
-0.390414 0.824561 -0.653049
0.053901 -0.217835 0.228423
0.390366 -0.828326 -0.648292
-0.228641 0.164158 -0.103968
0.228627 -0.164759 -0.103046
0.790072 0.400442 0.643126
-0.127688 -0.255294 -0.103760
-0.790019 -0.396700 0.645502
-0.228191 -0.051668 -0.134038
-1.082140 -0.003385 -0.039462
0.015509 -0.062070 -0.042006
-0.015514 0.061824 -0.042366
-0.132740 -0.252987 0.105737
0.057538 0.014753 0.044370
-0.049098 0.219016 -0.230214
0.132753 0.253599 0.104244
0.049069 -0.220353 -0.228940
1.082140 0.003150 -0.039490
-0.224597 0.170502 0.103271
0.224609 -0.169898 0.104233
-0.057532 -0.014493 0.044463

0.000000 0.000000 0.000000

0.228175 0.050887 -0.134367

0.000020 0.000888 0.304829

Br

-1.051210 -0.075641 -0.039571

-0.080824 -0.181025 0.211124

0.205926 0.026459 -0.201889

0.293078 1.012359 -0.039566

-0.017526 -0.069520 0.001983

0.071646 0.002650 0.001982

-0.130841 0.161662 -0.226588

0.193899 0.041318 0.211121

-0.068804 -0.195890 -0.201887

0.000000 0.000000 0.000000

0.345443 -0.426818 0.904639

-0.143486 0.177292 0.206363

-0.027351 0.033794 0.060097

0.091870 0.239862 -0.005983

0.182193 -0.225114 0.013442

-0.023760 0.029356 -0.063838

0.414149 -0.511703 -0.828460

-0.253743 -0.039855 -0.005979

-0.071668 -0.002723 -0.001941

-0.661476 0.817294 0.002141

0.142917 -0.176588 -0.206070

0.000000 0.000000 0.000000

0.253687 0.039640 0.005808

0.081431 0.183405 -0.213215

0.023732 -0.029322 0.063897

0.069597 0.197958 0.204040

1.036924 0.163477 0.002008

-0.178962 0.221122 -0.012861

-0.208115 -0.026805 0.204043

0.027232 -0.033648 -0.060240

-0.091647 -0.239852 0.005811

0.017602 0.069526 -0.001942
-0.376008 -0.980079 0.002008
-0.196352 -0.041416 -0.213212
0.130761 -0.161563 0.225845

Kr

0.225350 0.055979 0.133984
-0.225332 -0.055200 0.134339
-0.057289 -0.015421 -0.044366
-0.016297 0.061902 0.041884
0.000000 0.000000 0.000000
-0.000020 -0.000879 -0.302718
0.127674 0.254688 -0.105258
-0.053870 0.219157 0.227162
0.016303 -0.061658 0.042240
0.057283 0.015163 -0.044463
-0.390414 0.824561 -0.653049
0.053901 -0.217835 0.228423
0.390366 -0.828326 -0.648292
-0.228641 0.164158 -0.103968
0.228627 -0.164759 -0.103046
0.790072 0.400442 0.643126
-0.127688 -0.255294 -0.103760
-0.790019 -0.396700 0.645502
-0.228191 -0.051668 -0.134038
-1.082140 -0.003385 -0.039462
0.015509 -0.062070 -0.042006
-0.015514 0.061824 -0.042366
-0.132740 -0.252987 0.105737
0.057538 0.014753 0.044370
-0.049098 0.219016 -0.230214
0.132753 0.253599 0.104244
0.049069 -0.220353 -0.228940
1.082140 0.003150 -0.039490
-0.224597 0.170502 0.103271
0.224609 -0.169898 0.104233

-0.057532 -0.014493 0.044463

0.000000 0.000000 0.000000

0.228175 0.050887 -0.134367

0.000020 0.000888 0.304829

CH_4

-2.132842 2.141781 -12.464814

0.398052 1.770579 -12.492090

-1.544322 2.329314 -11.826170

-1.542280 3.194910 -11.625886

-2.042680 1.218420 -10.080894

-1.544322 2.329314 -11.826170

-0.734779 2.107073 -12.117069

-1.767425 1.873468 -11.096924

-1.568416 4.408693 -11.374412

-2.964262 1.919565 -13.357301

C_2H_4

9.000368 12.291288 10.926112

11.203127 11.162517 13.188001

10.804527 11.284707 11.151934

13.204725 14.558940 10.448824

12.283537 12.264063 10.149384

12.535289 12.744161 7.709610

10.697770 10.486660 10.865214

13.709885 12.198817 9.834751

12.933852 12.622085 9.745619

11.412338 11.614776 10.796641

13.045647 13.439121 10.078545

11.203127 11.162517 13.188001

12.750143 12.638245 8.875115

12.933852 12.622085 9.745619

10.056133 11.689681 11.074622

14.738200 11.615862 9.971933

10.804527 11.284707 11.151934

10.534183 9.347605 10.449259

NH_3

-6.578687 0.849364 0.422934

-7.117823 0.985983 0.028951

-7.551675 1.299082 0.254887

-6.464526 2.277649 -1.208536

-7.275438 0.450116 -0.361627

-7.520845 -0.565860 -0.998720

-7.564988 1.025564 0.405943

-5.633953 0.515328 1.125918

-6.900067 1.464229 -0.407807

-7.117823 0.985983 0.028951

H_2O

0.005330 0.287057 0.485888

-0.564735 0.037147 -0.321794

0.000000 0.000000 0.115651

-0.012831 -0.431875 0.239550

0.748955 0.000000 -0.462605

0.000000 0.000000 0.115651

-0.748955 0.000000 -0.462605

0.012826 0.431878 0.239546

0.564752 -0.037148 -0.321793

-0.005324 -0.287058 0.485889

HF

-0.282390 -0.307151 -0.400701

0.000000 0.000000 -0.261387

-0.124806 0.398133 -0.400701

-0.000000 0.000000 0.223540

0.407196 -0.090982 -0.400701

0.131389 -0.419134 -0.349319

0.297286 0.323353 -0.349319

0.000000 0.000000 1.442144

-0.428675 0.095781 -0.349319

0.000000 0.000000 -0.261387

References

[1] B. P. Pritchard, D. Altarawy, B. Didier, T. D. Gibson and T. L. Windus, *J. Chem. Inf. Model.*, 2019, **59**, 4814–4820.

[2] G. M. J. Barca, C. Bertoni, L. Carrington, D. Datta, N. De Silva, J. E. Deustua, D. G. Fedorov, J. R. Gour, A. O. Gunina, E. Guidez, T. Harville, S. Irle, J. Ivanic, K. Kowalski, S. S. Leang, H. Li, W. Li, J. J. Lutz, I. Magoulas, J. Mato, V. Mironov, H. Nakata, B. Q. Pham, P. Piecuch, D. Poole, S. R. Pruitt, A. P. Rendell, L. B. Roskop, K. Ruedenberg, T. Sattasathuchana, M. W. Schmidt, J. Shen, L. Slipchenko, M. Sosonkina, V. Sundriyal, A. Tiwari, J. L. Galvez Vallejo, B. Westheimer, M. Wloch, P. Xu, F. Zahariev and M. S. Gordon, *J. Chem. Phys.*, 2020, **152**, 154102.

[3] A. Martín Pendás and E. Francisco, Promolden. A QTAIM/IQA code (Available from the authors upon request).

[4] A. D. Becke and K. E. Edgecombe, *J. Chem. Phys.*, 1990, **92**, 5397–5403.

[5] H. Schmider and A. Becke, *J. Mol. Struct.: THEOCHEM*, 2000, **527**, 51–61.

[6] K. E. Schmidt and J. W. Moskowitz, *J. Chem. Phys.*, 1990, **93**, 4172–4178.

[7] A. Lüchow, S. Manten, C. Diedrich, A. Bande, T. C. Scott, A. Schwarz, R. Berner, R. Petz, A. Sturm, M. Hermsen, K. H. Mood, C. Schulte, L. Reuter, M. A. Heuer and J. Ludovicy, Amolqc (v7.1.0). Zenodo https://doi.org/10.5281/zenodo.4562745 (2021).

[8] N. Metropolis, A. W. Rosenbluth, M. N. Rosenbluth, A. H. Teller and E. Teller, *J. Chem. Phys.*, 1953, **21**, 1087–1092.

[9] W. K. Hastings, *Biometrika*, 1970, **57**, 97–109.

[10] D. C. Liu and J. Nocedal, *Math. Program.*, 1989, **45**, 503–528.